Aus der medizinischen Universitätsklinik Freiburg

- Abteilung Hämatologie und Onkologie -

Proteinsignatur der replikativen und prämaturen Seneszenz in humanen nicht-kleinzelligen Bronchialkarzinom- und Fibroblastenzelllinien

INAUGURALDISSERTATION

zur

Erlangung des Medizinischen Doktorgrades

der Medizinschen Fakultät der

Albert-Ludwigs-Universität Freiburg im Breisgau

Vorgelegt 2007 von

Wanda Kloos

Geboren in Bukarest

Meinen Eltern

TABLE OF CONTENTS

1. INTRODUCTION

1.1 The phenomenon of senescence

In response to diverse cell stressors such as telomere dysfunction, DNA damage and strong mitogenic signals, human cells are driven into a state of permanent cell cycle block in G_1/S-phase, termed senescence. Despite their static appearance, senescent cells are viable and metabolically active. Quiescence, a nonproliferative state in which cells are arrested in G_0-phase, can be instantly reversed due to mitogenes, whereas senescent cells do not abandon this phase in response to pro-mitogenic stimuli such as serum or growth factors (Dimri et al., 1994; Dimri et al., 1996; Narita et al., 2003; Narita, 2007).

1.1.1   Senescence as a hypermitogenic arrest

Cellular senescence can be characterized as a continuous growth stimulation in the absence of cell division (Blagosklonny, 2003).

In normal cells, mitogens (growth factors) both initiate and maintain the transition from G_1- to S-phase in the cell cycle (Blagosklonny, 2003). In order to force cells into senescence, two events are required: first a strong stimulation of mitogen-activated pathways, second, the blockage of cyclin-dependent kinases (CDKs) via inhibitors (CDKIs). Thus, cell cycle arrest can be triggered by either hypermitogenic stimuli, such as Ras or Raf-1 or direct inhibitors of CDKs such as p21 and p16 (Blagosklonny, 2006). This hypertrophic arrest is characterized by continuous mitogenic signaling which pushes the cell to grow despite its blocked cell cycle (Fig. 1), which might be an explanation to the typical senescent morphology of large cells which have an active metabolism and secrete mitogens in a futile attempt to overcome the cell cycle block.

The reversibility of senescence remains a much-discussed issue. Some authors insist on its irreversibility, whereas others suggest that, even if the senescent state cannot be reversed by growth factors, there are other means to do so. Therefore, abrogating the cell cycle block either by getting rid of CDKIs or activating the cell cycle downstream of CDKIs (c-myc, E2F, E1A) might reverse cellular senescence (Blagosklonny, 2006). For example, S-phase entry of senescent fibroblasts can be caused by inactivation of pRB and p53 and

overexpression of E2F and cyclin E/CDK2 (Gire and Wynford-Thomas, 1998; Sarraj et al., 2001; Beausejour et al., 2003).

Another interesting approach is the transition of senescent cells into quiescence which, theoretically, could be performed by inhibiting mitogen-activated pathways (Blagosklonny, 2006).
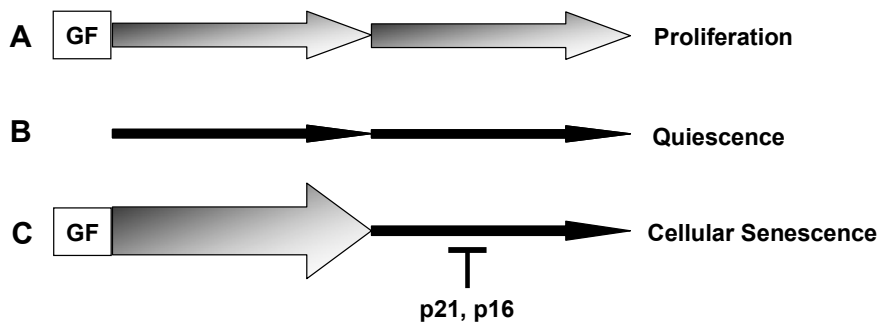
Figure 1. Cellular senescence as a hypermitogenic arrest. Adapted from Blagosklonny, 2006.

A. Proliferation. Since both upstream mitogen-activated pathways and downstream cell cycle pathways are activated, cells continue to grow and cycle.

B. Quiescence. If mitogen signaling is absent, cells neither grow nor cycle.

C. Cellular senescence. When cell cycle is blocked by CDK inhibitors, ongoing mitogenic signaling causes the senescent phenotype.

GF: growth factors

1.1.2 Triggers of cellular senescence

There are diverse factors which can switch on the senescence program: DNA damaging agents, irradiation, oxidative stress, inhibitors of histone deacetylases, microtubule-stabilizing agents, retinoids, strong mitogenic signaling, certain oncogenes and mitogen-activated kinases such as Ras and Raf-1 (Blagosklonny, 2006; Collado and Serrano, 2006). However, the confirmation *in vivo* of this previously *in vitro* established concept did not follow until recently. A series of studies could identify senescent cells *in vivo* using different models (Braig et al., 2005; Chen et al., 2005; Collado et al., 2005; Lazzerini Denchi et al., 2005; Michaloglou et al., 2005), as reviewed in (Narita, 2007).
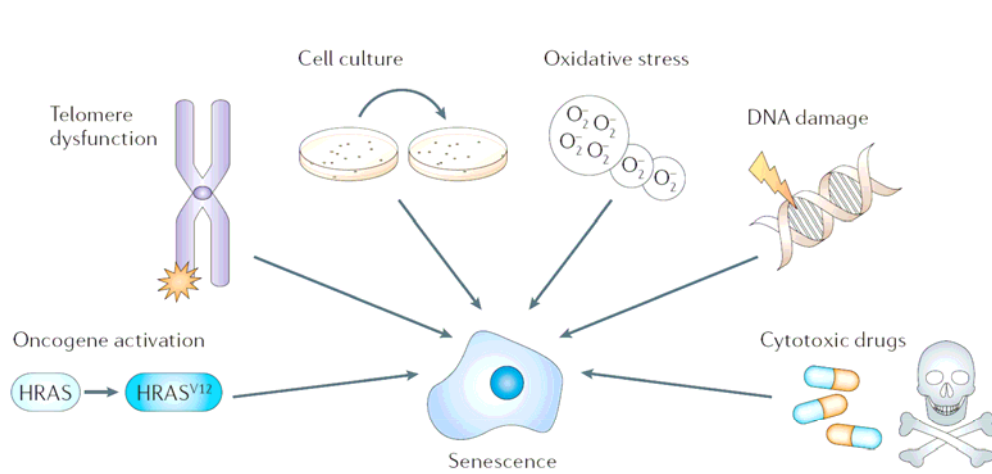
Figure 2. Many roads lead to senescence. From Collado and Serrano, 2006.

1.1.3 The senescent phenotype

The phenotype of senescent cells is characterized by a variety of changes, such as large cell size, a flat vacuolated morphology, the inability to synthesize DNA and the presence of the senescence-associated beta-galactosidase (SA-ß-gal) marker (Dimri et al., 1995; Severino et al., 2000; Campisi, 2001).

Furthermore, senescent cells are not able to express genes required for proliferation, even in a pro-mitogenic environment (Ben-Porath and Weinberg, 2004).

Besides the cessation to further proliferate, many senescent cell types become resistant to apoptotic signals (Campisi, 2005a). There are also functional changes which accompany the senescence response. Best described in human fibroblasts, they develop a secretory phenotype, characterized by an increased secretion of extracellular matrix remodeling enzymes, inflammatory cytokines and epithelial growth factors (Faragher, 2000; Krtolica et al., 2001). The secreted molecules may alter the microenvironment of the surrounding tissue, therefore having potential tumorigenic effects.

1.1.4 Histones

In terms of the regulation of senescence, one can distinguish between genetic and epigenetic mechanisms. Epigenetic mechanisms lead to changes in gene function without

an altered DNA sequence, e.g. alterations of high-order chromatin structure (Atkinson and Keith, 2007). Epigenetic processes such as post-translational modifications of histones are much involved in a variety of cellular regulations.

Histone proteins are crucial for the efficient packaging of DNA to the nucleus of the cell (Atkinson and Keith, 2007). Furthermore, the tight histone binding provides a barrier for factors which need access to DNA in order to regulate gene expression.

The histone formation is an octamer which consists of two copies each of histones H2A, H2B, H3 and H4 wrapped around the DNA. Their DNA-binding can be mediated by post-translational modifications, such as acetylation and methylation, which mainly occur on the histone N-terminal tail as well as on the globular domain (Atkinson and Keith, 2007). One possible role of these modifications might be to act as a 'histone code' for gene transcription, where combinations of histone modifications can be translated into an output signal, forming a histone pattern specific for DNA access and therefore gene transcription (Strahl and Allis, 2000; Jenuwein and Allis, 2001).

As it is now understood, histone phosphorylation is fundamental for mediating cellular responses to DNA damage, as incurred by various processes such as irradiation (Herskind and Rodemann, 2000), DNA-damaging drugs (Robles and Adami, 1998) and oxidative stress (von Zglinicki et al., 1995) which may all, ultimately, lead to senescence.

1.1.5 Chromatin organization

Generally, the senescent phenotype exhibits a specific gene expression profile. Some cell types show global changes in chromatin structure, leading to the accumulation of senescence-associated heterochromatin foci (SAHF) (Narita et al., 2003; Zhang et al., 2005; Narita et al., 2006). SAHF can provide a protective chromatin barrier against the transcription of growth-promoting genes by mitogenic transcription factors. At the sites of SAHF, which are formed by newly deposited heterochromatin, active transcription does not take place (Atkinson and Keith, 2007). Once initiated, SAHF become self-sustaining, being able to maintain the senescent state without requiring either the presence of DNA damage or cell cycle inhibitors (Bakkenist et al., 2004). This provides a strong correlation

between SAHF and the irreversibility of the senescence state (Beausejour et al., 2003; Narita et al., 2003).

In terms of the molecular pathways, the upregulation of $p16^{INK4a}$ inhibits the phosphorylation and therefore inactivation of retinoblastoma protein (pRB) which can now bind E2F, a transcription factor required for the regulation of genes associated with the transition from G_1- to S-phase in the cell cycle. This binding inactivates E2F, leading to a permanent growth arrest by silencing growth regulatory genes through changing the chromatin state of the promoter sequences (Atkinson and Keith, 2007). With this mechanism, pRB-mediated heterochromatin formation might lead to the stable repression of growth regulatory genes during senescence.

Presumably, pRB binding to regulatory sequences might be sufficient to form SAHF (Nielsen et al., 2001). Mutations in genes encoding pRB, $p16^{INK4a}$ or silencing events could lead to the bypass of senescence and therefore to a progression to cancer (Narita et al., 2003). In general, the formation of SAHF can be understood as to be directed towards certain genes and not as a global effect (Atkinson and Keith, 2007).

Silenced chromatin (heterochromatin) is characterized by a variety of histone modifications, such as hypoacetylation of H3 and H4 (Atkinson and Keith, 2007). Active chromatin (euchromatin), to the contrary, contains hyperacetylated histones. Additionally, DNA hypermethylation is rather associated with silent chromatin whereas DNA hypomethylation is connected to active chromatin. Notably, SAHF are enriched for markers of heterochromatin and exclude euchromatic markers (Fig. 3).

Another essential structural component of SAHF consists of high-mobility group A (HMGA) proteins which seem to contribute to the stable senescence arrest (Narita et al., 2006). It has been shown that the loss of linker histone H1 in senescent cells can be connected to the increased level of HMGA proteins, since H1 competes with HMGA in binding DNA (Funayama et al., 2006). HMGA1 and HMGA2 are senescence-associated chromatin binding proteins, not transcriptional factors, although they seem to have the ability to provide a chromatin environment suitable for transcription (Reeves, 2001).

A

P
RB P
P
P

Open
chromatin
structure

E2F

Gene
expression

B

Oncogenic insult
e.g. aberrant
Ras signalling

Increased p16
expression

HP1
SUV39H1 RB HDAC
E2F

SAHF formation

C

HP1

HP1
SUV39H1 RB HDAC
E2F

Closed
chromatin
structure

Gene
repression

○ H3 and H4 acetylation   ● K4 H3 methylation   ● K9 H3 methylation
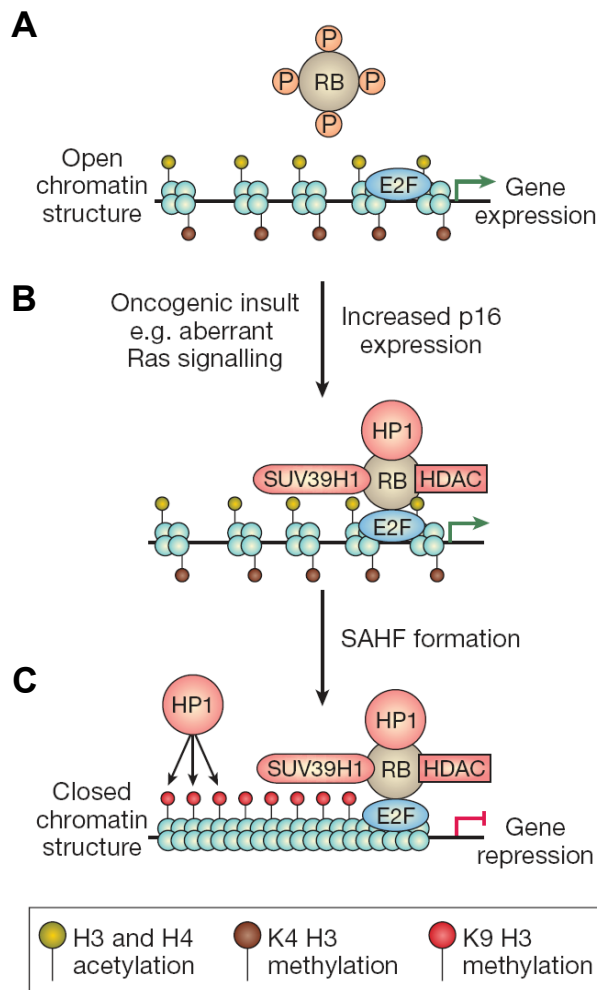
Figure 3. The formation of senescence-associated heterochromatin foci (SAHF) in response to oncogenic result.
Adapted from Atkinson and Keith, 2007.

A. An active gene promoter (e.g. cyclin D1) leads to an open (euchromatic) chromatin structure. Under these conditions, the transcription factor E2F is able to mediate transcription since retinoblastoma protein (pRB) remains inactivated due to its phosphorylated form, as a result of low $p16^{INK4a}$ levels.

B. Oncogenic insult increases $p16^{INK4a}$ levels which activate, i.e. hypophosphorylate pRB. Activated pRB binds to E2F together with several other proteins such as heterochromatin protein 1 (HP1), histone deacetylase (HDAC) and the Lys9 (K9) H3 methyltransferase SUV39H1.

C. The ultimate result is a closed (heterochromatic) chromatin structure which promotes the silencing of gene expression.

Interestingly, HMGA is known to be an oncogene, since its expression is induced by growth factors or serum stimulation (Lanahan et al., 1992). It can be found to a high extent in proliferating cells in the embryo or in tumors (Reeves, 2001). How can we explain its accumulation during senescence? One speculation is that HMGA proteins seem to be both pro- and antioncogenic, depending on the cellular context (Narita, 2007). Another finding claims that knockdown of HMGA1 abolishes SAHF architecture completely, whereas HMGA2 has a lesser impact (Narita, 2007).

SAHF formation appears to be largely dependent on the p16/Rb pathway in Ras-induced senescence, whereas the impact of p53 on SAHF is only marginal (Narita et al., 2003). p16 is an inhibitor of D-type CDKs which prosphorylate the Rb protein family and

consequently release the repression of E2F-target cell cycle genes. p16/Rb has thus major influence on SAHF formation and cell cycle gene silencing. Furthermore, codepletion of p16 and HMGA1 cause a higher incidence of senescence bypass which may indicate a cooperative effect between these two concerning the stability of the cell cycle arrest (Narita, 2007).

Nonetheless, the ambiguous role of HMGA proteins leaves room for speculation. Since HMGA is upregulated in many benign tumors, which are especially prone to oncogene-induced senescence, one could assume that HMGA upregulation happens within an early stage of tumorigenesis with the purpose of activating the senescence program. This process is destined to fail with additional mutations disabling the onset of senescence, such as mutated p53 and p16/Rb, which would then reveal the oncogenic activity of HMGA (Narita, 2007).

1.2 Telomere-dependent senescence or replicative senescence (RS)

Senescence was initially observed in long-term cultures of human diploid fibroblasts, being accompanied by progressive telomere shortening and eventual loss of telomere function (Hayflick, 1965; Rubin, 2002). In 1961, L. Hayflick made the observation that human cells derived from embryonic tissues can only divide 50 times, which became known as the Hayflick limit. This limit is due to the loss of telomeric DNA that happens when cells lacking the enzyme telomerase undergo DNA replication (Wright and Shay, 2001). Without telomerase activity or other telomere lengthening mechanisms, around 50-100 bp of telomeric sequence get lost at each cell division (Harley et al., 1990; Hastie et al., 1990).

The so-called telomere-dependent or replicative senescence (RS), also termed M1 (mortality state 1), occurs when primary cultured cells come to a specific number of divisions that is characteristic for each cell type and species (Barradas et al., 2002).

1.2.1   The human telomerase reverse transcriptase

Typically found in eukaryotes, telomeres are stretches of DNA tandem repeats (TTAGGG in vertebrates), terminating in a 3' single-stranded DNA overhang (d'Adda di Fagagna et

al., 2004). Telomeric DNA forms, together with specialized proteins, protective caps at the ends of chromosomes. These structures prevent the chromosomal ends from being recognized as DNA double-strand breaks (DSBs) which would consequently lead to their degradation or fusion by DNA repair machineries.

With each cell division, telomeres become shorter because DNA polymerases cannot fully replicate the 3' ends, referred to as the 'end-replication problem'. The maintenance of telomeres is done by a specialized RNA-templated polymerase called telomerase (Cech, 2004). The ribonucleoprotein core enzyme consists of a catalytic subunit, the human telomerase reverse transcriptase (hTERT) and a small template RNA component (hTERC). In normal human somatic cells, telomerase activity is suppressed mainly due to transcriptional repression of the hTERT transgene (Bodnar et al., 1998). Telomerase is known to be active in germ line as well as in some progenitor cells of proliferative tissues like hematopoietic stem cells.

Overexpression of hTERT in primary human cells is sufficient to prevent telomere shortening and enables these otherwise normal cells to proliferate indefinitely, a behavior typical of that of cancer cells (Artandi, 2006).

If senescence is bypassed through the inactivation of the p53 and Rb pathways, telomeres continue to shorten with cells dividing beyond their normal senescence point (Shay et al., 1991; Ben-Porath and Weinberg, 2004). These telomeres erode completely, making the cells enter the 'crisis', or M2 (mortality stage 2), a state characterized by massive cell death due to multiple chromosomal fusions and consequent genomic catastrophe. Thus, senescence is induced at a midway point of telomere attrition.

In telomerase-null mice, 'too-short' telomeres combined with p53 mutations lead to genomic instability and an increased risk of malignant transformation (Chin et al., 1999). This could explain the higher incidence of skin cancer with p53 mutations in patients with dyskeratosis congenita who have short telomeres either because of a defect in the integral RNA component of telomerase or in its processing pathway (Vulliamy et al., 2001).

Infrequently, cells during the crisis phase of genomic instability spontaneously activate telomerase, leading to indefinite telomere maintenance (Wong and Collins, 2003). Under selective pressure, a telomerase-independent alternative mechanism for lengthening of telomeres (ALT) can arise in human cells. In cells where ALT is used, telomere attrition

can be prevented by a recombination-based mechanism between telomeres (Dunham et al., 2000), resulting in telomere length heterogeneity (Bryan and Reddel, 1997). The ALT is detectable in some transformed fibroblasts and a small minority of cancers such as osteosarcomas, soft tissue sarcomas and glioblastoma multiforme (Henson et al., 2002; Atkinson and Keith, 2007). Interestingly, in normal mesenchymal tissues telomerase activity is more strictly repressed, which may explain the particular pressure for ALT activation over telomerase activity in these cell types.

Telomerase activity can be detected in about 85% of malignant tumors (Shay and Bacchetti, 1997), a fact that stresses the importance of telomerase in tumorigenesis.

Besides the actual prolongation of telomeres, telomerase, together with the specific telomere-binding proteins - now referred to as the shelterin complex as reviewed in (Verdun and Karlseder, 2007) - has also the function of creating a telomere 'cap', thus preventing the telomeres from being recognized as damaged DNA (Griffith et al., 1999). Telomeres capping the ends of linear chromosomes are essential chromosomal elements, and their loss causes genomic instability which is an enormous risk factor for malignant transformation (Artandi and DePinho, 2000; Shay and Wright, 2001; Kim Sh et al., 2002; Blasco, 2003). The lack of these protective caps leads to inappropriate joining of telomeres producing fused chromosomes, which are highly vulnerable to breakage (Artandi, 2006).

1.2.2 From telomere dysfunction to senescence

What part of telomere dysfunction triggers the senescence response? It seems that not the actual shortening of telomeres, but rather the process of their 'uncapping' may be responsible for the onset of cell cycle arrest (Blackburn, 2000; Blackburn, 2001). The main event to end the replicative life of primary human cells might be a deficiency in the protective function of critically shortened telomeres (Karlseder et al., 2002). Thus the exposed chromosome ends are recognized as damaged DNA, leading to consecutive activation of the senescence program.

The telomeric DNA 'cap' adopts a very unusual and specific structure, the so-called T-loop. In this conformation, the end of the chromosome is folded back and the single-stranded telomeric 3'-overhang invades into a portion of the double-stranded telomeric

DNA (Griffith et al., 1999). Forming a three-stranded structure, it is supposed to prevent telomere ends from being recognized as DNA damage. It remains unclear, whether the T-loop itself, the factors associated with it, or a combination of both, leads to the ultimate triggering of a DNA damage response (DDR) (d'Adda di Fagagna et al., 2004). The impairment of the DNA-binding function of TRF2, the mammalian telomere repeat binding protein which promotes T-loop formation, leads to either p53-dependent cell death or to permanent cell cycle arrest *in vivo,* depending on the cell type (Karlseder et al., 1999; Stansel et al., 2001).

1.3 Premature senescence (PS)

Cell cycle checkpoint activation can lead to growth arrest either by uncapped telomeres or by other DNA-damaging events, for instance induced by bleomycin, hydrogen peroxide, irradiation or inadequate culture conditions. In order to distinguish this growth arrest from the replicative senescent phenotype, terms such as PS (premature senescence), accelerated senescence or M0 (mortality stage 0) are used.

Hyperproliferative signaling and unscheduled DNA synthesis as a response to certain mitogenic oncogenes, such as the Ras/Raf prototypes, can lead to an early senescent growth arrest (Braig and Schmitt, 2006). An intact mitogen-activated protein kinase (MAPK) pathway, the kinase downstream of Ras, is crucial for this process. Constitutively mitogenic stimuli triggered by oncogenic Ras initially cause rapid cell proliferation (Serrano et al., 1997). This leads to the activation of the two tumor suppressor pathways of p53 and p16/Rb, which then eventually override cell proliferation and provoke PS. The bypass of senescence does indeed require the inactivation of both the p53 and the p16/Rb pathways (Serrano et al., 1997).

Oncogene-induced senescence (OIS) acts as an intrinsic anti-tumor response mechanism, allowing the cells to keep their proliferation within a tolerable range, although the mechanisms of how the threshold and the deviation from it are sensed, remain unknown. If oncogenic lesions are combined with mutations that disable the senescence machinery, such as p53, pRb and INK4aARF locus mutations, the outcome is full-blown cancer. Therefore, subsequent provocation of OIS contributes to the restriction from a benign to a

malignant state. Senescent cells can be found in premalignant or benign tissues, such as in BRAF- (a downstream effector of Ras) associated naevi (Michaloglou et al., 2005) or KRAS-associated lung adenomas (Collado et al., 2005), but not in malignant ones.

Many questions remain unanswered, e.g. how benign tumors seem to switch on the senescence pathway in order to avoid their malignant transformation, and whether OIS could probably be a natural process which happens in our bodies all the time. Could the capability to undergo senescence provide an explanation to what makes benign tumors actually benign?

Other speculations concern the question what kind of oncogene-driven cells may turn into manifest malignant tumors - the ones managing to bypass senescence, or the cells which emerge from senescence by having mutated essential senescence regulators.

Other ways of provoking PS can be performed by treating cells with chemotherapeutic agents, such as bleomycin, actinomycin D and cyclophosphamid. In response to these agents cells engage a p53/p16-dependent long-term senescence program (Robles and Adami, 1998; Schmitt et al., 2002). Furthermore, the acetylation of p53 seems to promote the expression of growth suppressive genes and induce cellular senescence (Luo et al., 2004; Furukawa et al., 2007).

1.4 From signal to senescence

Recently, it has been shown that both RS and PS share a common signal, recognized as DNA double strand breaks (DSBs) (Schmitt et al., 2007). These DSBs provoke DNA damage pathways in return. However, not every DNA damage leads to cellular senescence. The actual purpose of cell cycle arrest is to give a cell the opportunity to repair the DNA damage before progressing to the next phase of the cycle (Schmitt et al., 2007). In turn, if severely damaged cells manage to progress through the cell cycle inappropriately, this often ends in mitotic crisis, apoptosis and massive cell death.

In RS, DDR is initiated by telomere erosion and attrition, resulting in DSBs at chromosome ends (d'Adda di Fagagna et al., 2003; Herbig et al., 2004).

Increased intracellular levels of reactive species due to oncogenic activation lead to alterations in DNA replication fork progression and the appearance of DNA single- and double-strand breaks (Bartkova et al., 2006; Di Micco et al., 2006; Takahashi et al., 2006). Cells treated with sublethal concentrations of H_2O_2 (<0.45 mM) are oxidatively stressed and driven into senescence by means which are yet unclear. One suggestion is that oxidative stress triggers the hyperactivation of poly (ADP-ribose) polymerase (PARP), being responsible for subsequent NAD^+ depletion (Furukawa et al., 2007). This leads to a decreased activity of the NAD^+-dependent deacetylase SIRT1, the human homolog of the yeast Sir2 protein, which inactivates p53. Therefore acetylated p53 can accumulate and induce its transcriptional target, p21.

Furthermore, oxidative stress is regarded as one cause of telomere shortening (von Zglinicki, 2002). In multicellular organisms, an inability to repair DNA damage and/or prolonged checkpoint activation can end either in apoptosis (Rich et al., 2000) or in a permanent cell cycle arrest (Schmitt, 2003). In mammalian cells, the task to respond to DSBs belongs to the ataxia teleangiectasia mutated kinase (ATM), in which absence these functions can be overtaken by the ataxia teleangiectasia and Rad3 related kinase (ATR) (Shiloh, 2003). ATR is particularly important for the response to DNA damage during S-phase (Zou and Elledge, 2003). In humans, these two enzymes belong to the checkpoint phosphatidyl inositol 3-kinase-like kinase (PIKK) family (d'Adda di Fagagna et al., 2004). Once activated, the checkpoint PIKK proteins phosphorylate a range of factors, including the distal checkpoint serin/threonine kinases CHK1 and CHK2, which target various effector proteins involved in modulating DNA repair, transcription and cell-cycle progression (Bartek and Lukas, 2003). One such target is the C terminus of the histone H2A variant H2AX, which is phosphorylated at DNA damage sites (Fernandez-Capetillo et al., 2004). γ-H2AX, the resulting phosphorylated species of H2AX, is engaged in the DDR by inducing changes in local chromatin structure (SAHF) and by the accumulation of DNA repair and checkpoint proteins to the damaged regions. Another target of ATM/ATR and CHK1/CHK2 kinases is p53, which is phosphorylated and stabilized, leading to accumulation of the CDKI p21. p21 is responsible for a more sustained G_1/S cell cycle arrest as reviewed in (Schmitt et al., 2007; Shiloh, 2001).

The signaling pathways in telomere dysfunctional cancer cells are yet far away from being fully understood. There seem to be at least two different pathways which lead to senescence growth arrest: one is activated by upregulation of p53, the other induces p16 overexpression and activates pRB (Campisi, 2005b). Dysfunctional telomeres are supposed to trigger the first pathway via p53 upregulation whereas overexpression of oncogenes and suboptimal culture conditions are meant to activate the p16/pRB pathway (Fig. 4).

1.5 Senescence and cancer

The cause of both replicative as well as telomere-independent senescence boils down to a DDR, which is crucial for the induction of senescence (d'Adda di Fagagna et al., 2003; Herbig et al., 2004). SA-ß-gal positive cells can be found in tumors after being treated with DNA-damaging chemotherapeutical agents, as described in human breast cancer and in a lymphoma mouse model (Schmitt et al., 2002; te Poele et al., 2002).

The induction of PS in tumor cells may provide an attractive therapeutic target for anti-cancer therapy in the future (Roninson, 2003; Shay and Roninson, 2004). One interesting aspect hereby considers the senescence-associated changes in chromatin. Thus, a therapeutic option to induce PS could be through control of enzymes that catalyze epigenetic modifications (Atkinson and Keith, 2007), leading to a targeted up- or downregulation of senescence-associated genes.

Although senescence is supposed to be a powerful anticancer mechanism, accumulation of senescent cells is associated with dysfunctions that can contribute to age-related diseases, such as cancer, paradoxically.

Senescence as a hypermitogenic arrest, i.e. the combination of cell cycle arrest and hypertrophy due to strong mitogenic signaling, already bears an ambiguity. Cell cycle arrest prevents cancer, whereas growth stimulation is already a step towards cancer (Blagosklonny, 2006). In order to become cancerous, a cell would only need to overcome the cell cycle arrest (Green and Evan, 2002; Lowe et al., 2004; Campisi, 2005c).

The senescence response is therefore characterized as being 'antagonistically pleiotropic' (Campisi, 2005b; Campisi, 2005a). This definition implies that cancer suppressive features

of senescence are beneficial in young organisms, whereas due to the accumulation of secretorily active senescent cells in old organisms, they may eventually provide a pro-tumorigenic environment.
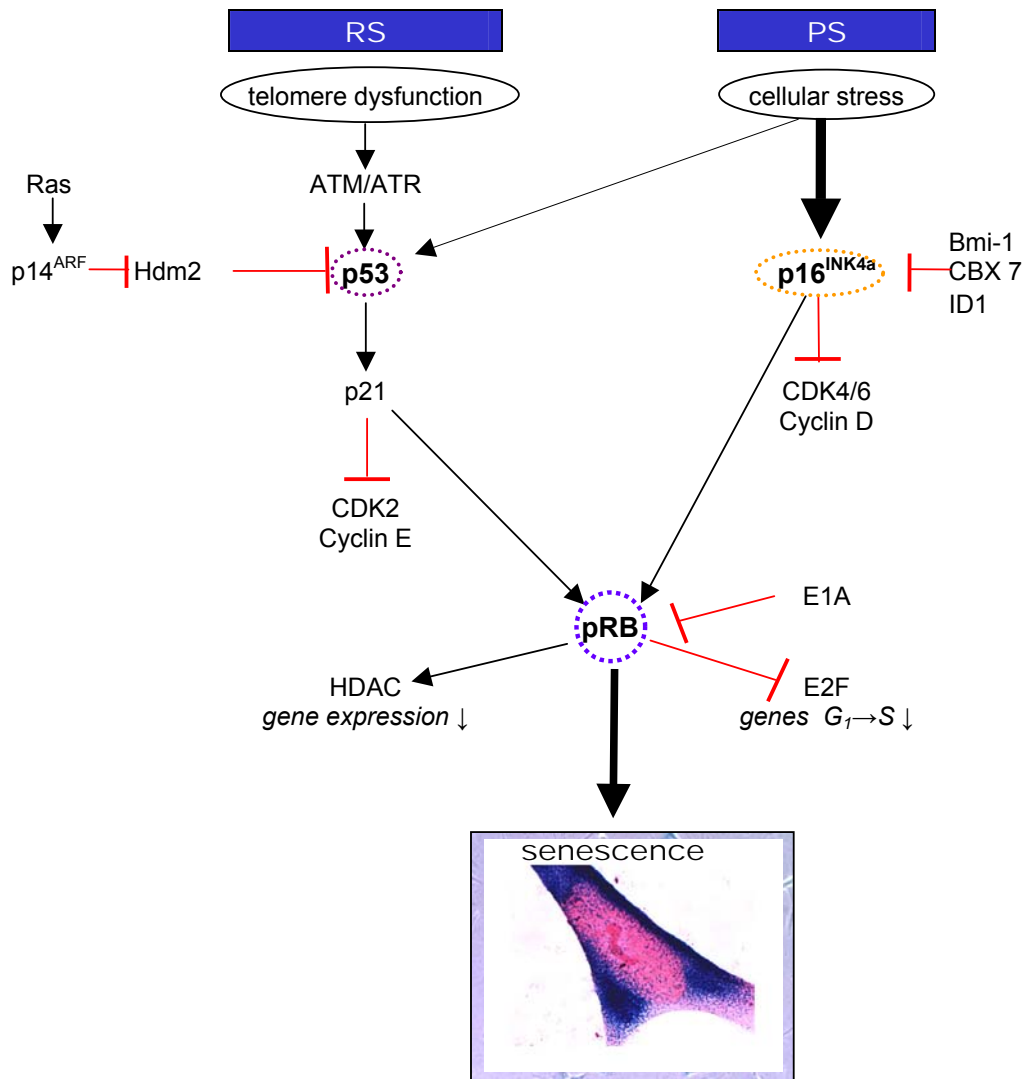
Figure 4. Molecular pathways of replicative senescence (RS) and premature senescence (PS).

RS and PS share one common signaling pathway: p53. On the other hand, most cellular stresses activate the p16^{INK4a} pathway which ultimately leads to the activation of pRB.

ATM: ataxia teleangiectasia mutated kinase; ATR: Ataxia teleangiectasia and Rad3 related kinase; p16^{INK4a}: cyclin-dependent kinase inhibitor 4A; p14^{ARF}: alternative reading frame product of *INK4a* gene locus; HDAC: histone deacetylases; Hdm2: Human-double minute-2; BMI-1: polycomb ring finger oncogene; CBX 7: chromobox homolog 7; ID 1: DNA-binding protein inhibitor 1; E2F: transcription factor; E1A: adenoviral protein

The incidence of cancer is age-dependent due to the fact that it requires the accumulation of multiple mutations (Bishop, 1995; Simpson and Camargo, 1998; Gray and Collins, 2000; Knudson, 2000), which, of course, takes time. However, there is increasing evidence that accumulated mutations are not the single reason for this phenomenon (Campisi, 2005a). Many cells with oncogenic mutations need a permissive tissue microenvironment in order to become malignant. Interestingly, the formation of epithelial tumors, the major type of age-related cancer, largely depends on the interactions between the epithelium and the underlying stroma (DePinho, 2000; Coussens and Werb, 2002). Furthermore, senescent stromal fibroblasts seem to be able to stimulate the proliferation of premalignant cells, converting them to malignant tumors *in vivo* (Krtolica et al., 2001).

The role of senescence in the process of tumorigenesis thus remains a controversial issue. Since senescent cells do not proliferate, it has been proposed that cellular senescence may act as a fundamental barrier to cancerous transformation (Campisi, 2001; Mathon and Lloyd, 2001), thereby being a self-defense mechanism to prevent the proliferation of potentially damaged cells.

Almost any type of cellular stress activates p53 which unleashes a complex transcriptional program ultimately resulting in the elimination from the proliferative pool by either apoptosis or senescence (Serrano, 2007). Strikingly, senescence is being recognized as a primary mechanism of tumor regression. Cancer regression can therefore be explained with a mechanism other than cell death and telomere-induced senescence can now be seen as effective as apoptosis in reducing cancer incidence (Sedivy, 2007).

1.6 Senescence and aging

Does senescence accelerate the process of aging? Indeed, it has been shown that fibroblasts from patients with premature aging syndromes such as Werner's disease develop SA-ß-gal activity earlier than those from young or healthy individuals (Narita, 2007). In addition, dyskeratosis congenita and aplastic anemia are linked to mutations in

telomerase or in proteins which affect telomerase activity, thus leading to a faster rate of telomere shortening with age (Mason and Bessler, 2004).

Senescence might contribute to aging by two simultaneous mechanisms: firstly by the accumulation of senescent cells in tissues, secondly by limiting the regenerative potential of stem cells (Collado et al., 2007). Recently, it has been discovered that p16 expression increases age-dependently and therefore contributes to aging in bone marrow, brain and pancreatic islets (Janzen et al., 2006; Krishnamurthy et al., 2006; Molofsky et al., 2006).

Nevertheless, a direct causative effect of cellular senescence on aging has yet not been shown.

1.7 Proteomic approaches

An promising way to elucidate the signaling pathways involved in establishing the senescent state is analyzing the specifically expressed proteins.

Comparing RS and PS at protein level in cultured cells gives hint to the fact that these two stages are different phenotypes, however sharing similarities (Dierick et al., 2002). Although premature senescent fibroblasts morphologically resemble their replicative counterparts, they exhibit different protein expression patterns (Cong et al., 2006). These differences specific to PS are defined as 'molecular scars' of subcytotoxic stress. It is of great interest to identify some of the proteins behind these scars to understand the pathophysiological consequences of the senescent cell cycle arrest.

In search of new biomarkers of senescence, techniques such as high resolution two-dimensional gel electrophoresis, matrix-assisted laser desorption/ionization mass spectrometry (MALDI-MS) and isobaric tagging for relative and absolute quantitation (iTRAQ) have been used (Dierick et al., 2002; Benvenuti et al., 2002; Cong et al., 2006). Nonetheless, a proteomic pattern specific for senescence has yet not been described.

1.8 Aim of the work

Our goal was to establish a protein signature for cellular senescence and to discover potentially existing similarities between RS and PS. What proteins characterize these two cell cycle stages, what are common features and where to find the differences? Is there a general senescence program similarly affecting all cell types?

Two cell lines were used, A549 non small cell lung cancer (NSCLC) cells, and the human diploid fibroblast cell line HK1. Cells were driven into PS by exposure to H_2O_2, bleomycin and irradiation, whereas RS was reached through ongoing cell culturing. Senescence was then detected by SA-ß-gal staining.

In the immortalized A549 NSCLC cells, suppression of telomerase was achieved by inserting a plasmid vector with a gene encoding for a dominant negative hTERT catalytic subunit. These cells were single cell cloned in a FACS-sorter according to their level of GFP expression.

For quantitative proteomic research, we analyzed the cell lysates using the novel technology of Surface-Enhanced Laser Desorption/Ionization Time-Of-Flight Mass Spectrometry (SELDI-TOF MS).

2. MATERIAL AND METHODS

2.1 Material

2.1.1 Chemicals

Chemicals were purchased from Baker (Deventer, Netherlands), Bio Whittaker (Verviers, Belgium), Invitrogen (Karlsruhe), Merck (Darmstadt) and Sigma-Aldrich (Steinheim).

2.1.2 Enzymes

Enzymes were purchased from NEB (Frankfurt) and Invitrogen (Karlsruhe).

2.1.3 Disposables

Cryo tubes	Corning (New York, NY, USA)
Gloves	Ansell (München)
Filter 0.45 µm	Millipore (Bedford, MA, USA)
Chamber Slides	Nalgene Nunc (Wiesbaden)
Cover slips	R. Langenbrinck (Emmendingen)
Combitips 0.1, 5, 10 ml	Eppendorf (Hamburg)
Cannulae 18 – 26 G	Braun (Melsungen)
Cuvettes Half-Micro	Greiner (Frickenhausen)
Slides	R. Langenbrinck (Emmendingen)
Hygromycin B in PBS 50 mg/ml	Invitrogen (Karlsruhe)
Parafilm 'M'	American National Can (Chicago, IL, USA)
PCR-tubes 200 µl	Applied Biosystems (Foster City, USA)
Pipette tips 5, 10, 25, 50 µl	Corning (New York, NY, USA)
Pipette tips ART 10, 20, 200, 1000 µl	Molecular Bioproducts (San Diego, CA, USA)
Pipette tips Multi-Guard	Sorenson (West Salt Lake City, UT, USA)

10, 30, 200, 1000 µl

Falcon tubes   Falcon BD (Le Pont de Claix, France)

5, 15, 50 ml

Falcon tubes 5 ml   Falcon BD (Le Pont de Claix, France)

Syringes 1, 2, 5, 10, 20 ml   Braun (Melsungen)

Sterile filters   Millipore (Bedford, MA, USA)

Sterile filter bottles   Nalgene Nunc (Wiesbaden)

Cell culture flask   Falcon BD (Le Pont de Claix, France)

25, 75, 175 cm^2

Cell culture dish   Falcon BD (Le Pont de Claix, France)

96, 48, 12, 6-well

Petri dish 35 mm   Nalgene Nunc (Wiesbaden)

Cell filter 40, 100µm   Falcon BD (Le Pont de Claix, France)

2.1.4 Buffers and Solutions

The buffers and solutions were produced with deionised water, or directly used
from the quoted companies. Cell culture solutions were sterile filtered with 0.22
µm filters.

Aqua ad iniectabilia   Delta-Pharma (Pfullingen)

10 % BSA   Invitrogen (Karlsruhe)

2.5 M CaCl$_2$ Invitrogen (Karlsruhe)

25 mM Chloroquin (2 000 x)   Invitrogen (Karlsruhe)

Bleomycin (3 mg/ml)   Central   cytostatic   drug   preparation,   Pharmacy
University Hospital Freiburg

DMEM Medium

87 % Dulbecco's MEM   Invitrogen (Karlsruhe)

10 % Fetal Bovine/Calf Serum (FCS)

1 % Penicillin/Streptomycin

1 % L-Glutamine (200 mM)

        1 % Sodium-Pyruvate (100 mM)

DMEM Medium + 0.1 % FCS

        97 % Dulbecco's MEM   Invitrogen (Karlsruhe)

        0.1 % Fetal Bovine/Calf Serum (FCS)

        1 % Penicillin/Streptomycin

        1 % L-Glutamine (200 mM)

        1 % Sodium-Pyruvate (100 mM)

RPMI Medium

        87 % RPMI   Invitrogen (Karlsruhe)

        10 % Fetal Bovine/Calf Serum (FCS)

        1 % Penicillin/Streptomycin

        1 % L-Glutamine (200 mM)

        1 % Sodium-Pyruvate (100 mM)

RPMI Medium + 0.1 % FCS

        97 % RPMI   Invitrogen (Karlsruhe)

        0.1 % Fetal Bovine/Calf Serum (FCS)

        1 % Penicillin/Streptomycin

        1 % L-Glutamine (200 mM)

        1 % Sodium-Pyruvate (100 mM)

Freeze medium (standard):

        70 % cell-type-specific medium (RPMI, DMEM etc.)

        20 % FCS

        10 % DMSO

Freeze medium (phoenix ampho cells):

        90 % FCS

        10 % DMSO

PBS Dulbecco's   Invitrogen (Karlsruhe)

PBS + 0.1, 2, 3 % BSA   Invitrogen (Karlsruhe)

Polybrene   Sigma-Aldrich (Steinheim)

RNAse, DNAse-free (0.5 µg/µl) Roche (Mannheim)

20 x SSC   3 M NaCl, 0.3 M Sodiumcitrat, pH 7.0

10 x TBE Buffer	Invitrogen (Karlsruhe)
TE	10 mM Tris-HCl, pH 7.5, 1 mM EDTA
1 x Trypsin-EDTA	Invitrogen (Karlsruhe)

2.1.5 Equipment

Centrifuge	Cytospin 3 SHANDON, Pennsylvania, USA
Centrifuge	Heraeus SEPATECH
ELISA Reader	Molecular devices, USA
FACS Machine	FACS Scan, Becton Dickonson, Heidelberg
Light Microscope	Leica, Bensheim
Fluorescence Microscope	ZEISS Axiophot II, Oberkochen
Photometer (Ultraspec 3100pro)	Biochrom, Cambridge, England
PCR Machine	Gene-Amp System 9700, AppliedBiosystems, USA

2.1.6 Computing

The following programs were used:

Microsoft Office 2000 Professional (WinWord, Excel und PowerPoint) and Adobe Photoshop 9.0 CS.

2.2 Methods

2.2.1 Cell culture

All procedures with eukaryotic cells took place under sterile conditions. Cells were cultured in incubators (BBD 6220; Heraeus, Stuttgart) at 37°C and 5 % CO_2. To count the cells Neubauer slides were used and dead cells were excluded with a trypan blue staining (Invitrogen, Karlsruhe). The cell concentration was measured as follows:

$$\text{cell count / ml} = \frac{\text{cell count}_{\text{4 big squares}}}{4} \times \text{dilution factor} \times 10\ 000$$

To determine the growth of synchronic dividing cells doubling rates were calculated using the cumulative population doubling level (CPDL) as follows:

$$PD = \frac{\log \text{cell count}_{\text{Output}} - \log \text{cell count}_{\text{Input}}}{\log 2} \qquad CPDL = \sum PD$$

The cell culture requirements of the different cell types are specified in the respective chapters. For storage, cells were frozen at -80°C in the appropriate medium. For permanent storage, the cells were transferred into liquid nitrogen. In order to thaw the cells they were first placed into the water bath at 37°C and then immediately transferred into a 15 ml Falcon tube with PBS + 0.1 % BSA or fresh culture medium. The mixture was centrifuged for 5 min at 300 x g, the supernatant removed, the cells washed twice with PBS, then counted and used for further processing.

2.2.2 Cell lines

2.2.2.1 A549
A human non small cell lung cancer cell line of type II-like alveolar epithelial cells, obtained from ATCC, Wesel, Germany.

2.2.2.2 HK1
A human preputial diploid fibroblast cell line generously provided by H. Veelken (University Hospital Freiburg). In addition to telomerase negative wild type cells, immortalized HK1 cells were used expressing ectopic hTERT (Zimmermann et al., 2004) whilst containing either one of the following retroviral vectors: pOS-hTERT-IRES-GFP or pBABE-hTERT-IRES-GFP.

2.2.3 Analytical Flow Cytometry

Flow cytometry is a method for the simultaneous analysis of single cells in suspension on basis of their fluorescence and light scattering properties. The cells are hereby led by a fluid stream into a measuring chamber where they are excited by a laser beam of a wave length of 488 nm. When the cells pass through the laser beam they disperse and scatter light. The emitted light is simultaneously detected by different gates. Forward light scatter (FSC) is a dimension for cell size, whereas side scatter (SSC) is mainly influenced by intracellular granularity. Gates of different emission spectra allow the measurement of fluorochromes such as green fluorescent protein (GFP), which was transferred to the cells as a reporter gene with a retroviral vector.

　　　FL1: 530 nm (maximum emission):　　　GFP

For determination of the GFP positivity 2×10^5 cells were washed with PBS, resuspended in 150 µl of PBS including 1 % Formalin and analyzed using a FACScan Cytometer (Becton Dickinson).

2.2.4 Fluorescence activated cell separation (FACS-sorter)

In addition, the FACS-sorter recognizes the above mentioned cell properties and contemporarily sorts the cells according to their appropriate attributes.

A549 cells were transduced with a retroviral GFP associated vector and grown in a T-75 (25 cm²) cell culture flask to receive a bulk of cells. From this bulk, single cell clones were gained by sorting according to their intensity of GFP expression in the *Core Facility I* of the Internal Medicine I department (University Hospital Freiburg). 10^6 cells were washed with PBS, diluted in 1 ml PBS + 0.1 % BSA and filtered through a 40 µm filter into a 5 ml Falcon tube. With help of Dr. M. Follo and K. Geiger single cells were sorted into a 96-well plate with RPMI medium using a *MoFlo high speed cell sorter* (Cytomation, Fort Collins, CO, USA). The first single cell clones were visible about two weeks later and transferred into 6-well plates. The day of beginning of transfection was designated as day 0.

2.2.5 Retroviral gene transfer

Retroviruses are RNA-viruses, since their genome is reversely transcribed from RNA to DNA and then stably integrated into the host cell after having infected a cell. This intermediate state is called provirus. There are certain criteria for recombinant retroviruses: on the one hand they should infect the cells very efficiently but only once whereas on the other hand they are not supposed to replicate in the host cell. The method used here is based on two components: a retroviral vector and the packaging cell line. The retroviral vector is a plasmid containing the packaging signal ψ and the retroviral 5'- and 3'-LTR which flank the gene of interest. In contrast, the packaging cell line carries the so-called helper genome encoding for retroviral structure proteins (gag, pol, env) whilst being deprived by a deleted packaging signal from the ability to pack viral RNA into virions in order to produce competent retroviruses.

Work with retroviruses and retroviral transduced cells were conducted only in security level L2 laboratories under defined safety conditions.

2.2.5.1 Packaging cell line

As a packaging cell line, phoenix ampho cells were used, based on the 293T cell line kindly provided by G. Nolan (Stanford University, Stanford, CA, USA). Phoenix ampho cells were cultured in DMEM medium and split by 70 – 80 % of confluence without Trypsin. Cells were cultured for six weeks and then one selection passaged for one week in 300 µg/ml Hygromycin (Sigma-Aldrich, Steinheim) or 1 µg/ml Diphtheria Toxin (Calbiochem, Merck, Darmstadt) to prove the successful integration of gag, pol and env genes.

2.2.5.2 Retroviral vectors

The used retroviral hybrid vector pOS was friendly provided by U. Klingmüller (Max Planck Institute for Immmunobiology, Freiburg). The cDNA of a dominant-negative (DN) hTERT mutant, generously provided by Robert Weinberg (MIT, Cambridge, MA, USA), was inserted into a pOS vector harboring an IRES GFP or a puromycin resistance gene (*SV40 puro*). There are five point mutations accounting for two changed amino acids in

the DNhTERT cDNA, leading to a complete telomerase inhibition *in vitro* (Hahn et al., 1999):

```
                          V  -  D  -  V
        WT    5' GTG GAT GTG 3'            2131-2139
        DN    5' GTC GCG ATC 3'            2131-2139
                          V  -  A  -  I
```

1. pOS-IRES-GFP (5731 bp)

2. pOS-hTERT-IRES-GFP (9143 bp)

3. pOS-DNhTERT-IRES-GFP (9143 bp)
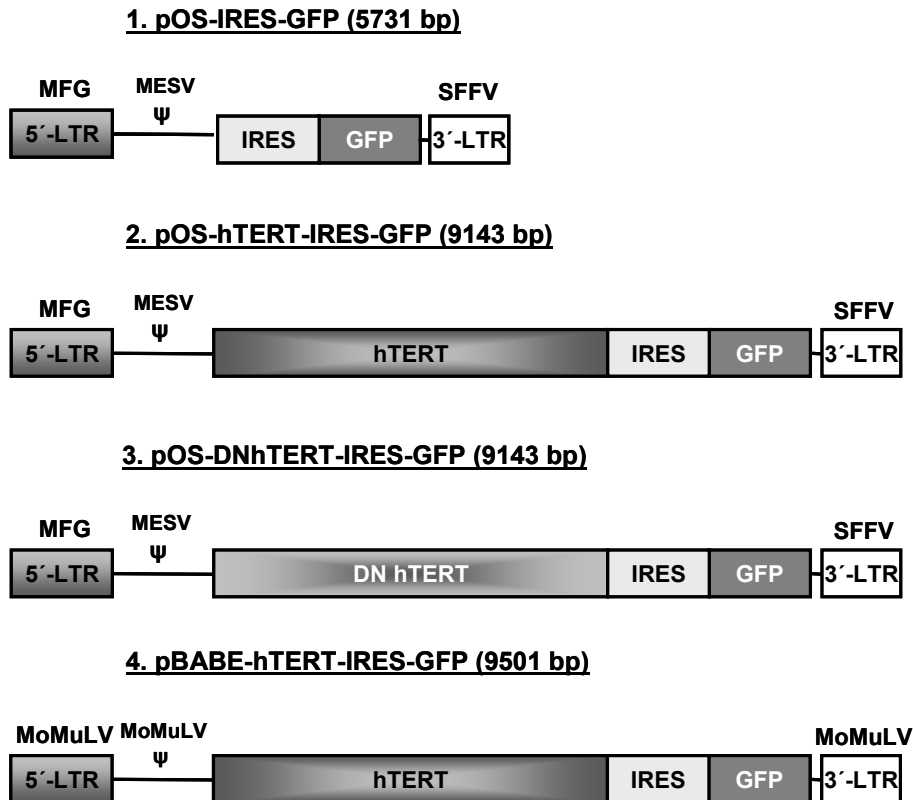

4. pBABE-hTERT-IRES-GFP (9501 bp)

Figure 5. Retroviral vectors.

Vectors 1, 2, 4 were used with HK1 cells, vectors 1, 2, 3 with A549 cells.

DN: dominant negative; GFP: Green Fluorescent Protein; IRES: Internal Ribosomal Entry Site; LTR: Long Terminal Repeats; MESV: Murine Embryonic Stem Cell Virus; MoMuLV: Moloney Murine Leukemia Virus; SFFV: Spleen Focus Forming Virus

2.2.5.3 Production of replicative incompetent retroviruses

Infectious particles were obtained with transient calcium-phosphate-transfection of the retroviral vectors in Phoenix ampho cells after a modified protocol (Pear et al., 1993).

8×10^5 Phoenix ampho cells were plated 20 h before transfection with RPMI medium into a 6-well plate. Directly before transfection the medium was replaced with RPMI medium + 12 µM chloroquin (Sigma-Aldrich, Steinheim) in order to inhibit lysosomal DNases by neutralizing the pH of the vesicles.

10 µl plasmid DNA (1 µg/µl) per transfection was diluted with H_2O, supplemented with 12.5 µl 2.5 M $CaCl_2$-solution and filled up with 125 µl HBS (pH 7.05). 250 µl of this transfection solution was distributed equally on top of the Phoenix ampho cells. After 10 h the medium was replaced by RPMI medium without chloroquin. Retroviral supernatants with high titers could be harvested within a time range of 36 – 72 h after transfection.

For the infections of the cells, only fresh retroviral supernatant was taken.

2.2.5.4 Retroviral infection of human non small cell lung cancer cells (A549)

Three days before the first retroviral infection, 4×10^4 NSCLC cells (A549) were plated into 6-well plates with RPMI medium. For the first infection, cells were treated with fresh retroviral supernatant + 3 µl Polybrene (8 mg/ml). Eight hours later, a second infection was performed. All in all, infections were repeated four times within 72 hours. Transduction efficiency was determined seven days later by flow cytometric assessment of the GFP expression and single cell cloning with the MoFlo high-speed cell sorter (Cytomation, Freiburg).

2.2.6 TRAP (Telomeric Repeat Amplification Protocol) Assay

Telomerase activity of the A549 NSCLC cells was determined by using the *TeloTAGGG* PCR ELISA[PLUS] kit (Roche, Mannheim) according to the manufacturer's protocol. Telomerase from the samples adds telomeric repeats (TTAGG) to the 3'-end of biotinylated primers. These elongation products get amplified by PCR. Then the PCR products (amplicons) are denaturized and hybridized to digoxigenin-labeled telomeric

probes. When antibodies conjugated to horseradish peroxidase are added to the approach, these amplicons can be detected by using the peroxidase sensitive substrate TMB (3,3- 5,5- tetramethylbemzidine) which leads to a visible color development.

2.2.6.1 Extract preparation

2×10^5 cells per reaction were transferred into fresh Eppendorf tubes. Cells were pelleted at 3000 x g for 10 minutes at 2 - 8°C, the supernatant carefully removed and the cells resuspended in PBS. After having repeated the centrifugation step, the supernatant was removed and the pelleted cells stored at –80°C until use. For preparation of the cell extracts, the cell pellets were resuspended in 200 µl of pre-cooled lysis reagent (solution 1), mixed and incubated on ice for 30 minutes. The lysate was then centrifuged at 16000 x g for 20 minutes at 2 - 8°C and the protein supernatant transferred into a fresh tube.

2.2.6.2 Elongation/Amplification

All steps were performed on ice. For each sample, 25 µl of the reaction mixture (solution 2) was transferred into a PCR tube. 1 - 3 µl cell extract (corresponding to 0.5 µg of total protein per sample) was filled up with dd H_2O to a final volume of 50 µl for each tube. As negative controls, 2 µl of RNase treated cell extract (5 µl extract incubated in 5 µl RNAse for 30 min at 37°C) and 23 µl dd H_2O per sample was added. For positive control, corresponding to a cell line with 100 % telomerase activity, cell extracts from Phoenix ampho cells were used. In a thermal cycler, combined primer elongation/amplification was performed as shown in Table 1.

2.2.6.3 Hybridization and photometric detection

For each sample, 20 µl of denaturizing reagent and 5 µl of the amplification product were incubated for 10 min at 15 - 25°C. 225 µl hybridization buffer was added to each tube and thoroughly mixed by vortexing briefly. 100 µl of this hybridization mix (Hybmix) were transferred to a Streptavidine coated microtiter plate (MTP), covered with foil and incubated for 2 h in a shaker (200 rpm) at 37°C. After 2 h the hybmix was removed and the PCR products, now fixed at the bottom of the MTP, were washed 3 times with 250 µl washing buffer. 100 µl of Anti-DIG-POD (peroxidase) were added per well, then the MTP

was covered with foil and incubated for 30 min on the shaker (300 rpm) at 15 - 25°C. After having removed the solution completely, each well was washed five times with 250 μl of washing buffer.

Finally, 100 μl of TMB substrate solution was added per well. The wells were covered with foil and incubated for color development at 15 - 25°C for 10 - 20 min on the shaker (300 rpm). Finally, without removing the reacted substrate, 100 μl stop reagent was added to each well in order to stop the color development. Using an ELISA reader (Molecular Devices), the absorbance of the samples was measured at 450 nm (with a reference wavelength of approx. 690 nm) within 30 min after having added the stop reagent. Additionally, an internal standard was used for each sample to exclude inhibitors of the Taq DNA polymerase.

Table 1. TRAP reaction.

	Time	Temperature	Cycles
Primer elongation	10-30 min	25°C	1
Telomerase inactivation	5 min	94°C	1
Amplification: Denaturation	30s	94°C	
Annealing	30s	50°C	1-30
Polymerization	90s	72°C	
	10 min	72°C	1
Hold		4°C	

2.2.6.4 Interpretation of the results

The ELISA signal of the sample was put in relation to the signal obtained by a control template with a known number of telomeric repeats. The so-called 'relative telomerase activity' (RTA) values were calculated according to the following formula:

$$RTA = \frac{(A_{bsorbance\ of\ sample} - A_{bsorbance\ of\ RNAse\ treated\ samples}) / A_{bsorbance\ of\ internal\ standard\ of\ the\ samples}}{(A_{bsorbance\ of\ control\ templates} - A_{bsorbance\ of\ lysis\ buffers}) / A_{bsorbance\ of\ internal\ standard\ of\ the\ control\ template}} \times 100$$

These values were translated in percentage of telomerase activity of the Phoenix ampho cells carried along with the test. Telomerase activity was considered as positive, if the

difference in absorbance ($A_{bsorbance\ of\ sample}$ - $A_{bsorbance\ of\ RNAse\ treated\ samples}$) was higher than the double amount of the background activity ($A_{bsorbance\ of\ RNAse\ treated\ samples}$).

2.2.7 Senescence Assay

Senescent cells are characterized by different features: a flat, enlarged morphology, short telomeres and growth arrest in culture. The pH-dependent expression of a certain type of beta-galactosidase, the so-called SA-ß-gal (senescence-associated beta-galactosidase), is the basic marker for senescence and can be detected histochemically with the Senescence Detection Kit (MBL, Woburn, MA, USA). SA-ß-gal activity is derived from the increased lysosomal content of senescent cells, which enables its detection at pH 6 (Collado and Serrano, 2006).

In cultured cells, SA-ß-gal activity is assayed using the chromogenic substrate of SA-ß-gal, X-gal, which exhibits a blue precipitate at the site where it is split. SA-ß-gal at pH 6 is only present in senescent cells and can not be found in pre-senescent, quiescent or immortal cells. The procedures were done according to the manufacturer's protocol.

1-3 x 10^3 cells were plated into chamber slides (Nalge Nunc, Wiesbaden) and left to grow for 2 - 3 days in the appropriate culture medium. Then the medium was removed and the cells washed once with 1 ml PBS. The cells were fixed with 0.5 ml of the Fixative Solution whilst freshly preparing the Staining Solution Mix. Calculated for each well, 470 µl of Staining Solution, 5 µl of Staining Supplement and 25 µl of 20 mg/ml X-gal in DMF (Dimethylformamide) were mixed in a Falcon tube. After the cells were washed again twice with PBS, 0.5 ml of the prepared Staining Solution Mix was added to each well. The cells were then incubated in a humidity chamber at 37°C for 12 - 16 h. As negative controls, either non-treated cells or not replicative senescent cells were used. Finally, the slides were washed with PBS and counterstained with Nuclear Fast Red for 5 min. Every cell with a blue cytoplasmatic or perinuclear staining was marked as positive.

2.2.8 Inducing Premature Senescence (PS)

PS in the A549 cells was induced by H_2O_2, bleomycin and irradiation. Within the HK1 cells, H_2O_2 and bleomycin were used.

2.2.8.1 H_2O_2

Early passage A549 and HK1 wild type cells were incubated in T-75 cell culture flasks with RPMI or DMEM medium, respectively, containing two different concentrations of H_2O_2.

For A549:   For HK1:

   - 240 µM   - 150 µM

   - 280 µM   - 180 µM

The cells were cultured with the specific H_2O_2 concentration for two hours, then rinsed thrice and let to recover for three days in fresh medium. Cultured cells were then harvested and pellets analyzed.

2.2.8.2 Bleomycin

Early passage A549 and HK1 wild type cells were treated with two different concentrations of bleomycin.

For A549:   For HK1:

   - 100 µg   - 15 µg

   - 150 µg   - 100 µg

The reagent was added to the RPMI or DMEM medium, respectively, wherein the cells were incubated for three days. Cells were then rinsed thrice with PBS and were left to recover for another three days in fresh RPMI medium. After harvest of the A549 cells, pellets were analyzed.

2.2.8.3 Irradiation

Early passage A549 cells were irradiated with two different intensities with help of Prof. Niedermann (Institute for Radiotherapy, University Hospital Freiburg):

   - 6 Gy (Gray)

   - 8 Gy

The cells were left to recover for seven days. Afterwards, cells were harvested and pellets analyzed.

2.2.9 Proteomic profiling with SELDI-TOF MS

2.2.9.1 Discovering biomarkers on the protein level

Biomarkers are biological compounds, such as proteins, which are either up- or downregulated in response to a particular physiological or pathological state. During the initial discovery phase, protein profiles for control and experimental groups are compared in an attempt to reveal statistically significant differences in protein expression.

Cell lysates from A549 and HK1 were analyzed and specific proteins identified as being either up- or downregulated during the process of senescence.

2.2.9.2 SELDI-TOF MS

SELDI-TOF MS (Surface-Enhanced Laser Desorption/Ionization Time-Of-Flight Mass Spectrometry) is a versatile new technology which can be applied for protein discovery as well as screening, diagnosis, prognosis and therapeutic considerations of cancer from several organ systems. Initially developed for the analysis of blood serum samples, SELDI-TOF soon proved to be also suitable for analyzing cell lysates.

The principles of the ProteinChip Array System (Ciphergen Biosystems, Fremont, CA, USA) are as follows:

Proteins from biological samples are diluted in the specific binding buffer for each chromatographic array and applied directly to the ProteinChip array where they are selectively retained on chromatographic surfaces on 8-spot chips. Using either CM10 (weak cationic exchange) or Q10 (weak anion exchange) binding buffers, with each wash the active spot surfaces experience a greater stringency, removing analytes with weak surface interaction potential and enriching for those of strong surface affinity.

After purification upon the SELDI surface, the analyte is detected by the use of a ProteinChip Reader PBS II (Ciphergen Biosystems). Desorption energy is provided by a

pulsed UV-laser. Upon laser activation, the sample becomes irradiated and desorption/ ionization liberates ions which are accelerated and ultimately strike a detector. Signal processing is promoted by a converter linked to a personal computer running the specific ProteinChip software. The detected analyte is displayed as a peak whose amplitude or area is proportional to the abundance. Time-of-flight (TOF) is related to the ion analyte mass-to-charge ratio (*m/z*). The generated mass spectral pattern for each sample consists of peaks whose mass-to-charge ratios, displayed in Dalton, are depicted on the x-axis, while the height of the peak (relative abundance or intensity) is disposed along the y-axis (Fig. 6).
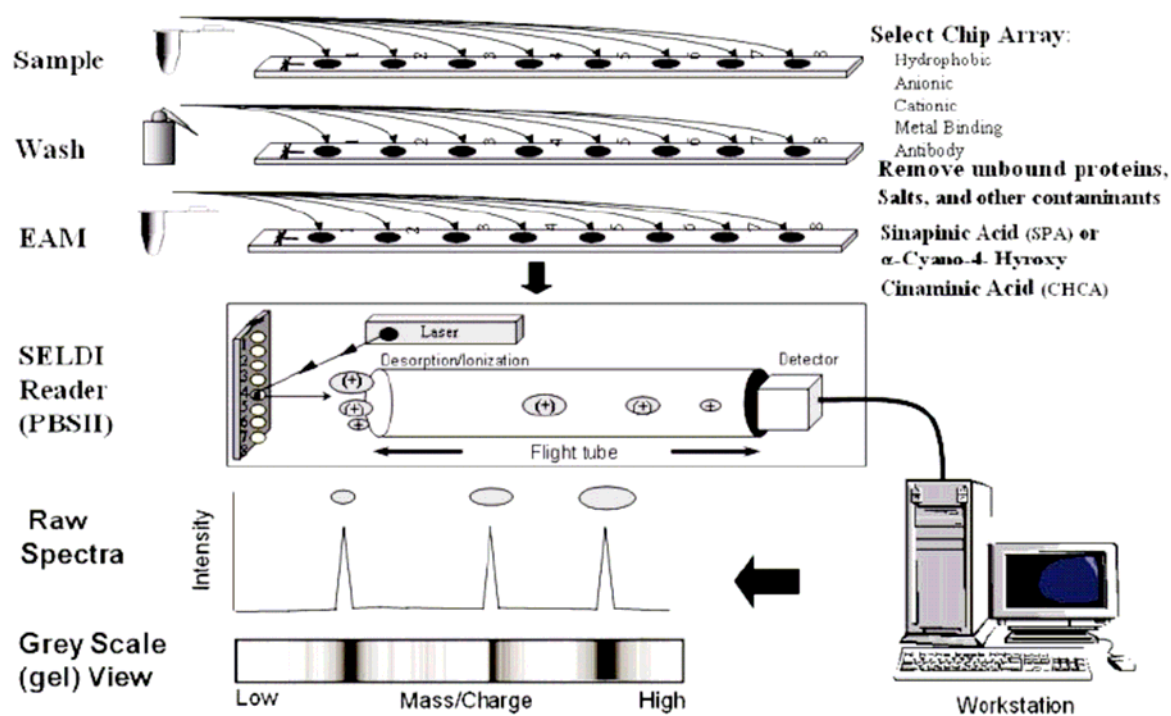

Figure 6. Procedures with the ProteinChip Array system.

From www.evms.edu/vpc/seldi/seldiprocess/fig2.jpg

A. Preparation of cell lysates

Cell pellets of A549 and HK1 were snap-frozen in liquid nitrogen and then lysed in DTC buffer (6 M Urea, 2 M Thiourea, 2 % CHAPS (3-3-cholamidopropyl-dimethylammonio-1-

propanesulfonic acid), DTT and a protease inhibitor cocktail. Cells were resuspended with 80 - 200 μl lysis buffer for 5 x 10^4 – 2 x 10^5 cells. After incubating on ice for 30 min, the lysed cells were centrifuged at 13000 x g / min at 4°C. The protein supernatant was carefully transferred into a fresh Eppendorf tube. Protein concentration was estimated using BioRad Bradford protein assay kit.

B. Sample loading and washing

25 μg sample per spot was incubated with the binding buffer specific for the array. The used ProteinChip arrays Q10 and CM10 were assembled into a deep-well type bioprocessor (Ciphergen Biosystems). Prior to loading, Q10 and CM10 arrays were equilibrated with 150 μl of binding buffer (100 mM TrisHCl, pH 9 for Q10 and 100 mM sodium acetate, pH 4 for CM10). After 5 min incubation for two consecutive times on a shaker (700 rpm), 100 μl of total cell lysate diluted in binding buffer was applied onto each spot in duplicate. All arrays were incubated on a shaker (700 rpm) for 30 min and then washed three times with 150 μl of the specific binding buffer. Last, after rinsing twice with 200 μl dd H_2O, the arrays were immediately removed from the bioprocessor and dried on a pre-warmed heating plate at 40°C for 3 min. 0.5 μl of SPA (saturated sinapinic acid, Ciphergen Biosystems) solution containing 200 μl 100 % ACN (acetonitrile) and 200 μl 1 % TFA (trifluoroacetic acid) was applied twice and the arrays were left to air-dry.

C. SELDI-TOF analysis

The MS analysis was performed using a PBS-II mass reader (Ciphergen Biosystems, CA, USA). Analysis was performed in two runs, providing a low mass (LM) and a high mass (HM) range.

Spectra were obtained with a laser intensity of 170 for LM (195 for HM) and a detector sensitivity of 7 (9) to acquire an optimal mass from 2 to 30 kDa (10 to 5 kDa). Mass accuracy was calibrated externally with the All-in-1 Protein molecular mass standards (Ciphergen Biosystems). Analysis of the mass spectra was performed using the ProteinChip software version 3.1 in combination with *Biomarker Wizard* (Ciphergen Biosystems). The spectra were imported into 'experiments' and sample groups were

designated. The different sample groups for each cell line consisted of RS, PS and controls. This was followed by automatic peak detection, eventually manually detected peaks were added. Noise and baseline subtraction were automatically performed for all spectra. Then all the spectra were normalized by the „Total Ion Content" method, as recommended in the Ciphergen manual. Peaks with *m/z* < 2500 were excluded, since the energy absorbing matrix signal generally interferes with peak detection in this region. In order to identify 'clusters' (sets) of peaks across spectra and across sample groups, the *Biomarker Wizard* module was used. The detected peaks had signal-to-noise ratios > 5 and a cluster mass detection window at 0.3 % of mass with a minimum peak threshold of 10 % of all spectra. For each cluster, which consists of peaks of similar masses from each spectrum, the p-value was determined by non-parametric two-sample comparison with the Wilcoxon rank sum test to assess the statistical significance of expression differences among the sample groups. From the peak intensities averaged for each sample group, fold-changes in expression were calculated compared to the average intensity of the control cell samples as reference. Clusters with significant expression differences ($p < 0.05$), containing peaks of signal-to-noise ratios ≥ 5, and having at least one of the fold changes ≥ 2.0 were considered as potential candidates for biomarkers.

Further analysis of spectra of all samples was performed by CiphergenExpress Software 3.0. Peaks of all spectra were clustered as above and the p-values determined by non-parametric two-sample comparison with the Mann-Whitney test. In addition, receiver operating characteristic (ROC) curves were created, which display the relationship between sensitivity (true-positive rate) and 1-specificity (false-positive rate) across all possible threshold values that define a disease or positivity of a condition. An area under the curve (AUC) value close to 0.0 or 0.99 of the ROC curves indicates that the respective peak is a good marker for distinguishing between RS or PS and control samples, respectively.

The coefficient of variation (CV) is a measure of dispersion of a distribution. The higher the CV value is, the higher the variance of the distribution.

3. RESULTS

3.1 A549 cell line (human non small cell lung cancer)

Among other tumor cell lines, A549 cells are known to express telomerase at a very high level which enables them to proliferate indefinitely. Telomere dysfunction was induced by inserting a retroviral vector containing a dominant negative mutant for hTERT, the core component of telomerase, into A549 bulk cells. A549 single cell clones were selected, and cultured until the state of replicative senescence (RS) was reached.

Premature senescence (PS) was induced in A549 wild type cells by H_2O_2 and bleomycin as well as irradiation.

3.1.1 Inducing RS

3.1.1.1 Retroviral gene transfer

In order to inhibit telomerase activity in the native A549 cancer cells and to consequently induce telomere dysfunction, telomerase positive A549 cells were retrovirally transduced with the following vectors:

> 1.) pOS-IRES-GFP (vc: vector control)
>
> 2.) pOS-hTERT-IRES-GFP (hT: hTERT)
>
> 3.) pOS-DNhTERT-IRES-GFP (DN: dominant negative hTERT)

The non-transduced wild type (wt) bulk was used as a negative control for GFP expression, whereas all three transduced bulks were positive controls, selected according to their GFP expression by FACS sorting for determining the transduction efficiency. Replicative senescence (RS) was induced by transduction with the dominant negative mutant (DN) of hTERT.

The date of the beginning of transfection was designated as day 0.

3.1.1.2 Cell selection with the FACS sorter and single cell cloning

The flow cytometric assessment of GFP expression showed that the efficiency of gene transfer was approximately 73 % in the GFP vector controls, 69 % in the hTERT cells

and 59 % in the DN hTERT cells. GFP positive cells were sorted and cloned at the core facility in Freiburg into 96-well plates. After three weeks of culture, the single cells which proliferated were firstly transferred into 6-well plates and then into T-75 flasks. A total amount of 54 clones grew out of 576 wells which corresponds to a cloning efficiency of approximately 9.4 %.

3.1.1.3 Growth capacity and GFP expression of the A549 cell clones

Representative clones were cultured and harvested at different time points. The levels of GFP expression and the cellular morphologies were analyzed with fluorescence activated cell sorting (FACS).

During cell culture, GFP levels remained stable above 80 % for 80 days. From day 80 onwards, a decrease in GFP expression was noticed for clone **DN 1**, the GFP expression levels of the remaining clones, however, were above 90 % for at least 110 days after the retroviral gene transfer (Fig. 7A and Fig. 8).

In the FACS analysis, the forward light scatter (FSC) channel is important for measuring the cell size. Senescent as well as preapoptotic cells undergo various morphological changes; among them, they increase their cellular size. We could see that replicative growth arrest of a representative DN A549 clone correlated with an increase in cell size, characterized by a shift in FSC (Fig. 8).

Eleven clones were selected according to their GFP expression and cultured for 160 days until the DN clones showed a significant decrease in their replication rate (i.e. no detectable population doubling within four weeks) or GFP expression dropped, respectively (Fig. 7B). The wt cells, as well as the vc and the hT clones, showed a continuously positive, exponential growth for over 160 days with cumulative population doubling levels (CPDL) ranging from 88 (**hT 2**) to 110 (**vc 2**).

Of the five dominant negative hTERT clones, only one (**DN 3**) continued growing exponentially for more than 160 days and reached a CPDL of 94.

The remaining four DN clones underwent permanent replicative growth arrest.

Clone **DN 2** already stopped growing after a CPDL of 28, therefore being in culture for only 40 days. **DN 5** underwent RS after 50 CPDLs and 130 days in culture. The longest

time for reaching RS took clone **DN 4**, remaining replicatively active until day 137 and a CPDL of 56.
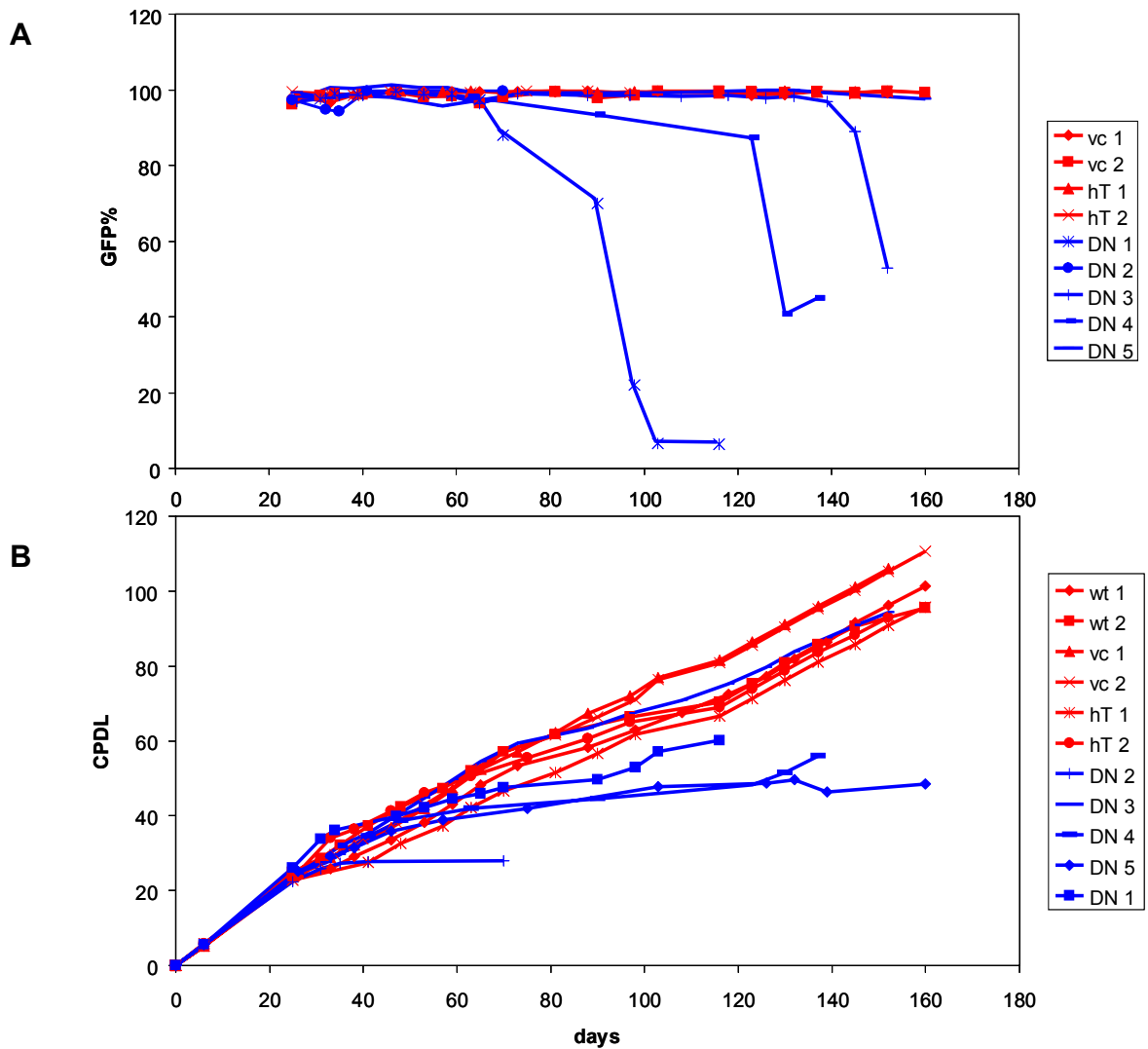
Figure 7. Transduced A549 clones.

The dominant negative (DN) clones for hTERT are represented by blue lines, whereas the hTERT-positive controls (wt, vc, hT) are labeled by red lines.

A. GFP expression intensities analyzed by FACS in nine clones.

B. Growth curves of eleven A549 clones. Note that there is one clone, DN 3, which keeps growing exponentially despite its transfection with the DN-hTERT vector.

wt: wild type; vc: vector control; hT: hTERT; DN: dominant negative hTERT
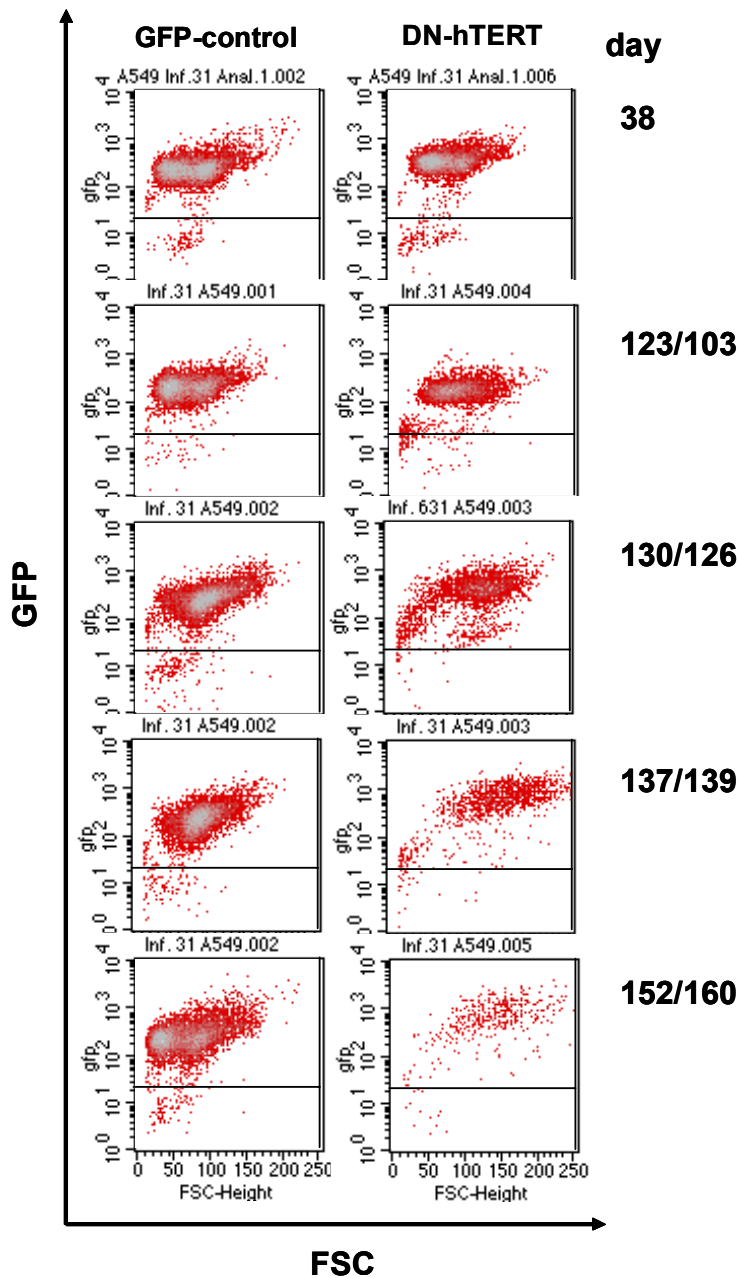
Figure 8. FACS analysis of the A549 vector control vc 1 and DN-hTERT clone DN 5 over time in culture.
The shift in the FSC (forward size scatter) at late passages of the DN 5 clone indicates the increased size of senescent cells.

3.1.1.4 Telomerase activity in clones

The telomerase activities of the A549 clones determined with the telomerase repeat amplification protocol (TRAP) assay correlated with their replicative capacities. As a telomerase-positive control, telomerase activity of Phoenix ampho cells, a derivative of the human embryonic kidney cell line 293T, was set as 100 %. Telomerase levels of the control clones (wt and vc) as well as of the hT clones ranged between 77.8 and 121 %

(Table 2). The clones **DN 2** and **DN 5** which stopped proliferating after having reached a CPDL of 28 and 50, respectively, had a detectable telomerase activity of approximately 5 %.

With a GFP level remaining constant for 140 days, clone **DN 3** continued growing exponentially in culture beyond 160 days. The TRAP assay showed that this clone had an actual telomerase activity of 20 %, thus having the highest value among all the DN clones. In addition, the clones which were transduced with the hTERT vector (**hT 1** and **hT 2**) showed an actual overexpression of telomerase, apparent in telomerase activities of 115 % and 121 % when compared to the wt and vc cells, which both had activities of approximately 78 %.

Table 2. Telomerase activity in % of A549 clones according to TRAP Assay PCR ELISA.

A549 clone	telomerase activity (%)
wt 1	77.8
vc 1	77.9
hT 1	115.0
hT 2	121.0
DN 2	4.69
DN 3	19.9
DN 5	5.06
Phoenix ampho	100.0

Phoenix ampho cells served as positive controls for telomerase, with an activity set as 100 %.
wt: wild type; vc: vector control; hT: hTERT; DN: dominant negative hTERT

3.1.1.5 SA-ß-galactosidase activity

A morphological biomarker for senescence is an increased pH-dependent expression of senescence-associated ß-galactosidase (SA-ß-gal), which can be detected by the use of the chromogenic substrate x-gal, leading to a blue-colored precipitate. Beta-gal expression in late passage A549 clones (day 155) was detected using a specific senescence detection kit.

Matching with the growth curves in cell culture, clones with a high telomerase activity (wt, vc and hT) displayed only minimal amount of the blue precipitate, whereas the DN clones showed an intense blue color development, corresponding to a high SA-ß-gal activity. In addition, the senescent cells of the DN clones were characterized through an enlarged and flattened morphology (Fig. 9).
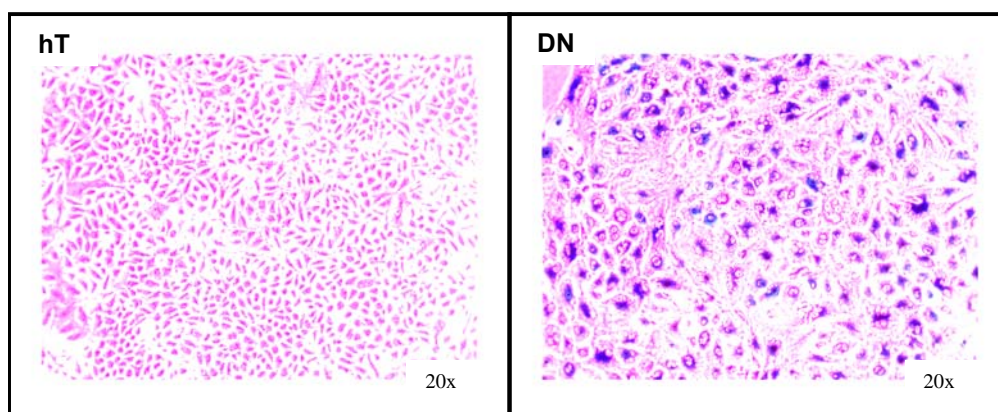
Figure 9. SA-ß-galactosidase expression of representative A549 control and replicative senescent clones.

The hTERT-positive clone (hT, left) with high telomerase activity, showed no blue color development, whereas the dominant-negative hTERT (DN, right) clone displayed an intense blue staining, indicating the state of senescence. Note the enlarged morphology of the replicative senescent cells.

3.1.1.6 SELDI-TOF MS

The cell lysate samples were processed using the technique of Surface-Enhanced Laser Desorption/Ionization Time-Of-Flight Mass Spectrometry (SELDI-TOF MS). Samples were loaded on Q10 and CM10 arrays, respectively, representing different chromatographic ion exchange surfaces. Spectra were then generated with the bioprocessor of Ciphergen Biosystems.

Samples of six clones in total, including the telomerase-positive controls wt, vc and hT were compared to late passages of DN clones (**DN 2**: day 70, **DN 5**: day 139), harvested when replicative growth arrest had occurred.

Table 3. Sample size (# of selected clones).

Controls		RS	
wt	vc	hT	DN
2	1	1	2

wt: wild type; vc: vector control; hT: hTERT; DN: dominant negative hTERT

The obtained protein mass spectra of six clones in compiled duplicates were analyzed according to the regulation of protein peaks using the CiphergenExpress Software. At indicated array types, a total amount of 64 significant protein peaks ($p < 0.05$) was revealed (Table 4).

Among the discovered peaks, 11.3 kDa has already been identified as Histone H4 (Zimmermann et al., 2007). Preliminary data suggest that peaks at 13.8 kDa, 14.0 kDa and 15.3 kDa might also have the identity of histone proteins. All these protein peaks appear to be downregulated with the onset of replicative senescence (Zimmermann et al., 2007). Likewise, we could find these four protein peaks significantly downregulated in late passages of replicative senescent A549 DN clones (Fig. 10 & 11).

In addition, the protein peaks at 48.0 kDa and 53.7 kDa were identified as potential candidates for cytokeratins 18 and 8, respectively (Zimmermann et al., 2007). Both were upregulated in the process of senescence, as well as in our A549 DN clones (Fig. 10 & 12).

In order to get an impression of the longitudinal dynamics of protein expression, successive time points in the culture of DN clones were analyzed by SELDI-TOF MS, starting at early passages (**DN 2**: day 35, **DN 5**: day 38). Once again, the downregulation of the protein peaks 11.3 kDa, 13.8 kDa, 14.0 kDa and 15.3 kDa could be observed whilst studying the successive time points of clone **DN 5** in culture (Fig. 12). In addition, a clear upregulation of the protein peaks at 48.0 kDa and 53.7 kDa occurred over time in culture in the **DN 5** clone.

Table 4. Summary of peaks in dominant negative hTERT (DN) A549 clones when compared to hTERT positive controls (p < 0.05).

Analysis was performed in compiled duplicates using CiphergenExpress Software.

Q10 array

mass (kDa)	regulation in DN	AUC	M/Z % CV
4.3	up	1	0.00
4.4	up	1	0.00
4.7	up	1	0.00
4.9	up	1	0.00
5.0	up	1	0.00
5.2	up	1	0.01
6.2	up	1	0.03
6.3	up	1	0.03
6.9	down	0	0.04
7.0	down	0	0.02
7.3	up	1	0.02
7.7	down	0	0.03
9.1	up	1	0.00
9.8	up	1	0.12
10.4	up	1	0.03
11.3	down	0	0.02
11.4	down	0	0.00
11.5	down	0	0.00
11.8	down	0	0.03
12.3	down	0	0.01
13.8	down	0	0.03
14.0	down	0	0.03
14.6	down	0	0.00
15.3	down	0	0.05
15.9	down	0	0.01
20.2	down	0	0.04
22.2	down	0	0.02
22.5	down	0	0.03
24.9	down	0	0.03
25.1	down	0	0.00
25.2	down	0	0.00
25.3	down	0	0.00
26.6	down	0	0.00
26.9	down	0	0.00
27.0	down	0	0.00
27.9	down	0	0.02
29.2	down	0	0.00
29.4	down	0	0.00
36.0	down	0	0.16
38.5	down	0	0.01

CM10 array

mass (kDa)	regulation in DN	AUC	M/Z % CV
4.0	up	1	0.15
4.2	up	1	0.06
4.4	up	1	0.07
4.5	up	1	0.07
4.6	up	1	0.05
4.7	up	1	0.07
4.9	up	1	0.00
5.0	up	1	0.06
5.1	up	1	0.02
5.3	up	1	0.00
5.8	up	1	0.01
5.9	up	1	0.04
6.7	up	1	0.10
6.9	down	0	0.04
7.0	down	0	0.07
8.5	up	1	0.11
9.1	up	1	0.00
9.8	up	1	0.05
10.0	up	1	0.02
10.4	up	1	0.00
10.8	up	1	0.07
11.1	up	1	0.04
11.4	down	0	0.14
11.7	up	1	0.08
12.4	up	1	0.09
13.8	down	0	0.12
14.0	down	0	0.05
14.6	down	0	0.00
15.3	down	0	0.05
18.4	up	1	0.05
18.6	up	1	0.00
21.3	down	0	0.07
21.8	down	0	0.03
22.2	down	0	0.13
22.5	down	0	0.12
22.8	down	0	0.08
30.6	down	0	0.31
33.5	up	1	1.54
41.7	up	1	0.57
43.8	up	1	0.60
46.1	up	1	0.68

AUC: Area under the curve

CV: Coefficient of variation

M/Z: Mass to charge ratio
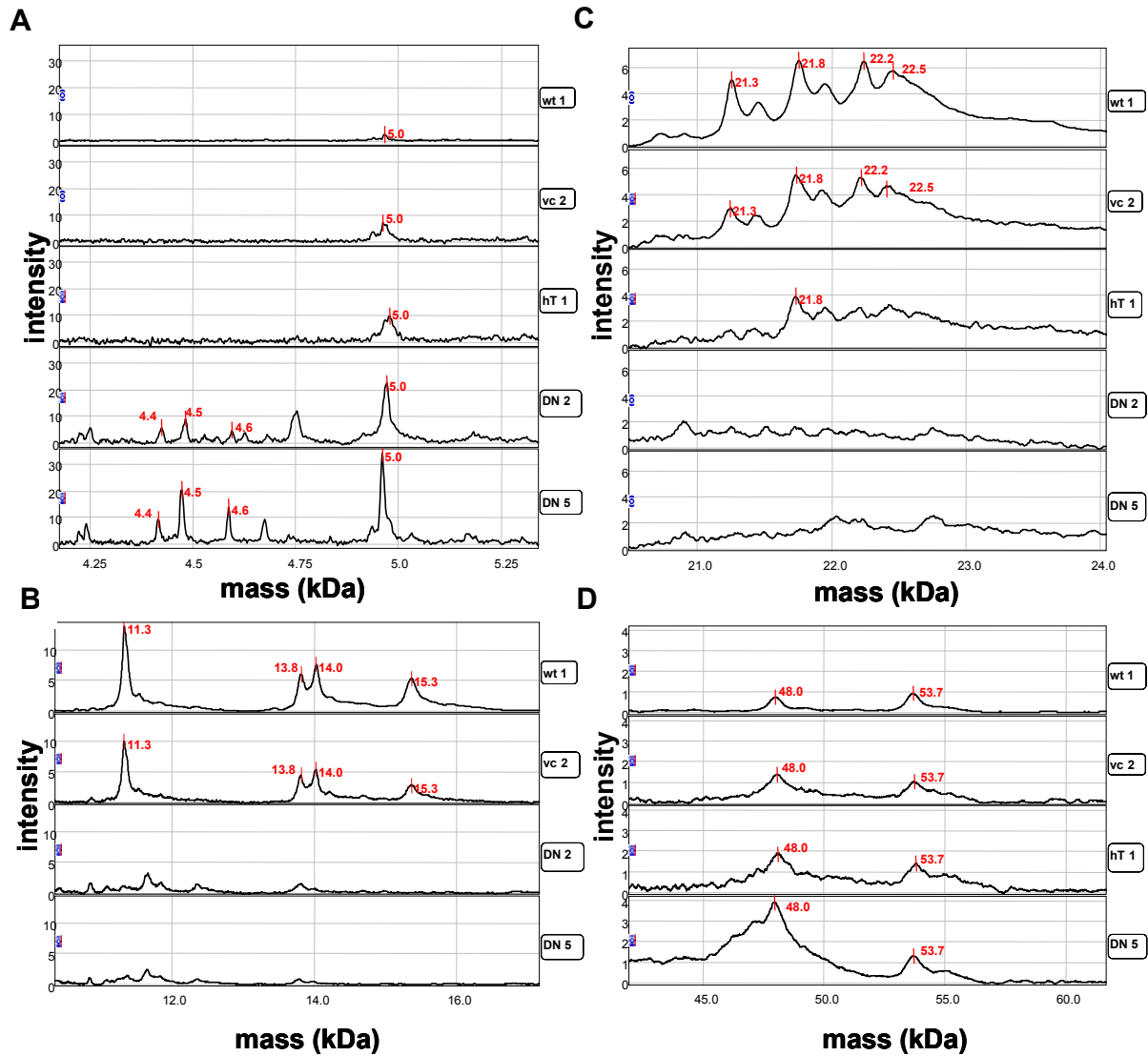
Figure 10. SELDI-TOF MS profiles of late-passage A549 clones (CM10).

The selected peaks are

A. 4.4 kDa, 4.5 kDa, 4.6 kDa and 5.0 kDa (all upregulated in DN clones)

B. 11.3 kDa, 13.8 kDa, 14.0 kDa and 15.0 kDa (all downregulated in DN clones)

C. 21.3 kDa, 21.8 kDa, 22.2 kDa and 22.5 kDa (all downregulated in DN clones)

D. 48.0 kDa and 53.7 kDa (both upregulated in DN clones).

wt: wild type; vc: vector control; hT: hTERT; DN: dominant negative hTERT
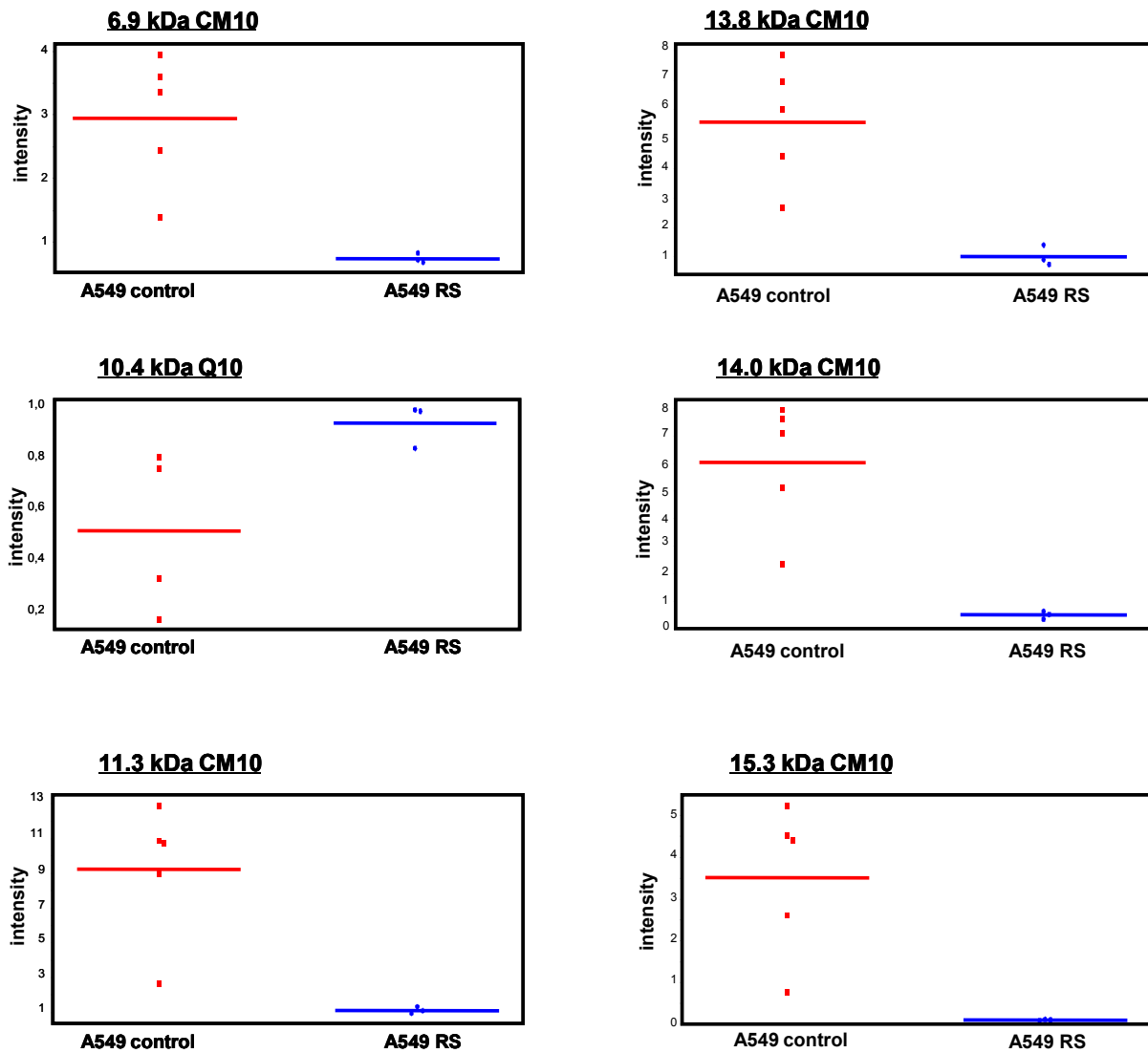
Figure 11. Regulation of protein peaks found in two replicative senescent (RS) DN A549 clones, compared to hTERT positive clones.

The analysis was conducted in compiled duplicates using CiphergenExpress Software.
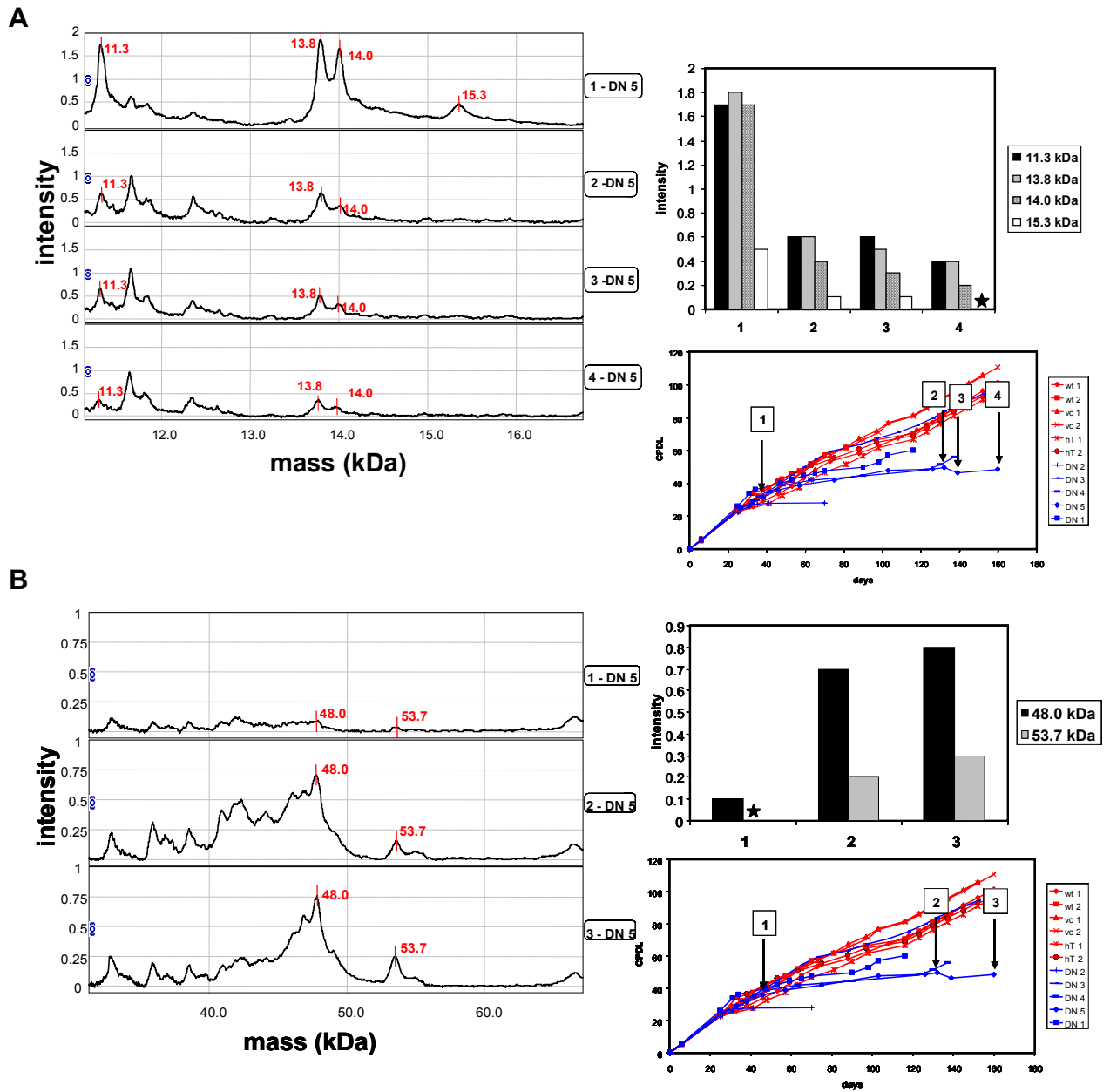
Figure 12. Longitudinal protein peak analysis of A549 DN 5 clone at successive time points.

A. Downregulation of the protein peaks 11.3 kDa, 13.8 kDa, 14.0 kDa, 15.0 kDa in the study of 4 successive time points (days 38, 126, 139, 160).

B. Upregulation of the protein peaks 48.0 kDa and 53.7 kDa in the process of 3 selected time points (days 46, 126, 160).

(*) = no detectable protein peak

3.1.2 Inducing PS

In order to induce PS, A549 cells were treated with toxic agents such as H_2O_2 and bleomycin, as well as irradiation.

3.1.2.1 H_2O_2

Early passage A549 wild type bulk cells were incubated with 230 µM and 280 µM H_2O_2 for two hours.

3.1.2.2 Bleomycin

In analogy, early passage A549 wild type cells were treated with 100 µg and 150 µg bleomycin over three days.

3.1.2.3 Irradiation

At last, young A549 cells were irradiated with 6 Gy (Gray) and 8 Gy, respectively.

3.1.2.4 SA-ß-galactosidase activity

Senescence was detected in early passage A549 control cells and treated ones by the usage of a senescence detection kit, in an analogous manner to the retrovirally transduced clones. A549 wild type cells showed only a minimal amount of the blue precipitate, whereas all the treated A549 cells exhibited a high intensity of blue color, corresponding to a high SA-ß-gal activity. The H_2O_2-incubated, as well as the bleomycin-treated and the irradiated A549 cells all showed features specific for senescence: a flattened shape with large cell size (Fig. 13).

Figure 13. **SA-ß-galactosidase expression of representative control and premature senescent A549 cells.**

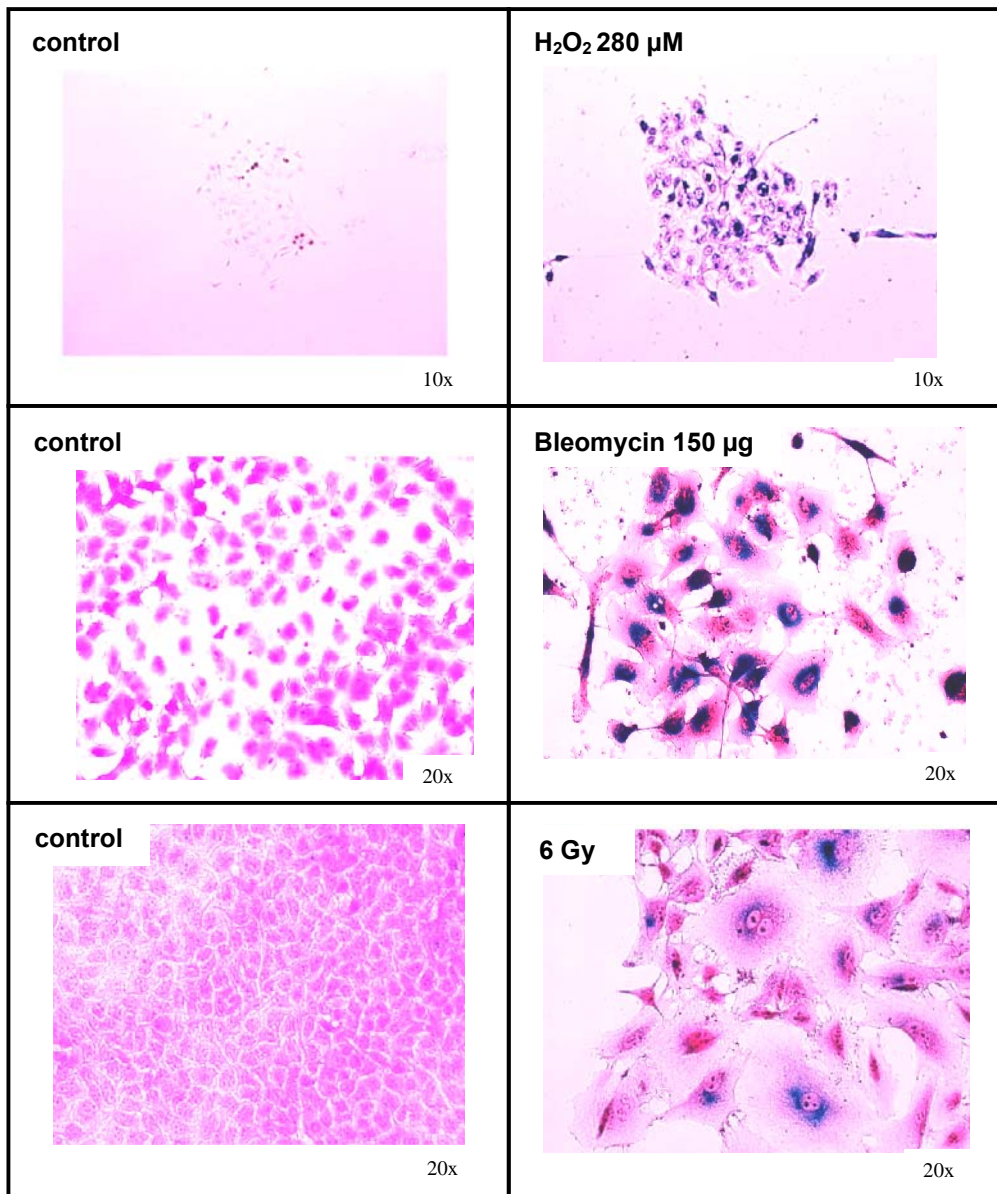The H$_2$O$_2$-incubated, the bleomycin-treated as well as the irradiated A549 cells (right) developed the characteristic blue precipitate of senescent cells when compared to A549 wild type control cells (left). Note the enlarged, flat shape of the premature senescent A549 cells.

3.1.2.5 SELDI-TOF MS

The cell lysate samples were processed with SELDI-TOF MS as mentioned above. After being loaded on Q10 and CM10 arrays, respectively, spectra were generated.

Table 5. Sample size (# of selected clones).

	controls	treated
A549 H_2O_2	1	2
A549 Bleo	1	2
A549 Irrad.	1	2
total	3	6

Peaks where first analyzed using *Biomarker Wizard* Software and were excluded unless found in at least two independent PS A549 experiments. A total amount of 17 equally regulated protein peaks was detected in all three premature senescent A549 cell populations (Table 6).

Among these peaks, we could again find the 13.8 kDa peak downregulated in all the three distinct phenotypes of PS. The additional protein peaks of 11.3 kDa and 15.3 kDa, downregulated in replicative senescent A549 clones, did not show significant differences in any of the premature senescent A549 cells. The 14.0 kDa peak, also downregulated in DN A549 cells, however, was similarly regulated in both the H_2O_2- and bleomycin-treated A549 cells, but not in the irradiated ones (Fig. 14).

Another pair of protein peaks, 48.0 kDa and 53.7 kDa, representing CK18 and CK8 and being upregulated in DN A549 clones, was found to be upregulated in the three PS variants of A549 cells as well.

These results suggest that the induction of PS harbors similarities to RS as well as differences, depending on the treatment agents.

Further comparison of the premature senescent A549 cells as one large experiment in compiled duplicates using CiphergenExpress Software revealed 25 statistically relevant peaks ($p < 0.05$) (Table 7). In this setting, the 15.3 kDa peak could be identified as being downregulated in the premature senescent A549 cells when compared to the controls. On the other hand, the 13.8 kDa peak did not appear to be differentially regulated in the new analysis (Fig. 15).

Table 6. Summary of SELDI peaks differentially regulated in at least two methods of inducing premature senescence (PS) in A549 cells.

Analysis was made using Q10 and CM10 ProteinChip arrays and *Biomarker Wizard* Software.

mass (kDa)	regulation in treated	A549 H_2O_2		A549 Bleo		A549 Irrad.	
x 4.0	**up**	**Q10**	**CM10**	**Q10**		**Q10**	**CM10**
x 4.2	**up**		**CM10**		**CM10**		**CM10**
x 4.4	**up**		**CM10**		**CM10**		**CM10**
4.5	up		CM10				CM10
4.6	up				CM10		CM10
x 4.8	**up**		**CM10**		**CM10**		**CM10**
5.0	up	Q10	CM10			Q10	CM10
x 5.2	**up**	**Q10**	**CM10**	**Q10**	**CM10**	**Q10**	
5.3	up		CM10				CM10
x 5.4	**up**		**CM10**	**Q10**			**CM10**
6.2	up			Q10		Q10	
6.3	up			Q10		Q10	CM10
6.5	up		CM10				CM10
6.7	down		CM10		CM10		
x 6.9	**down**		**CM10**		**CM10**		**CM10**
x 7.9	**down**		**CM10**		**CM10**		**CM10**
x 8.5	**up**		**CM10**		**CM10**		**CM10**
x 8.6	**down**		**CM10**		**CM10**		**CM10**
x 9.1	**up**		**CM10**		**CM10**	**Q10**	
9.8	up				CM10	Q10	
9.9	up			Q10		Q10	
x 10.1	**up**	**Q10**	**CM10**	**Q10**	**CM10**	**Q10**	
11.1	down				CM10		CM10
11.4	down	Q10		Q10			
11.7	down			Q10	CM10		CM10
x 13.8	**down**	**Q10**	**CM10**	**Q10**	**CM10**	**Q10**	**CM10**
14.0	down	Q10	CM10	Q10	CM10		
16.8	up		CM10			Q10	
20.2	up	Q10	CM10				
x 22.8	**down**		**CM10**		**CM10**		**CM10**
x 24.0	**down**		**CM10**	**Q10**			**CM10**
26.8	down			Q10	CM10		CM10
27.0	up				CM10	Q10	
28.7	down	Q10		Q10			
28.8	down	Q10		Q10			
28.9	down	Q10					CM10
32.7	down	Q10		Q10			
36.0	down	Q10		Q10			
x 48.0	**up**		**CM10**	**Q10**	**CM10**	**Q10**	
x 53.7	**up**		**CM10**	**Q10**	**CM10**	**Q10**	

(x): protein peaks commonly expressed in all the three variants of PS

Table 7. SELDI-TOF MS analysis of premature senescent A549 cells compared to the hTERT positive controls.

Samples were analyzed in compiled duplicates using CiphergenExpress software.

Q10 array

mass (kDa)	regulation in PS	p-value	AUC	M/Z % CV
4.2	down	0.02	0.06	0.00
5.2	up	0.04	0.88	0.02
6.2	up	0.04	0.88	0.04
6.3	up	0.04	0.88	0.02
7.7	up	0.04	0.88	0.00
12.0	down	0.02	0.06	0.02
44.0	up	0.04	0.88	0.15
90.5	up	0.02	0.94	0.01

CM10 array

mass (kDa)	regulation in PS	p-value	AUC	M/Z % CV
4.2	up	0.04	0.88	0.04
4.5	up	0.01	1.00	0.03
4.6	up	0.03	0.88	0.04
4.7	up	0.01	1.00	0.00
4.8	up	0.03	0.88	0.03
5.3	up	0.03	0.88	0.06
5.8	up	0.04	0.88	0.00
6.0	up	0.02	0.94	0.01
6.3	down	0.02	0.06	0.03
6.6	down	0.04	0.13	0.00
7.9	down	0.03	0.13	0.04
8.6	down	0.01	0.00	0.04
14.0	down	0.04	0.13	0.04
14.6	down	0.04	0.13	0.00
15.3	down	0.02	0.06	0.00
15.9	down	0.04	0.13	0.02
20.2	up	0.02	0.94	0.09
28.0	down	0.04	0.13	0.03
33.0	down	0.03	0.13	0.11

AUC: Area under the curve

CV: coefficient of variation

M/Z: Mass to charge ratio

A
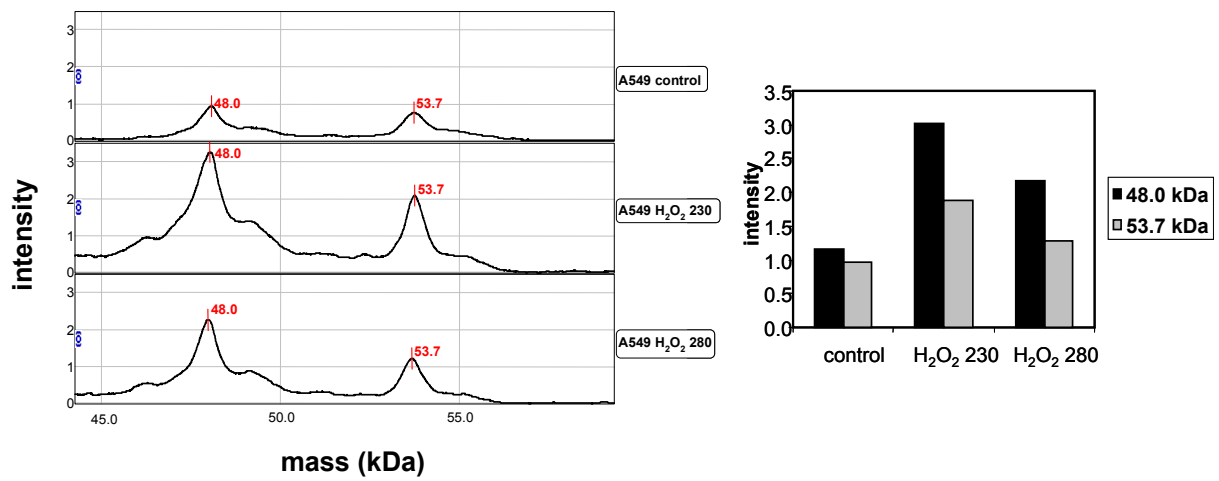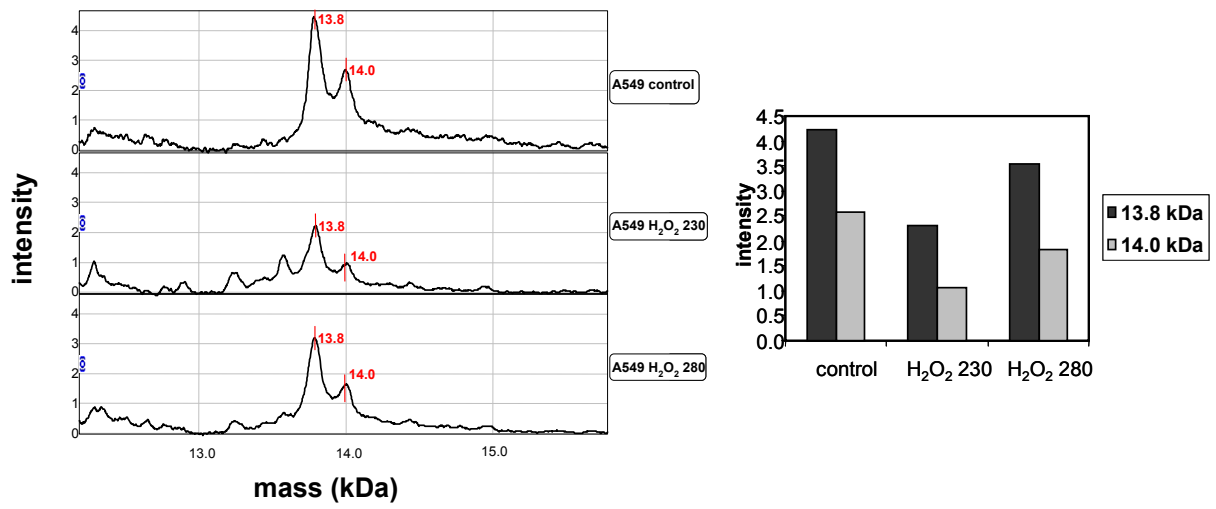
B
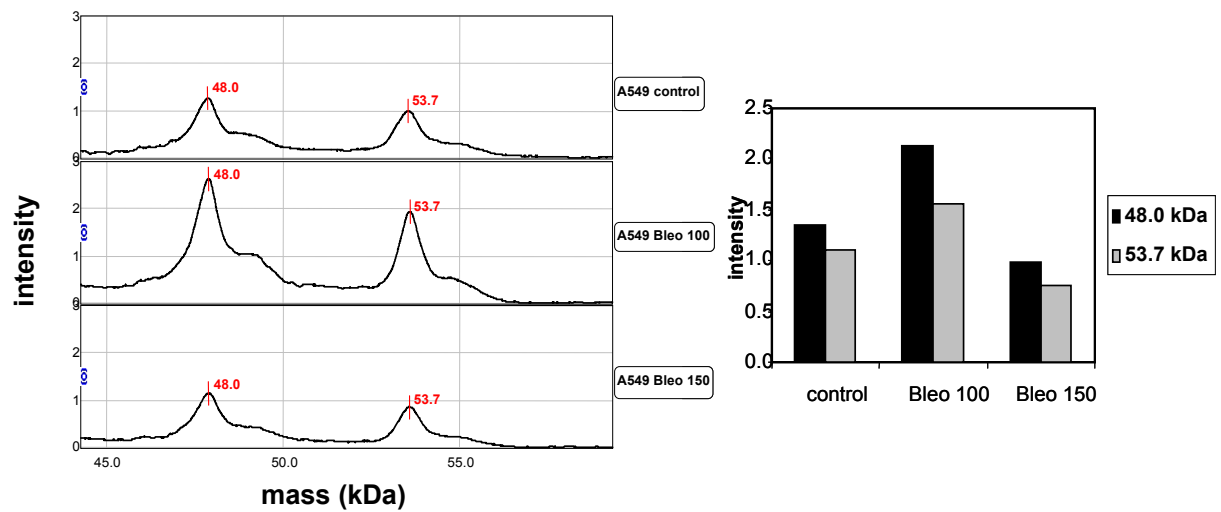
Figure 14. **SELDI-TOF MS profiles of selected peaks in premature senescent A549 cells (CM10).**

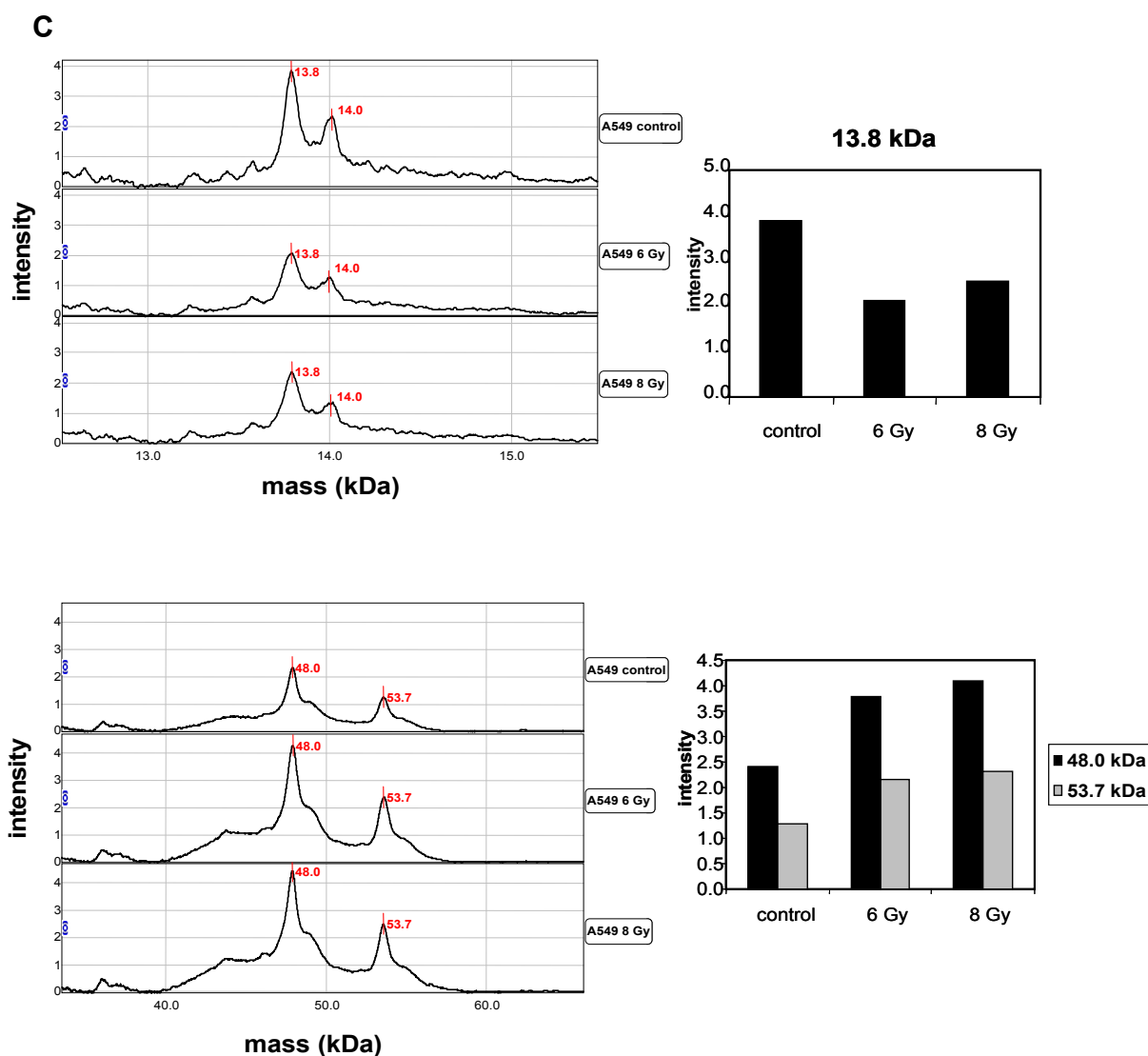**A.** H_2O_2-treated A549 cells: Note that the protein peaks of 13.8 kDa and 14.0 kDa are both downregulated when compared to the controls, but less distinctive within the higher H_2O_2 concentration of 280 µM versus 230 µM. The protein peaks of 48.0 kDa and 53.7 kDa are both upregulated, but again the effect is more pronounced in the 230 µM H_2O_2 concentration than in the 280 µM one.

B. Bleomycin-treated A549 cells: Protein peaks at 48.0 kDa and 53.7 kDa are both upregulated. Yet again, the medium concentration of 100 µg bleomycin shows a higher impact on the protein regulation than 150 µg.

C. Irradiated A549 cells: The 13.8 kDa protein peak is downregulated in premature senescent A549 cells. The A549 cells irradiated with 6 Gy exhibit a stronger downregulation than the A549 cells irradiated with 8 Gy. The 14.0 kDa protein peak showed hardly any differentiated expression. The protein peaks of 48.0 kDa and 53.7 kDa are both upregulated in irradiated A549 cells, with a clear concentration-dependent intensity increase.

4.2 kDa CM10

14.0 kDa CM10

13.8 kDa CM10

15.3 kDa CM10
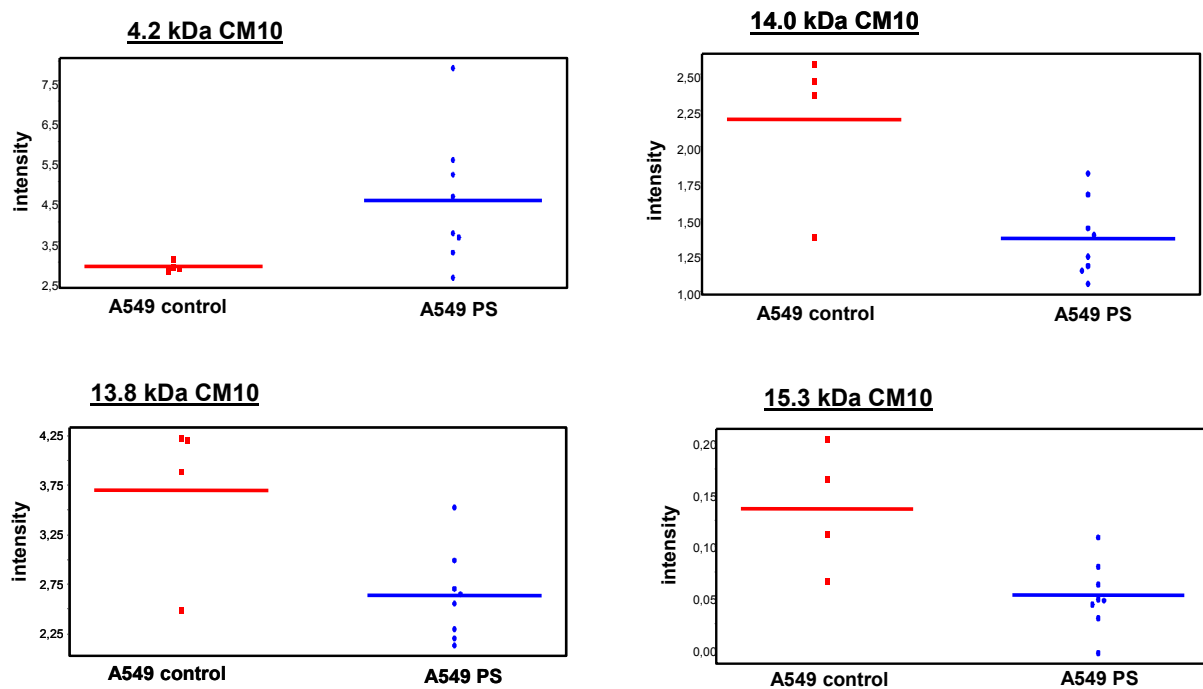
Figure 15. Selected protein peaks found differentially regulated in all three variants of premature senescent A549 cells.

The analysis was carried out in compiled duplicates using CiphergenExpress Software.

3.1.2.6 Summary of analysis of RS and PS in A549 cells

With CiphergenExpress Software, all the obtained data of both RS and PS experiments in A549 cells in compiled duplicates were analyzed. An amount of 12 peaks was found to be equally regulated in both cell populations (Table 8). Among these protein peaks, 14.0 kDa and 15.3 kDa were discovered to be downregulated in both RS as well as PS.

Table 8. Comparison of replicative senescent and premature senescent A549 cells.

Q10 array

mass (kDa)	regulation
5.2	up
6.2	up
6.3	up

CM10 array

mass (kDa)	regulation
4.2	up
4.5	up
4.6	up
4.7	up
5.3	up
5.8	up
14.0	down
14.6	down
15.3	down

3.2 HK1 cell line (human fibroblasts)

Human fibroblasts, as being telomerase-negative, are a well-studied and commonly used model for replicative senescence. We therefore decided to use human fibroblasts as an additional cell line to compare to the A549 NSCLC cells.

HK1 cells were cultured until they underwent RS. PS was induced analogously to the A549 cells by incubating young HK1 cells with H_2O_2 and bleomycin, respectively.

3.2.1 Inducing RS

In order to compare replicative senescent HK1 cells to immortalized ones, we used cells which had been transduced with three retroviral vectors:

      1.) pOS-IRES-GFP (vc: vector control)

      2.) pOS-hTERT-IRES-GFP (hT pOS)

      3.) pBABE-hTERT-IRES-GFP (hT pBABE)

HK1 cells containing vector number one (vc) acted as wild type cells together with the non-transduced wt HK1 cells. The second and third vectors contained hTERT, the core component of telomerase in order to immortalize the HK1 cell bulks. The transduced primary human fibroblasts proved to be immortalized by an hTERT-induced telomerase expression, which lead to a substantial telomere elongation in the range of 2 –2.5 kb as measured by flow-fluorescence in situ hybridization (flow-FISH) (Zimmermann et al., 2004).

3.2.1.1 Growth capacity and GFP expression of the HK1 cells

The telomerase-negative (wt, vc) and the two immortalized lines (hT pOS and hT pBABE) have been reactivated in culture for about 50 days with being cultured a total 186 days (Fig. 16). The GFP expression remained stable around 99 % for all three vector-transduced populations (data not shown). The wt as well as the vc HK1 bulks underwent RS after 150 days in culture and a CPDL of 56. Both transduced hTERT-positive HK1 cells continued their exponential growth beyond 186 days and 72 CPDLs.
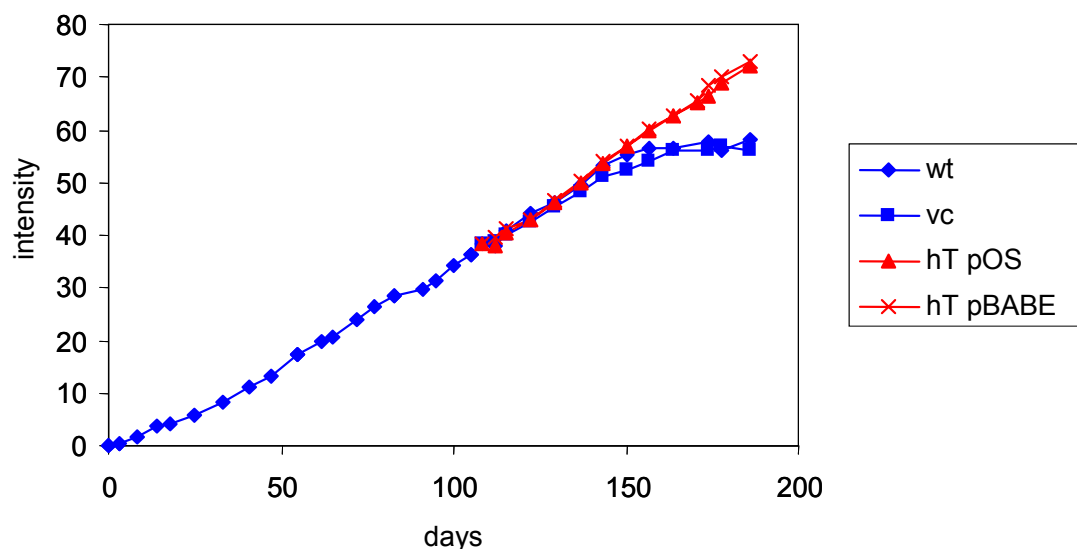
Figure 16. Growth curves of the four HK1 bulk cells.

Note the exponential growth of the immortalized hTERT-positive HK1 cells, represented by red lines. The wt and vc HK1 cells became replicative senescent after approximately 150 days in culture, being labeled with blue lines (Zimmermann et al., 2004).

wt: wild type; vc: vector control; hT pOS: hTERT pOS vector; hT pBABE: hTERT pBABE vector

3.2.1.2 SA-ß-galactosidase activity

Late passage HK1 cells (day 186) were treated with an x-gal solution mix in analogy to the A549 cells. Corresponding to the growth curves in cell culture, the retrovirally immortalized HK1 bulks hT pOS and hT pBABE remained pallid, whereas the telomerase-negative HK1 cells wt and vc developed a high intensity of blue precipitate, conforming to a high SA-ß-gal activity (Fig. 17).

3.2.1.3 SELDI-TOF MS

In analogy to the A549 cells, cell lysate samples from late passages (day 186) of replicative senescent HK1 wt and vc cells as well as immortalized hT pOS and hT pBABE cells were loaded on Q10 and CM10 ProteinChip Arrays, respectively. Using SELDI-TOF MS, analysis was conducted in compiled duplicates with CiphergenExpress Software. In total, 16 significant peaks with $p < 0.05$ were found (Table 10 & Fig. 18). Interestingly, the protein peaks already identified as differentially expressed in the

distinct senescence variants (PS and RS) of A549 cells, i.e. 11.3 kDa, 13.8 kDa, 14.0 kDa, 15.3 kDa, 48.0 kDa, 53.7 kDa, were not altered in this setting.
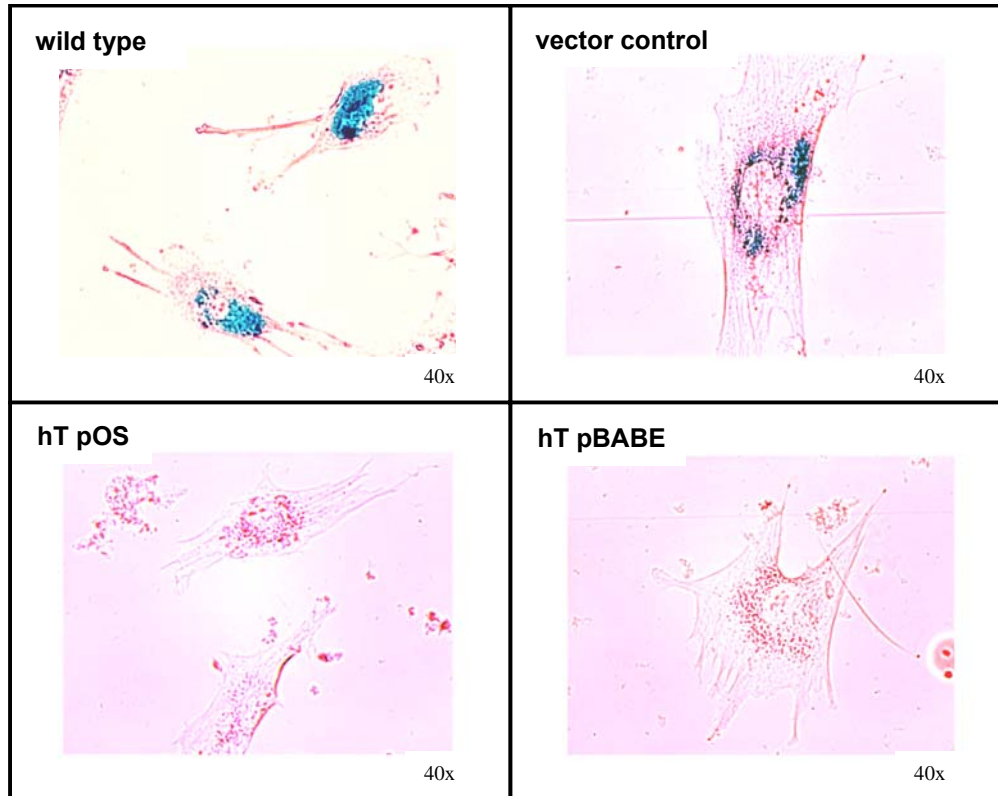
Figure 17. SA-ß-galactosidase expression of replicative senescent HK1 cells.
The replicative senescent wild type and vector control HK1 cells, which were telomerase-negative, developed a clear blue-colored precipitate (above) when compared to the immortalized HK1 cells hT pOS and hT pBABE (below) with high telomerase activity, thus remaining pallid.
hT pOS: hTERT pOS vector; hT pBABE: hTERT pBABE vector

Table 9. Sample size (# of selected clones).

RS		Controls	
wt	vc	hT pOS	hT pBABE
2	2	2	2

wt: wild type; vc: vector control; hT pOS: hTERT pOS vector; hT pBABE: hTERT pBABE vector

In order to take a differential look at the replicative senescent HK1 cells, analysis of HK1 wt and vc cells at an early time point 1 (day 150) and a late time point 2 (day 186) were performed with *Biomarker Wizard* Software (Table 11). Seventeen significant peaks

were equally regulated within these time points in the replicative senescent HK1 cells (p < 0.05). The protein peaks of 13.8 kDa and 15.3 kDa were downregulated in the native HK1 cells during the process of senescence (Fig. 19).

Table 10.   Summary of peaks in replicative senescent (RS) HK1 cells when compared to immortalized HK1 controls.

Analysis was performed in compiled duplicates using CiphergenExpress software.

Q10 array

mass (kDa)	regulation in RS	p-value	AUC	M/Z % CV
4.2	down	0.04	0.94	0.00
4.7	down	0.02	1.00	0.00
5.0	up	0.02	0.00	0.03
10.9	down	0.02	1.00	0.00
25.1	up	0.04	0.06	0.00
25.2	up	0.04	0.06	0.00
32.9	up	0.02	0.00	0.24
65.0	up	0.04	0.06	0.00

CM10 array

mass (kDa)	regulation in RS	p-value	AUC	M/Z % CV
4.1	down	0.02	0.00	0.00
5.3	down	0.02	0.00	0.04
8.6	up	0.02	1.00	0.05
8.7	up	0.04	0.94	0.06
11.8	up	0.04	0.94	0.05
28.2	up	0.04	0.94	0.36
33.0	up	0.04	0.94	0.07
92.0	down	0.04	0.06	0.75

AUC: Area under the curve; **CV**: Coefficient of variation; **M/**Z: Mass to charge ratio
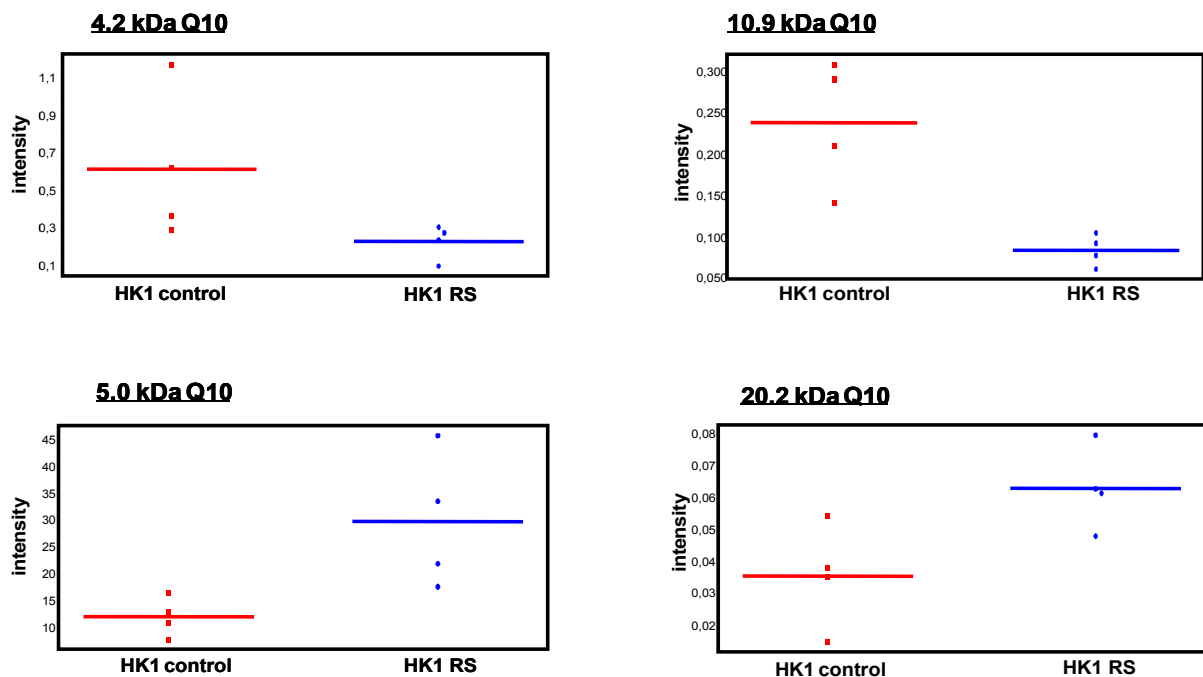

Figure 18. Protein peak regulation in replicative senescent HK1 bulks.

The analysis was carried out in compiled duplicates using CiphergenExpress Software.

HK1 control: hTERT pOS & hTERT pBABE; HK1 RS: wild type & vector control

Table 11. Protein peak intensities commonly regulated in replicative senescent HK1 cells.

Wild type and vector control HK1 cells are compared on an early time point 1 (day 150) and a late time point 2 (day 186).

Q10 array

mass (kDa)	regulation	p	Mean - RS HK1 1	SD - RS HK1 1	Mean - RS HK1 2	SD - RS HK1 2
6.2	up	0.02	0.21	0.12	1.17	0.42
6.3	up	0.04	0.30	0.22	0.75	0.14
8.6	up	0.02	0.09	0.06	1.11	0.09
10.1	up	0.04	0.23	0.12	0.41	0.07
14.3	down	0.04	0.18	0.25	0.03	0.01
33.1	up	0.04	0.50	0.16	0.85	0.21

CM10 array

mass (kDa)	regulation	p	Mean - RS HK1 1	SD - RS HK1 1	Mean - RS HK1 2	SD - RS HK1 2
4.2	down	0.02	1.07	0.15	0.35	0.16
4.5	down	0.02	1.83	0.87	0.67	0.42
5.0	up	0.02	1.01	0.12	2.02	0.53
5.7	down	0.02	0.98	0.31	0.33	0.06
8.5	down	0.02	3.03	0.51	1.84	0.24
8.6	up	0.02	0.98	0.37	3.16	0.33
11.1	up	0.02	0.40	0.10	0.77	0.09
13.8	down	0.04	0.84	0.08	0.68	0.11
15.3	down	0.04	0.63	0.28	0.28	0.08
20.3	up	0.02	0.59	0.05	0.86	0.17
22.6	up	0.02	1.42	0.22	2.50	0.39
25.0	up	0.04	0.43	0.12	0.64	0.11

SD: standard deviation

3.2.2 Inducing PS

In order to induce PS, wild type (wt) HK1 cells were treated with H_2O_2 and bleomycin.

3.2.2.1 H_2O_2

Early passage HK1 wt cells (CPDL 25) were incubated with 150 μM and 180 μM H_2O_2 for two hours.

3.2.2.2 Bleomycin

Early passage HK1 wt cells (CPDL 16-18) were treated with 15 μg and 100 μg of bleomycin for three days:
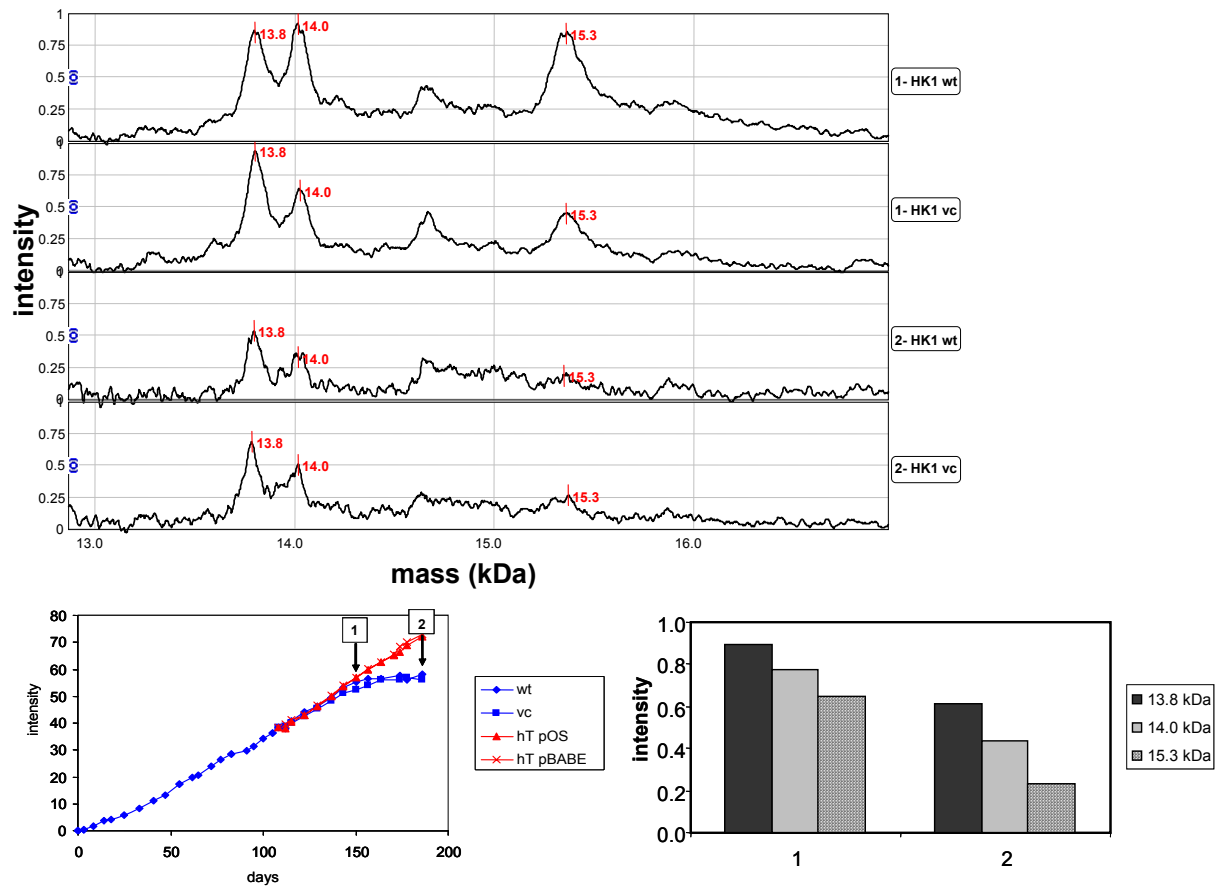
Figure 19. Regulation of 13.8 kDa, 14.0 kDa and 15.3 kDa protein peaks in replicative senescent HK1 cells at successive time points (CM10).

The peak intensities were analyzed between two passages (day 150 and day 186) of replicative senescent HK1 wild type and vector control cells. Note the clear downregulation of the respective peaks.

3.2.2.3 SA-ß-galactosidase activity

In analogy to the replicative senescent HK1 cells, early passage HK1 wt control cells and treated ones were incubated with the x-gal solution mix. Native HK1 wt cells remained pallid, whereas the treated HK1 cells developed a high amount of blue precipitate, corresponding to a high SA-ß-gal activity. The H_2O_2-incubated, as well as the bleomycin-treated HK1 cells all showed specific senescence-associated features such as a flat morphology and large cell size (Fig. 20).
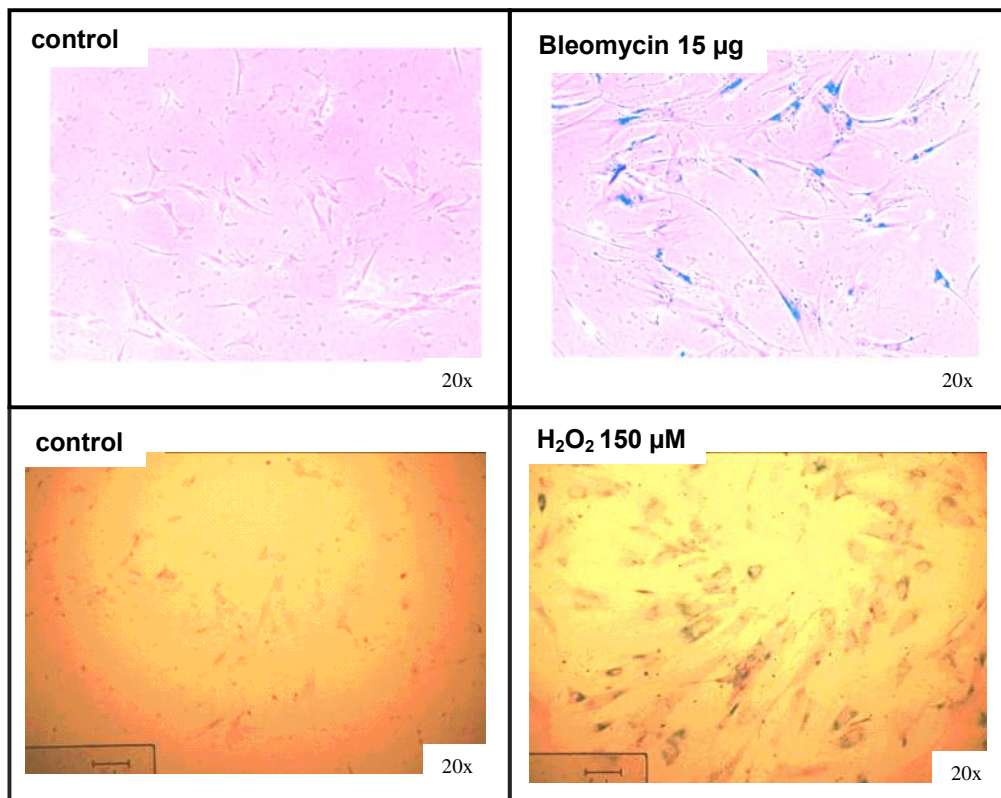
Figure 20. **SA-ß-galactosidase expression of premature senescent HK1 and HK1 controls cells.**
Treated HK1 cells (right) exhibited a blue-colored precipitate, whereas the control cells (left) remained
pallid. Note the enlarged, flat shape of the premature senescent HK1 cells.

3.2.2.4 SELDI-TOF MS

Similarly to the replicative senescent HK1 cells, cell lysates of the premature senescent
HK1 cells were processed with SELDI-TOF MS and then spectra were generated.

Table 12. Sample size (# of selected clones).

	controls	treated
HK1 H_2O_2	2	2
HK1 Bleo	1	2
total	3	4

Samples were initially analyzed with *Biomarker Wizard* Software. Twenty-four peaks
were equally regulated in both H_2O_2- and bleomycin-treated HK1 cells (Table 13).

Concerning the regulation of histone proteins, only the peak at 13.8 kDa was represented in all variants of premature senescent HK1 cells.

Interestingly, the 14.0 kDa peak intensity, on the other hand, was only altered within the bleomycin-treated HK1 cells (Fig. 21). The 15.3 kDa peak, however, could not be found in any of the PS populations.

Further analysis of all the variants of PS compared to the untreated HK1 controls in compiled duplicates with CiphergenExpress Software revealed 13 differentially regulated peaks with $p < 0.05$ (Table 14). The protein peaks of 13.8 kDa and 14.0 kDa reappeared as being downregulated in this setting (Fig. 22).

3.2.2.5 Comparison of RS and PS in HK1 cells

All the peaks found in replicative senescent and premature senescent HK1 cells obtained with CiphergenExpress Software were compared to each other. Only one peak was found to be equally regulated in both cell populations (Table 15).

3.2.2.6 Comprehensive SELDI-TOF MS data analysis of A549 and HK1 cells

All the significant peaks of RS and PS in A549 as well as RS and PS in HK1 cells which were detected in compiled duplicates with CiphergenExpress Software were summarized (Table 17). Protein peaks acquired during the longitudinal analysis of replicative senescent HK1 cells at two different time points were also included.

There was no single protein peak being represented in all four senescence states in both cell lines. Twelve protein peaks, however, were commonly expressed in senescent cells of both cell lines. Among these peaks the 11.3 kDa, 13.8 kDa, 14.0 kDa and 15.3 kDa ones were all downregulated.
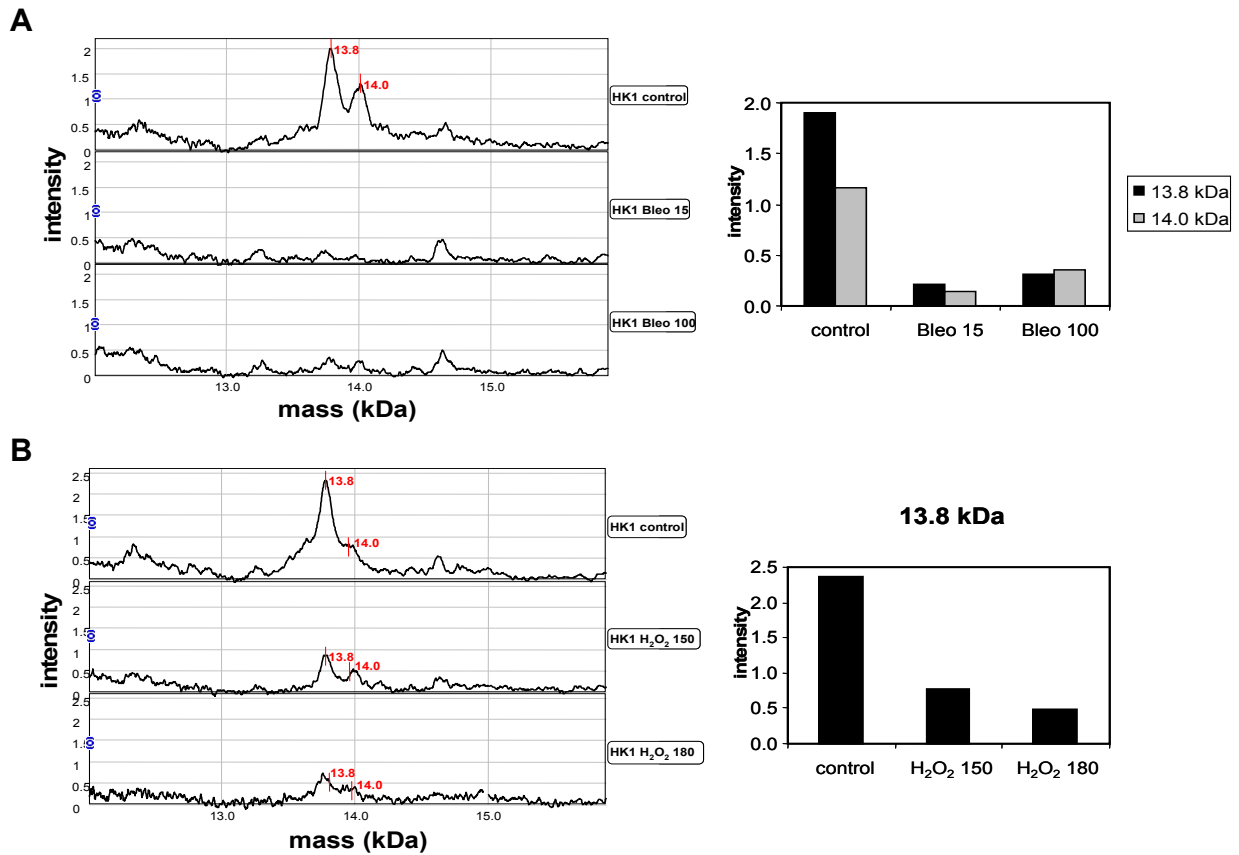
A

B

Figure 21. Regulation of selected peaks in premature senescent HK1 cells compared to controls (CM10).

A. Both 13.8 kDa and 14.0 kDa protein peaks are downregulated in the bleomycin-treated HK1 cells.

B. Downregulation of the 13.8 kDa protein peak in the H_2O_2-incubated HK1 cells. The 14.0 kDa peak is not differentially regulated.

mass (kDa)	regulation in treated	HK1 H₂O₂		HK1 Bleo	
4.0	*up*	Q10			
x 4.1	***up***		**CM10**		**CM10**
4.2	*down*	Q10	CM10		
4.3	*down*	Q10			
4.4	*down*	Q10			
4.5	*up*		CM10		
4.6	*down*	Q10	CM10		
4.7	*up*		CM10		
x 4.8	***down***		**CM10**	**Q10**	**CM10**
x 4.9	***down***	**Q10**	**CM10**	**Q10**	**CM10**
x 5.0	***up***	**Q10**		**Q10**	
x 5.0	***down***		**CM10**		**CM10**
x 5.2	***down***	**Q10**	**CM10**		**CM10**
5.3	*up*				CM10
x 5.4	***down***		**CM10**		**CM10**
5.5	*down*				CM10
5.6	*down*				CM10
6.0	*down*				CM10
x 6.2	***down***		**CM10**	**Q10**	
6.3	*down*	Q10			
6.5	*up*		CM10		
x 6.6	***down***		**CM10**		**CM10**
7.1	*down*	Q10			
x 7.9	***down***		**CM10**		**CM10**
8.2	*down*	Q10			
8.5	*down*		CM10		
8.6	*up*		CM10		
x 8.7	***down***		**CM10**		**CM10**
9.1	*up*		CM10		
9.8	*up*			Q10	
10.1	*down*	Q10	CM10		
10.2	*down*	Q10			
10.3	*up*				CM10
10.4	*up*			Q10	
x 10.9	***down***		**CM10**		**CM10**
x 11.1	***down***		**CM10**		**CM10**
x 11.4	***down***		**CM10**	**Q10**	
11.6	*down*	Q10			
11.7	*down*		CM10		
11.8	*down*	Q10			
11.9	*down*	Q10			
x 13.8	***down***	**Q10**	**CM10**	**Q10**	**CM10**
14.0	*down*				CM10
14.6	*down*	Q10	CM10		
16.8	*down*	Q10	CM10		
18.4	*down*			Q10	CM10
18.6	*down*		CM10		
20.2	*down*	Q10	CM10		
22.5	*down*				CM10
22.7	*down*			Q10	CM10
x 22.8	***down***	**Q10**			**CM10**
23.1	*up*			Q10	
23.2	*down*	Q10			
24.0	*down*			Q10	
24.9	*down*	Q10	CM10		
26.8	*down*			Q10	CM10
27.0	*up*				CM10
28.0	*down*	Q10			
x 28.4	***down***		**CM10**		**CM10**
x 28.9	***down***		**CM10**		**CM10**
32.8	*down*				CM10
32.9	*down*			Q10	CM10
x 33	***down***	**Q10**	**CM10**		**CM10**
35.9	*down*				CM10
36.0	*down*	Q10			
36.6	*down*		CM10		
x 37.2	***up***		**CM10**	**Q10**	
38.6	*up*				CM10
41.9	*down*	Q10			
x 46.2	***up***		**CM10**	**Q10**	**CM10**
x 46.5	***up***		**CM10**	**Q10**	
x 46.7	***up***		**CM10**	**Q10**	
47.3	*up*	Q10			
x 47.9	***up***	**Q10**			**CM10**
48.0	*down*		CM10		
48.3	*down*		CM10		
49.3	*up*				CM10
53.5	*up*			Q10	CM10

Table 13. Summary of SELDI peaks regulated in the two HK1 variants of PS (Q10 & CM10). For analyses, *Biomarker Wizard* Software was used.

(x): protein peaks commonly expressed in both PS variants of HK1 cells

Table 14. Summary of SELDI-peaks in premature senescent HK1 cells.

Analysis was carried out in compiled duplicates using CiphergenExpress software.

Q10 array

mass (kDa)	regulation in PS	p-value	AUC	M/Z % CV
6.9	down	0.03	1	0.00
7.7	down	0.03	1	0.00
10.9	down	0.03	1	0.00
11.3	down	0.03	1	0.00
11.5	down	0.03	1	0.00
12.3	down	0.03	1	0.00
22.7	down	0.03	1	0.23

CM10 array

mass (kDa)	regulation in PS	p-value	AUC	M/Z % CV
4.1	up	0.03	0	0.04
6.7	down	0.03	1	0.11
10.0	down	0.03	1	0.04
11.1	down	0.03	1	0.03
13.8	down	0.03	1	0.04
14.0	down	0.03	1	0.02

AUC: Area under the curve; **CV**: Coefficient of variation; **M/Z**: Mass to charge ratio
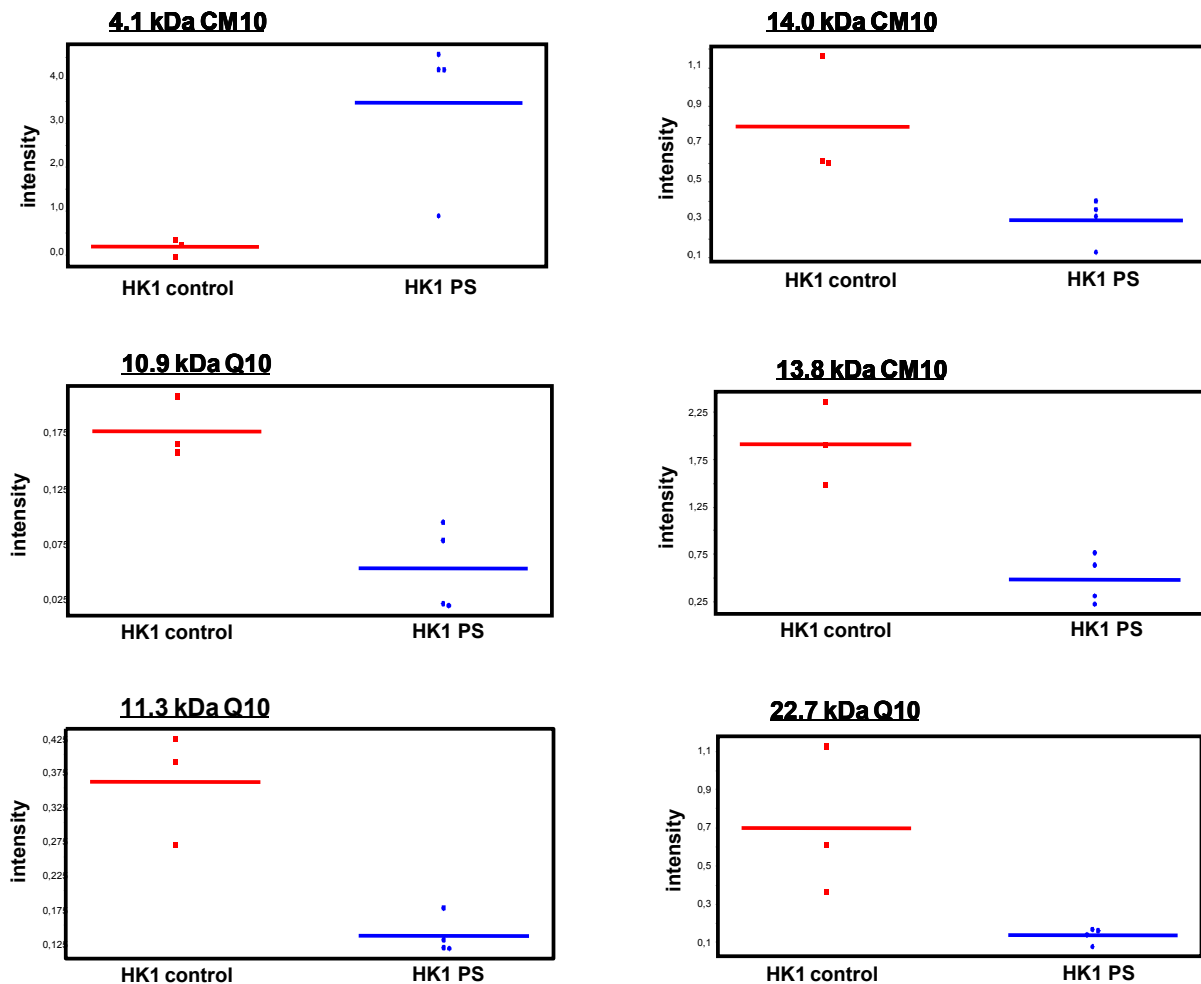
Figure 22. Regulation of protein peaks found in all premature senescent HK1 cells compared to HK1 controls.

The analysis was performed in compiled duplicates using CiphergenExpress software.

Table 15. Comparison of replicative senescent vs. premature senescent HK1 cells (Q10).

The only commonly regulated peak found in both is 10.9 kDa, which is downregulated.

mass (kDa)	regulation
10.9	down

Table 16. Sample size (# of selected clones).

	A549		HK1	
	RS	PS	RS	PS
controls	3	3	4	2
senescent	2	6	4	4
	5	9	8	6
total				**28**

Table 17. Comparison of both replicative and premature senescent A549 and HK1 cells (Q10 & CM10).

mass (kDa)	regulation	A549 RS	A549 PS	HK1 RS	HK1 PS
4.2	up	X	X		
4.5	up	X	X		
4.6	up	X	X		
4.7	up	X	X		
5.0	**up**	**X**		**X**	
5.2	up	X	X		
5.3	up	X	X		
5.8	up	X	X		
6.2	**up**	**X**	**X**	**(X)**	
6.3	**up**	**X**	**X**	**(X)**	
6.7	**down**	**X**			**X**
6.9	**down**	**X**			**X**
7.7	**down**	**X**			**X**
10.9	down			X	X
11.3	**down**	**X**			**X**
11.5	**down**	**X**			**X**
12.3	**down**	**X**			**X**
13.8	**down**	**X**		**(X)**	**X**
14.0	**down**	**X**	**X**		**X**
14.6	down	X	X		
15.3	**down**	**X**	**X**	**(X)**	
15.9	down	X	X		
20.2	up	X	X		

bold: peaks commonly expressed in both cell lines

(x): proteins peaks detected in the longitudinal analysis of two time points of replicative senescent HK1 cells

4. DISCUSSION

4.1   Aims and objectives

In order to develop a protein signature for human cellular senescence, we performed a proteomic survey using SELDI-TOF MS. A NSCLC tumor cell line (A549), and human diploid fibroblasts (HK1) were both forced into RS as well as PS. Our initial goal was to describe the different cellular states of senescence triggered by telomere dysfunction, irradiation and treatment with bleomycin and H_2O_2. Are there any differences in protein peak expression or are these morphologically undistinguishable states actually very similar?

The second purpose of our work was to examine whether there is a general senescence program affecting all cell types in the same way.

Studies concerning the gene expression during cellular senescence are abundant to find, whereas experiments about the protein expression profiles associated with the onset of senescence are rather scarce. Additionally, there has not yet been an approach using the novel SELDI-TOF MS technology for this purpose.

In our experiments, we used two statistical approaches (*Biomarker Wizard* and CiphergenExpress software) in order to thoroughly investigate the protein peak expression. In addition, analysis of replicative senescent cells consisted of a comparison of senescent cells and controls at late passages as well as longitudinal studies of successive time points of senescent cells in culture. This way, we could shed light from different sides on how RS might affect protein expression.

4.2   SELDI-TOF MS

The proteomic survey we conducted was done with the ProteinChip SELDI system, a unique method that uses chromatographic surfaces to retain proteins according to their physicochemical characteristics, followed by TOF MS using a ProteinChip Reader. Protein peaks in the mass range between 4 and 150 kDa can be detected with a resolution higher than MALDI-TOF (Matrix-Assisted Laser Desorption/Ionization Time-Of-Flight Mass Spectrometry) or any of the recent techniques. This novel technology

offers a variety of advantages, such as high-throughput capacity, sensitivity and resolving power, allowing semi-quantitative and statistical analysis whilst requiring only small sample volumes, thus offering a fast, effective route to biomarker discovery.

4.3   Replicative senescence (RS)

For studying the mechanisms of telomerase inhibition in the A549 NSCLC cells, we used clones instead of bulk cultures. We could thereby achieve a more accurate monitoring of telomere dynamics and proliferation capacities.

The retroviral gene transfer for suppressing telomerase activity in wild type A549 cells proved to be successful since the GFP levels remained constant over time in culture and four out of five selected clones underwent RS. Interestingly, one clone already stopped proliferating after only 40 days in culture and a CPDL of 28, whereas the clone which took the longest time to become senescent needed 137 days and a CPDL of 56. Overall, the rate at which RS was reached showed a great variation throughout the DN hTERT clones. This heterogeneity has already been described (von Zglinicki, 2002). It is known that with increasing CPDLs fewer and fewer cells remain actively proliferating. A possible molecular explanation might be a random variation in the position of the most distal primer for lagging-strand synthesis, telomeric recombination or stress-mediated single-strand breakage. However, most likely the distinct clones exhibit variable initial telomere lengths explaining the heterogeneity of their proliferative capacities. It is therefore of interest to answer the question whether cells which enter senescence earlier than others have initially shorter telomeres. One view postulates that only cells which divide until the very end undergo 'real' telomere-driven senescence, whereas the other cells would become senescent by telomere-independent stress ("culture shock") (von Zglinicki, 2002).

The A549 clone DN 2 did not enter RS, but rather showed a telomerase activity of 20 %, which could be sufficient for telomere maintenance and accounting for its continuously exponential growth. Therefore, a telomerase activity of 20 % enabled this clone to escape RS. The remaining clones, however, were successfully telomerase-suppressed, which on the one hand correlated with their limited proliferative potential and SA-ß-gal

expression when compared to the hTERT-positive A549 cells, as well as with their actual telomerase activity of only 5 % as detected by the TRAP assay.

Another noteworthy observation is that the clones transfected with the vectors containing wild type hTERT had an actual overexpression of telomerase, with rates of 115 and 121 %, respectively, when compared to the vector control or the wild type A549 cells, which showed activities of approximately 78 % in relation to the control tumor cell line.

The SELDI-TOF MS analysis of the replicative senescent A549 cells revealed a significant amount of 64 differentially regulated protein peaks, among them, 10 peaks already described in (Zimmermann et al., 2007) as differentially regulated in DN hTERT clones of at least three out of five cancer cell lines: 4.5 kDa (up), 4.7 kDa (up), 6.9 kDa (down), 7.0 kDa (down), 10.4 kDa (up), 11.3 kDa (down), 13.8 kDa (down), 14.0 kDa (down), 15.3 kDa (down) and 22.8 kDa (down). Zimmermann et al. had induced telomere dysfunction in five cancer cell lines, representing four different tumor tissues (lung, prostate, breast, colon), among them also A549 cells, and then analyzed their proteome using SELDI-TOF MS technology. In his experiments, a signature of six proteins common to all five cell lines could be detected: 6.9 kDa (down), 10.4 kDa (up), 11.3 kDa (up), 13.8 kDa (down), 14.0 kDa (down) and 15.3 kDa (down). In our experiments with the replicative senescent A549 cells, we could also identify these six protein peaks as being differentially regulated when compared to the immortal A549 controls (wild type, vector control, hTERT vector).

The 11.3 kDa protein peak has been identified and validated by nanoflow-HPLC-MS/MS (High-Performance Liquid Chromatography coupled with Tandem Mass Spectrometry) and immunoblotting as histone H4 (Zimmermann et al., 2007).Similarly, a protein peak at 11.3 kDa was identified as histone H4 in a proteomic analysis of invasive head and neck cancer (Roesch-Ely, et al. 2007). The 13.8 kDa and 14.0 kDa protein peaks revealed several histone proteins, among them histone H2B (Zimmermann et al., 2007). In addition, the 15.3 kDa peak correlated with the calculated mass of histone H3, which is 15.328 - 15.404 kDa, depending on the variant of this protein.

Thus it seems that a set of up to four histone protein peaks (11.3 kDa, 13.8 kDa, 14.0 kDa and 15.3 kDa) is downregulated during RS in A549 clones. However, further

investigations have to be made in order to confirm the true identity of the proteins behind these peaks.

In the longitudinal analysis of the A549 DN 5 clone at successive time points, two other protein peaks could have been detected as being upregulated with the onset of RS: 48.0 kDa and 53.7 kDa. The proteins behind these peaks were identified as cytokeratins 8 and 18 (Zimmermann et al., 2007). Cytokeratins belong to the intermediate filament (IF) proteins. In a study with senescence-accelerated mice using MALDI-TOF MS technique, among 85 discovered differentially expressed proteins, cytokeratins were found to be upregulated more than two-fold when compared to the control mice (Cho et al., 2003). Another IF protein identified to be upregulated in senescent cells is Vimentin (Nishio et al., 2001, Nishio and Inoue, 2005). The upregulated expression of IF proteins could be a possible explanation for the changes in cellular morphology during senescence. Recently, another protein involved in cytoskeleton remodeling, human profilin-1, was discovered to be upregulated in a SELDI-TOF MS analysis of T-cell clones after long-term culture, probably playing an important role in inducing the senescent phenotype and serving as a potential marker of immunosenescence (Mazzati et al., 2007).

In the replicative senescent HK1 cells, SELDI-TOF analysis revealed mostly other protein peaks to be differentially regulated when compared to the replicative senescent A549 cells. Only the 5.0 kDa peak was upregulated in both settings. However, in the longitudinal analysis of the replicative senescent HK1 cells during two successive time points, four additional differentially regulated peaks could be detected: 6.2 kDa (up), 6.3 kDa (up), 13.8 kDa (down) and 15.3 kDa (down). In summary, five protein peaks were uniformly regulated in RS within A549 and HK1 cells. Among these peaks were the putative histone proteins H2B and H3. This finding suggests that there might actually exist a similar regulative mechanism of senescence, especially in histone protein downregulation caused by telomere dysfunction, which can be found independently of the cell type.

In addition, it can not be assured that cellular senescence as the direct effector causes all the proteins identified to be differentially regulated in this study. Another possible explanation would be a differentiated expression triggered by a more general mechanism in correlation with an altered cell cycle progression.

4.4   Premature senescence (PS)

In both cell strains the PS experiments showed no real dose-dependent effects. Furthermore, in H_2O_2-treated A549 cells the concentration of 230 μMol showed more effects on the intensity of differential protein peak regulation than the higher concentration of 280 μMol. A similar phenomenon could be observed within the bleomycin-treated A549 cells, correlating with the hypothesis that mild stress, allowing at least some cells to proliferate, might be more effective than high agent concentrations (von Zglinicki, 2002).

The three different ways of inducing PS in A549 cells (H_2O_2, bleomycin, and irradiation) had 17 differentially regulated protein peaks in common, among them, again the peaks of 13.8 kDa (down), 48.0 kDa (up) and 53.7 kDa (up) already detected in the replicative senescent A549 clones. Interestingly, the 14.0 kDa peak was only downregulated in the agent treated A549 cells, but not in the irradiated ones. It seems that the three ways of inducing PS share a common mechanism, on the other hand subtle differences could be observed depending on how senescence had been provoked. The H_2O_2- and bleomycin-treated cells, however, seemed to have more differentially regulated peaks in common when compared to the irradiated ones.

In conclusion, within all three variants, the potential histone H2B and the already mentioned CK 8 and CK 18 were down- or upregulated, respectively.

DNA damage by irradiation is known to induce a direct downregulation of histone gene expression, concerning all subtypes (H1, H2A, H2B, H3 and H4) and being mediated through the G_1 checkpoint pathway (Su et al., 2004; Zhao, 2004). In molecular terms, DNA damage inhibits cyclin E-Cdk2 activity with a consecutive suppression of its substrate NPAT, ultimately leading to a downregulation of histone gene expression (Fig. 23). The fact that NPAT is required for both S-phase entry as well as histone gene expression demonstrates the strong coupling between histone gene transcription and cell cycle progression. Dysfunctional telomeres are known to trigger a DDR (DNA damage response), therefore it would be interesting to investigate whether NPAT is also involved in global histone expression in RS.
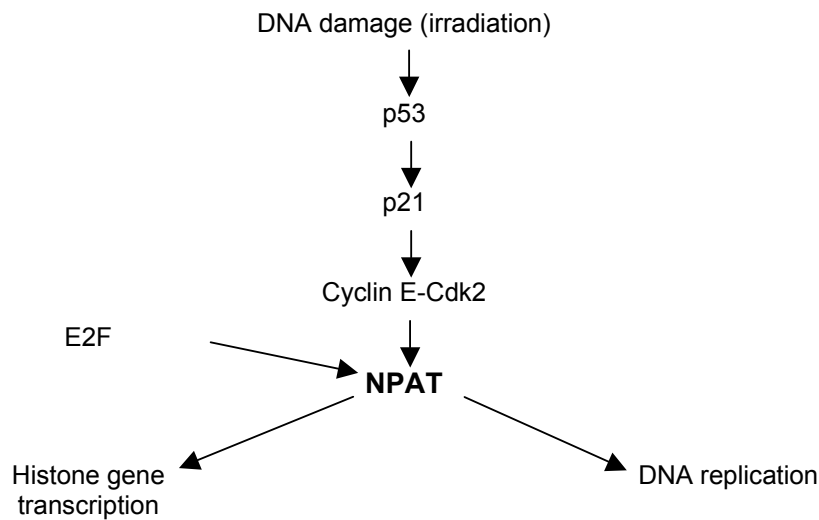
DNA damage (irradiation)

↓

p53

↓

p21

↓

Cyclin E-Cdk2

E2F   →   ↓

NPAT

↙   ↘

Histone gene   DNA replication
transcription

Figure 23. The role of NPAT in the coordination of histone gene expression and S-phase entry.
Adapted from Zhao, 2004.

When compared to the replicative senescent A549 clones, a panel of 12 commonly regulated peaks confirm that there might be plenty of similarities between RS and PS. Among these protein peaks, the two downregulated ones of 14.0 kDa and 15.3 kDa could be identified to be represented in the two different states of senescence, thus leaving room for the interpretation that in both RS and PS the cell cycle arrest correlates with a downregulation of histone proteins.

The HK1 cells treated with H_2O_2 or bleomycin, respectively, revealed a panel of 24 equally regulated protein peaks. The 11.3 kDa protein peak, identified as histone H4, was downregulated in both H_2O_2- as well as in the bleomycin-incubated HK1 cells.

In addition, the peak at 13.8 kDa was also downregulated in both variants of PS, whereas the 14.0 kDa was only downregulated in the bleomycin-treated HK1 cells. Interestingly, in contrast to A549, HK1 cells could not be forced into PS by irradiation, as could be seen in the lack of SA-β-gal expression (data not shown).

When comparing the premature senescent HK1 cells to the replicative senescent ones, only a single differentially regulated peak could be detected: 10.9 kDa (down). However, when we additionally interpreted the longitudinal analysis of the replicative senescent HK1 cells, the histone protein peak at 13.8 kDa also appeared downregulated in both RS and PS within HK1 cells.

Having only two protein peaks in common within the premature senescent and replicative senescent HK1 cells versus 12 peaks within the A549 cells, suggests that it is rather difficult to directly compare the single experiments between the two cell lines, because of varying sample sizes and possible interexperimental fluctuations.

Nonetheless, we have increased evidence that there is a correlation between senescence and downregulation of histones, as a complete loss of linker histone H1 has already been reported (Funayama et al., 2006) and connected to the induction of the senescent phenotype. Recently, it has been discovered in yeast cells, that histone variant H2A.Z is a negative regulator of p21 expression, and that depletion of H2A.Z in human cells leads to p21 activation and consecutively to PS (Gévry et al., 2007).

4.5   A protein signature for cellular senescence

In an approach to compare all the protein peaks we have found to be differentially expressed in both cell strains as well as variants of cellular senescence, a protein signature of 12 protein peaks in similar regulation common to both cell lines was detected with 5.0 kDa, 6.2 kDa and 6.3 kDa being upregulated, and the peaks of 6.7 kDa, 6.9 kDa, 7.7 kDa, 11.3 kDa, 11.5 kDa, 12.3 kDa, 13.8 kDa, 14.0 kDa and 15.3 kDa being downregulated during senescence.

Interestingly, our results were congruent with five out of the six discovered peaks which were part of a protein signature of telomere dysfunction in five cancer cell lines (Zimmermann et al., 2007), i.e. the protein peaks of 6.9 kDa, 11.3 kDa, 13.8 kDa, 14.0 kDa and 15.3 kDa were all downregulated in the respective replicative senescent cancer cell lines, as well as in our A549 and HK1 cells with onset of senescence.

In conclusion, cellular senescence triggered by telomere dysfunction as well as toxic agents and irradiation unleashes biomarkers, which might be part of a general protein signature of senescence overcoming the barriers of different cell types. We discovered a panel of 12 uniformly regulated protein peaks in senescent A549 NSCLC cells and HK1 fibroblasts. Among these peaks was a set of suspected histone proteins, with histone H4 being clearly identified and histones H2B and H3 behind the other peaks with great probability, which were consecutively downregulated with reaching of senescence within

the two cell lines. Due to our small sample size, further investigations will have to be made with other senescing cell strains in order to evaluate these findings. In addition, it would be interesting to show if these proteins are suitable as biomarkers for detecting senescent cells *in vivo*.

4.6   Approaches to novel strategies in cancer treatment

Although a lot of research has been dedicated to the study of apoptosis in cancer treatment, there is a paucity of data regarding the induction and clinical relevance of cellular senescence (Keith et al., 2007). It has been shown that the effects of many anti-cancer therapeutics result in a senescence-response. Future challenges should comprise why certain tissues initiate apoptosis while others seem more prone to activate the cellular senescence program, and whether senescent cancer cells are irreversibly growth arrested *in vivo*, or if an escape into malignancy is possible. Thus, the question is whether induction or avoidance of senescence in patients is a desired clinical outcome in therapy.

In our opinion, it seems favored in anti-cancer therapy to induce tumor regression by forcing the transformed cells into senescence. Recently, it has been shown that restoration of p53 function *in vivo* lead to tumor regression (Martins et al., 2006; Ventura et al., 2007). This mechanism appeared to be tumor type specific: in lymphomas, tumor cells consequently underwent apoptosis after p53 restoration, whereas sarcoma cells also answered with a rapid regression *in vivo*, which was first thought to be apoptosis. Surprisingly, sarcoma cells showed an irreversible cell cycle arrest, appeared flat and enlarge Ned as well as expressed SA-ß-gal, all characteristic features of cellular senescence.

In a mosaic mouse model of liver carcinoma brief activation via RNA interference of endogenous p53 also lead to a complete tumor regression with the onset of a cellular senescence program (Xue et al., 2007). A possible explanation for this fast tumor regression might be a rapid clearance from the tumor mass, due to the innate immune system, as reviewed in (Finkel et al., 2007). Examinations following p53 restoration revealed a dramatic inflammatory reaction with infiltrating neutrophils, macrophages and

natural killer cells, followed by a destruction of tumor cells via phagocytosis and direct cytotoxic killing (Xue et al., 2007). The leukocytes seem to be attracted by a variety of inflammatory cytokines and other immune modulators which are known to be secreted by senescent stromal cells. On the one hand, this chronical inflammation can promote a pro-tumorigenic environment, but on the other hand can trigger innate immune cells to fight against senescent cells which has anti-tumor benefits as well. Normal cells, however, did not seem to respond to p53 reactivation, underlining the tumor specific effect of this treatment. These findings are relevant, since standard chemotherapy and radiotherapy might function partly by inducing senescence within the tumor mass. Furthermore, the tendency might lead towards specific targeting strategies, for example aimed at restoring p53 function in human cancers.

Drug-induced PS in tumor cells is known to be telomerase-independent, as reviewed in (Roninson, 2003). Notably, in some tumor cell lines, cellular senescence seemed to even occur spontaneously, presumably due to subtle changes in the cell environment.

The future goal is to establish sensitive potential protein biomarkers for detecting senescent cells *in vivo*, thus providing crucial information about the response to anti-cancer treatment and prognosis in patients.

5. ZUSAMMENFASSUNG

Kürzlich wurde entdeckt, dass der Erfolg einer Vielzahl von Krebstherapien nicht durch Apoptose, sondern durch einen irreversiblen Zellzyklusarrest, die Seneszenz, zu erklären ist. In der vorliegenden Arbeit wurden zwei Arten der Seneszenz untersucht, zum einen die durch Telomerdysfunktion getriggerte replikative Seneszenz (RS), sowie die telomerunabhängige, durch Bestrahlung und toxische Agenzien auslösbare prämature Seneszenz (PS). Dazu wurden humane nicht-kleinzellige Bronchialkarzinomzellen (A549), die Telomerase exprimieren und Fibroblasten (HK1) verwendet. Aus den A549 Zellen konnten mittels retroviralen Vektoren telomerase-supprimierte Klone generiert werden, die nach einer bestimmten Zeit in Zellkultur replikativ seneszent wurden. PS wurde durch Behandlung mit Bleomycin, H_2O_2 sowie durch Bestrahlung erreicht. Die HK1 Zellen wurden solange kultiviert, bis sich ein Zellzyklusarret einstellte und mit transduzierten HK1 verglichen, die durch retrovirale Überexpression von hTERT, der katalytischen Komponente der Telomerase, immortalisiert waren. Analog zu den A549 Zellen wurde PS durch Behandlung mit Bleomycin und H_2O_2 ausgelöst. Die Zelllysate wurden mittels SELDI-TOF MS analysiert und die dabei erzeugten Massenspektren auf differentielle Proteinexpression untersucht. Hierbei fanden sich zahlreiche gemeinsam regulierte Proteinpeaks sowohl zwischen RS und PS derselben Zellinie als auch unter den beiden Zelllinien. So konnte zellinienübergreifend eine Proteinsignatur, bestehend aus 12 Proteinpeaks der Massen 5.0 kDa, 6.2 kDa und 6.3 kDa, die alle in seneszenten Zellen hochreguliert waren, sowie 6.7 kDa, 6.9 kDa, 7.7 kDa, 11.3 kDa, 11.5 kDa, 12.3 kDa, 13.8 kDa, 14.0 kDa, 15.3 kDa, die im Rahmen der Seneszenz herunterreguliert wurden, charakterisiert werden. Unter diesen Proteinen befanden sich zahlreiche Histone, darunter Histon H4 als sicher identifiziert, deren Expression in Zellen, die seneszent werden, abnimmt. Mit diesen Ergebnissen postulieren wir, dass es zellinienübergreifende Gemeinsamkeiten in dem Mechanismus gibt, der abhängig von spezifischen Triggern den Prozess der zellulären Seneszenz in Gang setzt. Das zukünftige Ziel ist es, Biomarker zu identifizieren, die ein sicheres Erkennen seneszenter Zellen *in vivo* und damit Hinweise auf Therapieerfolg und Prognose ermöglichen.

6. SUMMARY

Recently, it was discovered that the underlying mechanism of tumor regression after anti-cancer treatment cannot be explained with the induction of apoptosis, but rather with a permanent cell cycle arrest termed cellular senescence. We compared two different types of senescence, i.e. telomere-dependant replicative senescence (RS) and premature senescence (PS), whithin two cell strains, the telomerase-positive human non small cell lung cancer cell line A549 and the human fibroblast cell line HK1. By using retroviral vectors, telomerase-suppressed clones could be generated out of the A549 cells, which entered RS after being a certain time in culture. PS was obtained by treating the cells with bleomycin and H_2O_2 as well as irradiation. HK1 cells were cultured until RS occured and were then compared with transduced cells, which had been immortalized by retroviral overexpression of hTERT, the catalytic subunit of telomerase. Similarily to the A549 cells, PS of HK1 was reached by treating the cells with bleomycin and H_2O_2.

Cell lysates were analyzed using a novel technology, the SELDI-TOF MS ProteinChip Array System, which enables a high through-put and therefore the establishment of a sensitive protein profile of complex biological samples. The generated mass spectra were analyzed onto differential protein expression and several commonly regulated protein peaks in both cell strains as well as variants of cellular senescence could have been found.

A protein signature, containing a panel of 12 uniformly regulated protein peaks was detected with 5.0 kDa, 6.2 kDa and 6.3 kDa as being upregulated and 6.7 kDa, 6.9 kDa, 7.7 kDa, 11.3 kDa, 11.5 kDa, 12.3 kDa, 13.8 kDa, 14.0 kDa and 15.3 kDa being downregulated during senescence. Among these peaks was a set of suspected histone proteins, with histone H4 as being clearly identified, which was consecutively downregulated in cells reaching the senescent stage.

In conclusion, cellular senescence triggered by telomere dysfunction as well as toxic agents and irradiation unleashes biomarkers, strongly suggesting that there might be a general protein signature of senescence overcoming the barriers of different cell types. The future goal is to identify potential protein biomarkers for detecting senescent cells *in vivo*, thus providing crucial information about the response to anti-cancer treatment as well as being able to evaluate prognosis in patients.

7. REFERENCES

Artandi, S.E., and R.A. DePinho. 2000. A critical role for telomeres in suppressing and facilitating carcinogenesis. *Curr Opin Genet Dev*. 10:39-46.

Artandi, S.E. 2006. Telomeres, telomerase, and human disease. *N Engl J Med*. 355:1195-7

Atkinson, S.P., and W.N. Keith. 2007. Epigenetic control of cellular senescence in disease: opportunities for therapeutic intervention. *Expert Rev Mol Med*. 9:1-26.

Bakkenist, C.J., R. Drissi, J. Wu, M.B. Kastan, and J.S. Dome. 2004. Disappearance of the telomere dysfunction-induced stress response in fully senescent cells. *Cancer Res*. 64:3748-52.

Barradas, M., E.S. Gonos, Z. Zebedee, E. Kolettas, C. Petropoulou, M.D. Delgado, J. Leon, E. Hara, and M. Serrano. 2002. Identification of a candidate tumor-suppressor gene specifically activated during Ras-induced senescence. *Exp Cell Res*. 273:127-37.

Bartek, J., and J. Lukas. 2003. Chk1 and Chk2 kinases in checkpoint control and cancer. *Cancer Cell*. 3:421-9.

Bartkova, J., N. Rezaei, M. Liontos, P. Karakaidos, D. Kletsas, N. Issaeva, L.V. Vassiliou, E. Kolettas, K. Niforou, V.C. Zoumpourlis, M. Takaoka, H. Nakagawa, F. Tort, K. Fugger, F. Johansson, M. Sehested, C.L. Andersen, L. Dyrskjot, T. Orntoft, J. Lukas, C. Kittas, T. Helleday, T.D. Halazonetis, J. Bartek, and V.G. Gorgoulis. 2006. Oncogene-induced senescence is part of the tumorigenesis barrier imposed by DNA damage checkpoints. *Nature*. 444:633-7.

Beausejour, C.M., A. Krtolica, F. Galimi, M. Narita, S.W. Lowe, P. Yaswen, and J. Campisi. 2003. Reversal of human cellular senescence: roles of the p53 and p16 pathways. *Embo J*. 22:4212-22.

Ben-Porath, I., and R.A. Weinberg. 2004. When cells get stressed: an integrative view of cellular senescence. *J Clin Invest*. 113:8-13.

Benvenuti, S., R. Cramer, J. Bruce, M.D. Waterfield, and P.S. Jat. 2002. Identification of novel candidates for replicative senescence by functional proteomics. *Oncogene*. 21:4403-13.

Bishop, J.M. 1995. Cancer: the rise of the genetic paradigm. *Genes Dev*. 9:1309-15.

Blackburn, E.H. 2000. Telomere states and cell fates. *Nature*. 408:53-6.

Blackburn, E.H. 2001. Switching and signaling at the telomere. *Cell*. 106:661-73.

Blagosklonny, M.V. 2003. Cell senescence and hypermitogenic arrest. *EMBO Rep*. 4:358-62.

Blagosklonny, M.V. 2006. Aging and immortality: quasi-programmed senescence and its pharmacologic inhibition. *Cell Cycle*. 5:2087-102.

Blasco, M.A. 2003. Mammalian telomeres and telomerase: why they matter for cancer and aging. *Eur J Cell Biol*. 82:441-6.

Bodnar, A.G., M. Ouellette, M. Frolkis, S.E. Holt, C.P. Chiu, G.B. Morin, C.B. Harley, J.W. Shay, S. Lichtsteiner, and W.E. Wright. 1998. Extension of life-span by introduction of telomerase into normal human cells. *Science*. 279:349-352.

Braig, M., S. Lee, C. Loddenkemper, C. Rudolph, A.H. Peters, B. Schlegelberger, H. Stein, B. Dorken, T. Jenuwein, and C.A. Schmitt. 2005. Oncogene-induced senescence as an initial barrier in lymphoma development. *Nature*. 436:660-5.

Braig, M., and C.A. Schmitt. 2006. Oncogene-induced senescence: putting the brakes on tumor development. *Cancer Res*. 66:2881-4.

Bryan, T.M., and R.R. Reddel. 1997. Telomere dynamics and telomerase activity in in vitro immortalised human cells. *Eur J Cancer*. 33:767-73.

Campisi, J. 2001. Cellular senescence as a tumor-suppressor mechanism. *Trends Cell Biol*. 11:S27-31.

Campisi, J. 2005a. Aging, tumor suppression and cancer: high wire-act! *Mech Ageing Dev*. 126:51-8.

Campisi, J. 2005b. Senescent cells, tumor suppression, and organismal aging: good citizens, bad neighbors. *Cell*. 120:513-22.

Campisi, J. 2005c. Suppressing cancer: the importance of being senescent. *Science*. 309:886-7.

Campisi, J., and F. d'Adda di Fagagna. 2007. Cellular senescence: when bad things happen to good cells. *Nat Rev Mol Cell Biol.* 8:729-40.

Cech, T.R. 2004. Beginning to understand the end of the chromosome. *Cell*. 116:273-9.

Chen, Z., L.C. Trotman, D. Shaffer, H.K. Lin, Z.A. Dotan, M. Niki, J.A. Koutcher, H.I. Scher, T. Ludwig, W. Gerald, C. Cordon-Cardo, and P.P. Pandolfi. 2005. Crucial role of p53-dependent cellular senescence in suppression of Pten-deficient tumorigenesis. *Nature*. 436:725-30.

Chin, L., S.E. Artandi, Q. Shen, A. Tam, S.L. Lee, G.J. Gottlieb, C.W. Greider, and R.A. DePinho. 1999. p53 deficiency rescues the adverse effects of telomere loss and cooperates with telomere dysfunction to accelerate carcinogenesis. *Cell*. 97:527-38.

Cho, Y., S. Bae, B. Choi, S. Cho, C. Song, J. Yoo, and Y. Paik. 2003. Differential expression of the liver proteome in senescence accelerated mice. *Proteomics*. 3:1883-94.

Collado, M., J. Gil, A. Efeyan, C. Guerra, A.J. Schuhmacher, M. Barradas, A. Benguria, A. Zaballos, J.M. Flores, M. Barbacid, D. Beach, and M. Serrano. 2005. Tumour biology: senescence in premalignant tumours. *Nature*. 436:642.

Collado, M., and M. Serrano. 2006. The power and the promise of oncogene-induced senescence markers. *Nat Rev Cancer*. 6:472-6.

Collado, M., M. Blasco, and M. Serrano. 2007. Cellular senescence in cancer and aging. *Cell.*130:223-33.

Cong, Y.S., E. Fan, and E. Wang. 2006. Simultaneous proteomic profiling of four different growth states of human fibroblasts, using amine-reactive isobaric tagging reagents and tandem mass spectrometry. *Mech Ageing Dev*. 127:332-43.

Coussens, L.M., and Z. Werb. 2002. Inflammation and cancer. *Nature*. 420:860-7.

d'Adda di Fagagna, F., P.M. Reaper, L. Clay-Farrace, H. Fiegler, P. Carr, T. Von Zglinicki, G. Saretzki, N.P. Carter, and S.P. Jackson. 2003. A DNA damage checkpoint response in telomere-initiated senescence. *Nature*. 426:194-8.

d'Adda di Fagagna, F., S.H. Teo, and S.P. Jackson. 2004. Functional links between telomeres and proteins of the DNA-damage response. *Genes Dev*. 18:1781-99.

DePinho, R.A. 2000. The age of cancer. *Nature*. 408:248-54.

Di Micco, R., M. Fumagalli, A. Cicalese, S. Piccinin, P. Gasparini, C. Luise, C. Schurra, M. Garre, P.G. Nuciforo, A. Bensimon, R. Maestro, P.G. Pelicci, and F. d'Adda di Fagagna. 2006. Oncogene-induced senescence is a DNA damage response triggered by DNA hyper-replication. *Nature*. 444:638-42.

Dierick, J.F., D.E. Kalume, F. Wenders, M. Salmon, M. Dieu, M. Raes, P. Roepstorff, and O. Toussaint. 2002. Identification of 30 protein species involved in replicative senescence and stress-induced premature senescence. *FEBS Lett*. 531:499-504.

Dimri, G.P., E. Hara, and J. Campisi. 1994. Regulation of two E2F-related genes in presenescent and senescent human fibroblasts. *J Biol Chem*. 269:16180-6.

Dimri, G.P., X. Lee, G. Basile, M. Acosta, G. Scott, C. Roskelley, E.E. Medrano, M. Linskens, I. Rubelj, O. Pereira-Smith, and et al. 1995. A biomarker that identifies senescent human cells in culture and in aging skin in vivo. *Proc Natl Acad Sci U S A*. 92:9363-7.

Dimri, G.P., A. Testori, M. Acosta, and J. Campisi. 1996. Replicative senescence, aging and growth-regulatory transcription factors. *Biol Signals*. 5:154-62.

Dimri, G.P. 2005. What has senescence got to do with cancer? *Cancer Cell*. 7:505-12.

Dunham, N.A., A.A. Neumann, C.L. Fasching, and R.R. Reddel. 2000. Telomere maintenance by recombination in human cells. *Nat Genet*. 26:447-50.

Faragher, R.G. 2000. Cell senescence and human aging: where's the link? *Biochem Soc Trans*. 28:221-6.

Fernandez-Capetillo, O., A. Lee, M. Nussenzweig, and A. Nussenzweig. 2004. H2AX: the histone guardian of the genome. *DNA Repair (Amst)*. 3:959-67.

Finkel, T., M. Serrano, and M. Blasco. 2007. The common biology of cancer and ageing. *Nature.* 448:767-774.

Funayama, R., M. Saito, H. Tanobe, and F. Ishikawa. 2006. Loss of linker histone H1 in cellular senescence. *J Cell Biol*. 175:869-80.

Furukawa, A., S. Tada-Oikawa, S. Kawanishi, and S. Oikawa. 2007. H2O2 accelerates cellular senescence by accumulation of acetylated p53 via decrease in the function of SIRT1 by NAD+ depletion. *Cell Physiol Biochem*. 20:45-54.

Gévry, N., H. Chan, L. Laflamme, D. Livingston, and L. Gaudreau. 2007. p21 transcription is regulated by differential localization of histone H2A.Z. *Genes Dev.* 21:1869-81.

Gire, V., and D. Wynford-Thomas. 1998. Reinitiation of DNA synthesis and cell division in senescent human fibroblasts by microinjection of anti-p53 antibodies. *Mol Cell Biol*. 18:1611-21.

Gray, J.W., and C. Collins. 2000. Genome changes and gene expression in human solid tumors. *Carcinogenesis*. 21:443-52.

Green, D.R., and G.I. Evan. 2002. A matter of life and death. *Cancer Cell*. 1:19-30.

Griffith, J.D., L. Comeau, S. Rosenfield, R.M. Stansel, A. Bianchi, H. Moss, and T. de Lange. 1999. Mammalian telomeres end in a large duplex loop. *Cell*. 97:503-14.

Hahn, W.C., S.A. Stewart, M.W. Brooks, S.G. York, E. Eaton, A. Kurachi, R.L. Beijersbergen, J.H. Knoll, M. Meyerson, and R.A. Weinberg. 1999. Inhibition of telomerase limits the growth of human cancer cells. *Nat Med*. 5:1164-70.

Harley, C.B., A.B. Futcher, and C.W. Greider. 1990. Telomeres shorten during ageing of human fibroblasts. *Nature*. 345:458-460.

Hastie, N.D., M. Dempster, M.G. Dunlop, A.M. Thompson, D.K. Green, and R.C. Allshire. 1990. Telomere reduction in human colorectal carcinoma and with ageing. *Nature*. 346:866-8.

Hayflick, L. 1965. The Limited in Vitro Lifetime of Human Diploid Cell Strains. *Exp Cell Res*. 37:614-36.

Henson, J.D., A.A. Neumann, T.R. Yeager, and R.R. Reddel. 2002. Alternative lengthening of telomeres in mammalian cells. *Oncogene*. 21:598-610.

Herbig, U., W.A. Jobling, B.P. Chen, D.J. Chen, and J.M. Sedivy. 2004. Telomere shortening triggers senescence of human cells through a pathway involving ATM, p53, and p21(CIP1), but not p16(INK4a). *Mol Cell*. 14:501-13.

Herskind, C., and H.P. Rodemann. 2000. Spontaneous and radiation-induced differentiationof fibroblasts. *Exp Gerontol*. 35:747-55.

Janzen, V., R. Forkert, H.E. Fleming, Y. Saito, M.T. Waring, D.M. Dombkowski, T. Cheng, R.A. DePinho, N.E. Sharpless, and D.T. Scadden. 2006. Stem-cell ageing modified by the cyclin-dependent kinase inhibitor p16INK4a. *Nature*. 443:421-6.

Jenuwein, T., and C.D. Allis. 2001. Translating the histone code. *Science*. 293:1074-80.

Karlseder, J., D. Broccoli, Y. Dai, S. Hardy, and T. de Lange. 1999. p53- and ATM-dependent apoptosis induced by telomeres lacking TRF2. *Science*. 283:1321-5.

Karlseder, J., A. Smogorzewska, and T. de Lange. 2002. Senescence induced by altered telomere state, not telomere loss. *Science*. 295:2446-9.

Keith, W., C. Thomson, J. Howcroft, N. Maitland, and J. Shay. 2007. Seeding drug discovery: integrating telomerase cancer biology and cellular senescence to uncover new therapeutic opportunities in targeting cancer stem cells. *Drug Discov Today.* 12:611-21.

Kim Sh, S.H., P. Kaminker, and J. Campisi. 2002. Telomeres, aging and cancer: in search of a happy ending. *Oncogene*. 21:503-11.

Knudson, A.G. 2000. Chasing the cancer demon. *Annu Rev Genet*. 34:1-19.

Krishnamurthy, J., M.R. Ramsey, K.L. Ligon, C. Torrice, A. Koh, S. Bonner-Weir, and N.E. Sharpless. 2006. p16INK4a induces an age-dependent decline in islet regenerative potential. *Nature*. 443:453-7.

Krtolica, A., S. Parrinello, S. Lockett, P.Y. Desprez, and J. Campisi. 2001. Senescent fibroblasts promote epithelial cell growth and tumorigenesis: a link between cancer and aging. *Proc Natl Acad Sci U S A*. 98:12072-7.

Lanahan, A., J.B. Williams, L.K. Sanders, and D. Nathans. 1992. Growth factor-induced delayed early response genes. *Mol Cell Biol*. 12:3919-29.

Lazzerini Denchi, E., C. Attwooll, D. Pasini, and K. Helin. 2005. Deregulated E2F activity induces hyperplasia and senescence-like features in the mouse pituitary gland. *Mol Cell Biol*. 25:2660-72.

Lowe, S.W., E. Cepero, and G. Evan. 2004. Intrinsic tumour suppression. *Nature*. 432:307-15.

Luo, J., M. Li, Y. Tang, M. Laszkowska, R.G. Roeder, and W. Gu. 2004. Acetylation of p53 augments its site-specific DNA binding both in vitro and in vivo. *Proc Natl Acad Sci U S A*. 101:2259-64.

Martins, C.P., L. Brown-Swigart, and G.I. Evan. 2006. Modeling the therapeutic efficacy of p53 restoration in tumors. *Cell*. 127:1323-34.

Mason, P., and M. Bessler. 2004. Heterozygous telomerase deficiency in mouse and man: when less is definitely not more. *Cell Cycle.* 3:1127-9.

Mathon, N.F., and A.C. Lloyd. 2001. Cell senescence and cancer. *Nat Rev Cancer*. 1:203-13.

Mazzatti, D., G. Pawelec, R. Longdin, J. Powell, and R. Forsey. 2007. SELDI-TOF-MS ProteinChip array profiling of T-cell clones propagated in long-term culture identifies human profilin-1 as a potential bio-marker of immunosenescence. *Proteome Sci.* 5:7.

Merchant, M., and S.R. Weinberger. 2000. Recent advancements in surface-enhanced laser desorption/ionization-time of flight-mass spectrometry. *Electrophoresis*. 21:1164-77.

Michaloglou, C., L.C. Vredeveld, M.S. Soengas, C. Denoyelle, T. Kuilman, C.M. van der Horst, D.M. Majoor, J.W. Shay, W.J. Mooi, and D.S. Peeper. 2005. BRAFE600-associated senescence-like cell cycle arrest of human naevi. *Nature*. 436:720-4.

Molofsky, A.V., S.G. Slutsky, N.M. Joseph, S. He, R. Pardal, J. Krishnamurthy, N.E. Sharpless, and S.J. Morrison. 2006. Increasing p16INK4a expression decreases forebrain progenitors and neurogenesis during ageing. *Nature*. 443:448-52.

Narita, M., S. Nunez, E. Heard, M. Narita, A.W. Lin, S.A. Hearn, D.L. Spector, G.J. Hannon, and S.W. Lowe. 2003. Rb-mediated heterochromatin formation and silencing of E2F target genes during cellular senescence. *Cell*. 113:703-16.

Narita, M., V. Krizhanovsky, S. Nunez, A. Chicas, S.A. Hearn, M.P. Myers, and S.W. Lowe. 2006. A novel role for high-mobility group a proteins in cellular senescence and heterochromatin formation. *Cell*. 126:503-14.

Narita, M. 2007. Cellular senescence and chromatin organisation. *Br J Cancer*. 96:686-91.

Nielsen, S.J., R. Schneider, U.M. Bauer, A.J. Bannister, A. Morrison, D. O'Carroll, R. Firestein, M. Cleary, T. Jenuwein, R.E. Herrera, and T. Kouzarides. 2001. Rb targets histone H3 methylation and HP1 to promoters. *Nature*. 412:561-5.

Nishio, K., A. Inoue, S. Qiao, H. Kondo, and A. Mimura. 2001. Senescence and cytoskeleton: overproduction of vimentin induces senescent-like morphology in human fibroblasts. *Histochem Cell Biol.* 116:321-7.

Nishio, K., and A. Inoue. 2005. Senescence-associated alterations of cytoskeleton: extraordinary production of vimentin that anchors cytoplasmic p53 in senescent human fibroblasts. *Histochem Cell Biol*.123:263-73.

Pear, W.S., G.P. Nolan, M.L. Scott, and D. Baltimore. 1993. Production of high-titer helper-free retroviruses by transient transfection. *Proc Natl Acad Sci U S A*. 90:8392-6.

Reeves, R. 2001. Molecular biology of HMGA proteins: hubs of nuclear function. *Gene*. 277:63-81.

Rich, T., R.L. Allen, and A.H. Wyllie. 2000. Defying death after DNA damage. *Nature*. 407:777-83.

Robles, S.J., and G.R. Adami. 1998. Agents that cause DNA double strand breaks lead to p16INK4a enrichment and the premature senescence of normal fibroblasts. *Oncogene*. 16:1113-23.

Roesch-Ely, M., M. Nees, S. Karsai, A. Ruess, R. Bogumil, U. Warnken, M. Schnölzer, A. Dietz, P. Plinkert, C. Hofele, and F. Bosch. 2007. Proteomic analysis reveals successive aberrations in protein expression from healthy mucosa to invasive head and neck cancer. *Oncogene.* 26:54-64.

Roninson, I.B. 2003. Tumor cell senescence in cancer treatment. *Cancer Res*. 63:2705-15.

Rubin, H. 2002. The disparity between human cell senescence in vitro and lifelong replication in vivo. *Nat Biotechnol*. 20:675-81.

Sarraj, S., R. Farb, and R.E. Martell. 2001. Reconstitution of dna synthetic capacity in senescent normal human fibroblasts by expressing cellular factors E2F and Mdm2. *Exp Cell Res*. 270:268-76.

Schmitt, C.A., J.S. Fridman, M. Yang, S. Lee, E. Baranov, R.M. Hoffman, and S.W. Lowe. 2002. A senescence program controlled by p53 and p16INK4a contributes to the outcome of cancer therapy. *Cell*. 109:335-46.

Schmitt, C.A. 2003. Senescence, apoptosis and therapy--cutting the lifelines of cancer. *Nat Rev Cancer*. 3:286-95.

Schmitt, E., C. Paquet, M. Beauchemin, and R. Bertrand. 2007. DNA-damage response network at the crossroads of cell-cycle checkpoints, cellular senescence and apoptosis. *J Zhejiang Univ Sci B*. 8:377-97.

Sedivy, J.M. 2007. Telomeres limit cancer growth by inducing senescence: long-sought in vivo evidence obtained. *Cancer Cell*. 11:389-91.

Serrano, M., A.W. Lin, M.E. McCurrach, D. Beach, and S.W. Lowe. 1997. Oncogenic ras provokes premature cell senescence associated with accumulation of p53 and p16INK4a. *Cell*. 88:593-602.

Serrano, M. 2007. Cancer regression by senescence. *N Engl J Med*. 356:1996-7.

Severino, J., R.G. Allen, S. Balin, A. Balin, and V.J. Cristofalo. 2000. Is beta-galactosidase staining a marker of senescence in vitro and in vivo? *Exp Cell Res*. 257:162-71.

Shay, J.W., O.M. Pereira-Smith, and W.E. Wright. 1991. A role for both RB and p53 in the regulation of human cellular senescence. *Exp Cell Res*. 196:33-9.

Shay, J.W., and S. Bacchetti. 1997. A survey of telomerase activity in human cancer. *Eur J Cancer*. 33:787-91.

Shay, J.W., and W.E. Wright. 2001. Telomeres and telomerase: implications for cancer and aging. *Radiat Res*. 155:188-193.

Shay, J.W., and I.B. Roninson. 2004. Hallmarks of senescence in carcinogenesis and cancer therapy. *Oncogene*. 23:2919-33.

Shiloh, Y. 2001. ATM and ATR: networking cellular responses to DNA damage. *Curr Opin Genet Dev*. 11:71-7.

Shiloh, Y. 2003. ATM and related protein kinases: safeguarding genome integrity. *Nat Rev Cancer*. 3:155-68.

Simpson, A.J., and A.A. Camargo. 1998. Evolution and the inevitability of human cancer. *Semin Cancer Biol*. 8:439-45.

Stansel, R.M., T. de Lange, and J.D. Griffith. 2001. T-loop assembly in vitro involves binding of TRF2 near the 3' telomeric overhang. *Embo J*. 20:5532-40.

Strahl, B.D., and C.D. Allis. 2000. The language of covalent histone modifications. *Nature*. 403:41-5.

Su, C., G. Gao, S. Schneider, C. Helt, C. Weiss, M. O'Reilly, D. Bohmann, and J. Zhao. 2004. DNA damage induces downregulation of histone gene expression through the G1 checkpoint pathway. *EMBO J.* 23:1133-43.

Takahashi, A., N. Ohtani, K. Yamakoshi, S. Iida, H. Tahara, K. Nakayama, K.I. Nakayama, T. Ide, H. Saya, and E. Hara. 2006. Mitogenic signalling and the p16INK4a-Rb pathway cooperate to enforce irreversible cellular senescence. *Nat Cell Biol*. 8:1291-7.

te Poele, R.H., A.L. Okorokov, L. Jardine, J. Cummings, and S.P. Joel. 2002. DNA damage is able to induce senescence in tumor cells in vitro and in vivo. *Cancer Res*. 62:1876-83.

Ventura, A., D.G. Kirsch, M.E. McLaughlin, D.A. Tuveson, J. Grimm, L. Lintault, J. Newman, E.E. Reczek, R. Weissleder, and T. Jacks. 2007. Restoration of p53 function leads to tumour regression in vivo. *Nature*. 445:661-5.

Verdun, R., and J. Karlseder. 2007. Replication and protection of telomeres. *Nature*. 447:924-31.

von Zglinicki, T., G. Saretzki, W. Docke, and C. Lotze. 1995. Mild hyperoxia shortens telomeres and inhibits proliferation of fibroblasts: a model for senescence? *Exp Cell Res*. 220:186-93.

von Zglinicki, T. 2002. Oxidative stress shortens telomeres. *Trends Biochem Sci.* 27:339-44.

Vulliamy, T., A. Marrone, F. Goldman, A. Dearlove, M. Bessler, P.J. Mason, and I. Dokal. 2001. The RNA component of telomerase is mutated in autosomal dominant dyskeratosis congenita. *Nature*. 413:432-5.

Wong, J.M., and K. Collins. 2003. Telomere maintenance and disease. *Lancet*. 362:983-8.

Wright, W.E., and J.W. Shay. 2001. Cellular senescence as a tumor-protection mechanism: the essential role of counting. *Curr Opin Genet Dev*. 11:98-103.

Xue, W., L. Zender, C. Miething, R.A. Dickins, E. Hernando, V. Krizhanovsky, C. Cordon-Cardo, and S.W. Lowe. 2007. Senescence and tumour clearance is triggered by p53 restoration in murine liver carcinomas. *Nature*. 445:656-60.

Zimmermann, S., S. Glaser, R. Ketteler, C.F. Waller, U. Klingmüller, and U.M. Martens. 2004. Effects of telomerase modulation in human hematopoietic progenitor cells. *Stem Cells*. 22:741-749.

Zimmermann S., M.L. Biniossek, M. Pantic, D. Pfeifer, C. Peters, H. Veelken, U.M. Martens. Proteomic analysis of tumor cells reveals a loss of core histones associated with telomere dysfunction. 2007. *Submitted.*

Zhao, J. 2004. Coordination of DNA synthesis and histone gene expression during normal cell cycle progression and after DNA damage. *Cell Cycle.* 3:695-97.

Zou, L., and S.J. Elledge. 2003. Sensing DNA damage through ATRIP recognition of RPA-ssDNA complexes. *Science*. 300:1542-8.

8. ABBREVIATIONS

ALT   Alternative lengthening of telomeres

ATCC   American Type Culture Collection

ATM   Ataxia teleangiectasia mutated kinase

ATR   Ataxia teleangiectasia and Rad3 related kinase

bp   Base pairs

BSA   Bovine serum albumin

CDK   Cyclin-dependent kinase

CDKI   Cyclin-dependent kinase inhibitor

CK   Cytokeratin

CHK 1,2   Checkpoint kinase 1,2

d   Days

dd   Double distilled

DDR   DNA damage response

DIG   Digoxygenin

DMEM   Dulbecco's Modified Eagle's Medium

DMSO   Dimethylsulfoxide

DN   Dominant negative

DNA   Desoxyribonucleic acid

ds   Double stranded

DSB   Double strand breaks

E2F   Transcription factor

EDTA   Ethylendiamine tetraacetic acid

ELISA   Enzyme linked immuno sorbent assay

env   Envelope protein

FACS   Fluorescence activated cell sort

FISH   Fluorescence in situ hybridization

FCS   Fetal calf serum

FSC   Forward light scatter

g   G-force, earth gravity acceleration defined as 9.80665 m/s^2

gag	Group specific antigens
GFP	Green fluorescent protein
Gy	Gray, SI unit of absorbed radiation
h	Hour
H_2O_2	Hydrogen peroxide
HMGA	High-mobility group A
hTERT	Human telomerase reverse transcriptase
hTERC	Human telomerase RNA
IF	Intermediate Filament
kbp	Kilo base pairs
kDa	Kilo Dalton
LTR	Long Terminal Repeats
M	Molar
M1, M2	Mortality stage 1 and 2
MALDI-TOF MS	Matrix-Assisted Laser Desorption/Ionization Time-Of-Flight Mass Spectrometry
mg	Milligrams
min	Minute
ml	Milliliter
MTP	Micro titer plate
MW	Molecular weight
n	Number
NSCLC	Non Small Cell Lung Cancer
OIS	Oncogene-induced senescence
p21, p53	Protein 21, 53
PBS	Phosphate-buffered saline
PCR	Polymerase chain reaction
PD	Population doubling
PIKK	Phosphatidyl inositol 3-kinase-like kinase
pol	Polyprotein
PS	Premature senescence

pRB	Retinoblastom protein
RNA	Ribonucleic acid
RNase	Ribonuclease
rpm	Rounds per minute
RPMI 1640	Roswell Park Memorial Institute (Medium)
RS	Replicative senescence
RT	Room temperature
RTA	Relative telomerase activity
S	Synthesis
s	Second
SA-β-gal	Senescence-associated beta-galactosidase
SAHF	Senescence-associated heterochromatin foci
SELDI-TOF MS	Surface-Enhanced Laser Desorption/Ionization Time-Of-Flight Mass Spectrometry
SDS	Sodiumdodecylsulfat
SSC	Side scatter
SV40	Simian Virus 40
TBS	Tris-buffered saline
TMB	Tetramethylbemzidine
TRAP	Telomere Repeat Amplification Protocol
µg	Microgram
µl	Microliter
µM	Micromolar
vc	Vector control
wt	Wild type

9. ACKNOWLEDGEMENTS

10. CURRICULUM VITAE

Wanda Kloos, geboren 10.10.1982 in Bukarest, Rumänien

Schulausbildung

1993 - 2002 – Freihofgymnasium Göppingen/ South Carroll High School, Maryland, USA

2000 - Graduation in USA, High School Diploma

2002 - Abitur in Göppingen

Studium

2002 – 2008 - Medizinstudium an der Albert-Ludwigs-Universität Freiburg i. Br.

2004 – Physikum

05.2005 - 11.2007 Anfertigung der Doktorarbeit bei Prof. Dr. Martens, Abt. Hämatologie/Onkologie, Innere Medizin I, Universitätsklinikum Freiburg

2008 – 2. Staatsexamen